ugr | Universidad de Granada

A BAYESIAN APPROACH TO FATIGUE DAMAGE ASSESSMENT IN COMPOSITE MATERIALS

BY:

Juan Chiachío Ruano

A THESIS SUBMITTED TO:

University of Granada

ADVISOR:

Dr. Guillermo Rus Carlborg

Department of Structural Mechanics & Hydraulic Engineering
University of Granada
Granada (Spain)

October 2014

Editor: Editorial de la Universidad de Granada
Autor: Juan Chiachío Ruano
D.L.: GR 2225-2014
ISBN: 978-84-9083-298-1

A Bayesian approach to fatigue damage assessment in composite materials

El doctorando Juan Chiachío Ruano y el director de la tesis Dr. Guillermo Rus Carlborg, garantizamos, al firmar esta tesis doctoral, que el trabajo ha sido realizado por el doctorando bajo la dirección del director de la tesis y hasta donde nuestro conocimiento alcanza, en la realización del trabajo, se han respetado los derechos de otros autores a ser citados, cuando se han utilizado sus resultados o publicaciones.

En Granada, a 19 de Septiembre de 2014,

Director de la Tesis

Fdo.: GUILLERMO RUS CARLBORG

El Doctorando

Fdo.: JUAN CHIACHIO RUANO

Summary

Modeling the fatigue behavior of fiber-reinforced polymer composites is a challenging problem with important implications for safety and cost in a wide range of engineering applications. The fatigue phenomena in composites is governed by a partially-understood damage process driven by several multi-scale fracture mechanisms that lead to the progressive alteration of mechanical properties such as strength and stiffness, and ultimately to the final failure of the material. The inherent complexity of this process implies uncertainty in modeling, that not only includes the uncertainty as a consequence of uncertain inputs and model parameters (loading and environmental conditions, mechanical parameters, fitting "constants", etc.), but also the uncertainty arising from the idealization of the damage process by means of a hypothesized model for damage behavior. As a result, not a single model but numerous *model classes* can be formulated to represent the actual damage process based on different assumptions and hypothesis about it.

Over the last few decades, numerous fatigue modeling approaches have been proposed in the literature as a consequence of the aforementioned lack of knowledge about the actual damage mechanisms that govern the fatigue behavior in composites. At the same time, structural health monitoring (SHM) technology has experienced a considerable development and a large variety of experimental data can be readily acquired and processed to assess the various health-related properties of composite materials. However, comparatively less effort has gone into integrating both sources of information, namely, damage models and SHM data, to quantify the modeling uncertainty under real testing conditions and, as a by-product, to select and rank the most plausible models among candidates.

In this thesis, several model classes are proposed to simulate the observed fatigue behavior in composite materials given by SHM data. These model classes belong to physically different families of models representing different hypothesis about damage progression. First, a set of Markov chain model classes for damage evolution is proposed under the hypothesis that fatigue damage follows an irreversible memoryless stochastic process. It is accomplished through a novel model parameterization for the Markov chains that efficiently accounts for the non-stationarity of the damage process. Alternatively, a set of physics-based model classes is proposed based on several damage-mechanics models that address the relationship between the internal damage mechanisms and their macro-scale manifestation based on physics-based first principles. These damage-mechanics models are previously

parameterized through a sensitivity analysis and further embedded stochastically to allow for uncertainty quantification.

The performance of these families of model classes is investigated using a rigorous *Bayesian inverse problem* approach that allows to simultaneously estimate the *posterior probability* of a particular model class within a set of candidates for representing the observed damage response, along with the uncertainty of the underlying model parameters of the model class. This is accomplished by Bayes' Theorem, that aims at updating the *prior probability* of both, model parameters and model classes, to obtain the aforementioned posterior (updated) probability given the data.

In this framework, probability is interpreted as a multi-valued (not Boolean) logic that expresses the relative *degree of plausibility* of each model class within a set of candidates for representing the system based on incomplete information from the system response. Model class assessment is thus considered as an inference about plausible model classes given the data and not as a quest for the "true model". Based on the entire posterior probability of the model class, robust predictive analyses of damage evolution are obtained. Additional robustness is achieved by combining the robust predictions of the overall model classes within the set of candidates, where the contribution of each model class is weighed by its posterior probability given by Bayes' Theorem.

The proposed Bayesian framework implies various computational issues and mathematical complexities that have lead to dedicated computational and algorithmic solutions, which are also contributions of this thesis. In particular one of them, the ABC-SubSim algorithm, has raised to an original contribution in the specialized literature for Approximate Bayesian Computation, since it has demonstrated higher computational efficiency as compared to the other recent ABC algorithms.

Several case studies are presented to investigate the performance of the proposed model classes using SHM data from CFRP and GFRP laminates subjected to tension-tension fatigue loads. In this thesis, a reinterpretation of the Popperian paradigm for the inverse problem is adopted [Karl R. Popper, *The logic of scientific discovery*, Basic Books (1959)], by which experimental data is not intended to be used to validate or falsify a hypothesis/model for the system, but, instead, to estimate the degree of belief of such hypothesis/model for representing the observed system response by the data. A key finding from the case studies is that the simpler model classes turn out to be the best (most plausible) candidates when selected by striking a balance between average goodness of fit and model complexity, related with the amount of information extracted from data. Therefore, the principle of Ockham's razor seems to hold true for the fatigue modeling framework investigated here, that in this context can be stated as *simpler models that are consistent with data are to be preferred over unnecessarily complicated ones*. This statement is not an imposed condition but a natural outcome when dealing with models informed by the data in a Bayesian approach, since the application of Bayes' Theorem is shown to automatically enforce a quantitative Ockham's razor.

Resumen

La modelización del comportamiento a fatiga de los materiales compuestos poliméricos reforzados con fibras es un problema complejo con importantes implicaciones en seguridad y coste en un amplio rango de aplicaciones de ingeniería. El fenómeno de la fatiga en materiales compuestos está gobernado por un proceso interno de daño parcialmente conocido que es dirigido por varios mecanismos de fractura a diferentes escalas, dando lugar a la alteración progresiva de propiedades mecánicas como la resistencia y la rigidez, y finalmente al fallo último del material. La complejidad inherente de este proceso de daño implica incertidumbre en la modelización, que no solo incluye la incertidumbre como consecuencia de inputs y parámetros inciertos, sino también la incertidumbre derivada de la idealización del proceso de daño mediante un modelo hipotético de comportamiento a fatiga. Como resultado, no solo un único modelo sino numerosas clases de modelos pueden ser formuladas para idealizar el proceso de daño a partir de diferentes supuestos e hipótesis sobre el mismo.

En las últimas décadas se han propuesto diferentes aproximaciones al problema de modelización como consecuencia de la mencionada falta de conocimiento sobre los mecanismos reales de daño que gobiernan el comportamiento a fatiga en materiales compuestos. Al mismo tiempo, la tecnología de monitorización de salud estructural ha experimentado un grado de desarrollo considerable y, en consecuencia, una gran variedad de datos experimentales pueden ser fácilmente adquiridos y procesados para conocer el estado de salud estructural de los materiales compuestos. Sin embargo, comparativamente menos esfuerzo de investigación se ha puesto en la integración de ambas fuentes de información, es decir, modelos de daño y datos de monitorización de salud estructural, para cuantificar la incertidumbre de la modelización en condiciones reales de ensayo y, como subproducto, seleccionar y clasificar los modelos más plausibles de entre un conjunto de modelos candidatos.

En esta tesis se proponen varias clases de modelos de evolución de daño para simular el comportamiento a fatiga en materiales compuestos usando datos de monitorización. Estas clases pertenecen a familias de modelos físicamente diferentes que representan a su vez hipótesis diferentes acerca de la progresión del daño. En primer lugar se propone un conjunto de modelos de daño basados en la teoría de cadenas de Markov bajo la hipótesis de que el daño por fatiga sigue un proceso estocástico, irreversible y sin memoria. Esto es llevado a cabo mediante una novedosa parametrización de las cadenas de Markov que tiene en cuenta de forma eficiente la no estacionariedad del proceso de acumulación de daño. Alternativamente, se propone un conjunto de modelos basados en mecánica del daño que dan cuenta

de la relación entre los mecanismos de daño interno y su manifestación a macro-escala mediante principios físicos. Estos modelos de mecánica del daño son previamente parametrizados mediante un análisis de sensibilidad y posteriormente embebidos estocásticamente para permitir la cuantificación de incertidumbre de los mismos.

El comportamiento de estas familias de modelos es investigado mediante un enfoque basado en el *problema inverso Bayesiano*, que permite estimar simultáneamente la *probabilidad a posteriori* de un modelo dentro de un conjunto de clases de modelos candidatos, junto con la incertidumbre de los parámetros del modelo. Esto se lleva a cabo mediante el Teorema de Bayes, que tiene por objeto actualizar la *probabilidad a priori* de los parámetros del modelo, así como estimar la probabilidad de las clases de modelos candidatos. En este marco Bayesiano, la probabilidad es interpretada como una sentencia lógica de varios valores (no Booleana) que expresa el *grado de plausibilidad* de cada clase de modelos dentro de un conjunto de clases para representar la respuesta del sistema basada en información incompleta de la misma. Por tanto, la evaluación del comportamiento de cada clase se considera como una inferencia sobre el conjunto de clases de modelos plausibles dados los datos y no como una búsqueda del "modelo verdadero". Basado en la probabilidad total a posteriori de la clase de modelos, puede obtenerse mediante simulación la predicción robusta de la evolución del daño. Una robustez adicional en la predicción se consigue combinando las predicciones robustas de las distintas clases dentro del conjunto de clases candidatas, donde la contribución de cada clase es multiplicada por su probabilidad a posteriori dada por el Teorema de Bayes.

El marco Bayesiano propuesto implica una serie de complejidades computacionales y matemáticas que han dado lugar a soluciones computacionales y algoritmos específicamente diseñados, que son también contribuciones de esta tesis doctoral. En particular uno de ellos, el algoritmo ABC-SubSim, ha emergido como contribución original en la literatura especializada de Cálculo Bayesiano Aproximado (ABC, por sus siglas en inglés), ya que ha demostrado mayor eficiencia computacional en comparación con otros algoritmos recientes de ABC.

Las clases de modelos investigados en esta tesis han sido evaluadas mediante varios casos de estudio utilizando datos de monitorización de daño en laminados de fibra de carbono y fibra de vidrio sometidos a cargas de fatiga tipo tensión-tensión. En esta tesis se ha adoptado una reinterpretación del paradigma Popperiano para el problema inverso [Karl R. Popper, *The logic of scientific discovery*, Basic Books (1959)], por el cual los datos experimentales no son entendidos para ser usados para validar o falsar una hipótesis/modelo del sistema, sino en cambio, para estimar el grado de plausibilidad de dicha hipótesis/modelo para representar la respuesta del sistema dada por los datos. Un resultado clave de los casos de estudio investigados es que los modelos más simples resultan ser los mejores candidatos (más plausibles) cuando son seleccionados mediante un equilibrio entre la bondad de ajuste y la complejidad del modelo, relacionada con la cantidad de información que el modelo extrae de los datos. Por tanto, el principio conocido como "cuchillo de Ockham" parece ser cierto para el marco de modelización a fatiga investigado en esta tesis, que en este contexto

puede enunciarse como *los modelos más simples que sean consistentes con los datos son preferibles a los innecesariamente complicados*. Esta sentencia no es una condición impuesta, sino un resultado natural cuando se trata de modelos informados por datos de monitorización en un marco Bayesiano, ya que se demuestra que la aplicación del Teorema de Bayes implica una expresión cuantitativa del principio del cuchillo de Ockham.

Acknowledgments

I would like to thank the responsible of the direction of my research, Dr. Guillermo Rus Carlborg from the Department of Structural Mechanics and Hydraulic Engineering of the University of Granada. He supported me to bring me back to the University to work in the exciting area of the inverse problem in composites materials. His research vision has had a big impact on my work throughout these years. I would also like to thank my colleges from the Non Destructive Evaluation lab and from the Department of Structural Mechanics for their friendly help and support. I couldn't forget to my advisors during my research stays abroad: Prof. James L. Beck from Caltech (USA), Prof. Karl Schulte from Technical University of Hamburg (Germany), and Dr. Abhinav Saxena and Dr. Kai Goebel from NASA Ames Research Center (USA). The collaboration with all of them and their teams has been really fruitful and beneficial for my PhD research. A special mention goes to Prof. James L. Beck, my mentor, for his valuable guidance through the Bayesian methodology along these years. He has had a great influence not only on my research work but also in my scientific education.

This doctoral thesis has led me to long periods working and studying very hard, not only at home but also abroad. So I need to express my sincere gratitude to my family and friends for the comprehension and help I have received during these years. I am definitively in debt with them.

Finally, I would like to thank the Ministry of Education of Spain for the FPU grant no. P2009-4641, the NASA ARMD/AvSafe project SSAT, the Structures and Composites lab at Stanford University for experimental data, the Spanish Ministerio de Economía y Competitividad for project DPI2010-17065, and the regional Junta de Andalucía for projects P11CTS-8089 and GGI3000IDIB.

Abbreviations

ABC	Approximate Bayesian Computation
AGF	Average goodness of fit
BK	Bogdanoff and Kozin model
CDF	Cumulative distribution function
CFRP	Carbon fiber reinforced polymer
COD	Crack opening displacement
DC	Duty cycle
EIG	Expected information gained
FRP	Fiber reinforced polymer
GA	Genetic Algorithms
GFRP	Glass fiber reinforced polymer
GPU	Graphics processing unit
GSA	Global sensitivity analysis
M-H	Metropolis-Hasting algorithm
MA	Moving average
MC	Monte Carlo method
MCMC	Markov chain Monte Carlo
MMA	Modified Metropolis algorithm
PCoE	Prognostics Center of Excellence
PDF	Probability density function
PMC	Population Monte Carlo
PMIE	Principle of Maximum Information Entropy
PRC	Partial Rejection Control
PT	Parallel Tempering
PZT	Piezoelectric sensor
RIG	Relative information gain
SDOF	Single degree of freedom
SHM	Structural health monitoring
SMC	Sequential Monte Carlo
TTMC	Time transformation-condensation method

List of Symbols

Symbol	Description
θ	Model parameter vector
$\boldsymbol{\Theta}$	Set of possible values of model parameters
$\mathcal{M}_j$	Parameterized model class
$\mathbf{M}$	Set of model classes
$\mathfrak{M}$	Superset of model sets
$\mathcal{D}$	Experimental dataset
$\mathfrak{D}$	Region of possible outcomes of the system
$\boldsymbol{x}$	Simulated outcome vector from stochastic model
$\bar{x}_n^i$	i-th latent damage state at cycle n
$\mathbf{y}$	Experimental measurements vector
y_n	Damage measurement at cycle n
X_{n_N}	Sequence of n_N simulated outcomes
Y_{n_N}	Sequence of n_N experimental outcomes
$\mathcal{X}$	Subregion of $\boldsymbol{x}$-outcomes
$\mathcal{T}$	Set of consecutive fatigue cycles
$\mathcal{T}_\mathcal{D}$	Set of opportunistically staggered fatigue cycles
I	Set of latent damage states
p_n^i	Probability of $\bar{x}_n^i$
$p_n^{i,j}$	Conditional probability of transition: $p_n^{i,j} = p(\bar{x}_{n+1}^j \vert \bar{x}_n^i)$
$\mathbf{p}_n$	Probability mass function of damage at cycle n
$\mathbf{P}_n$	Probability transition matrix at cycle n
$g(\theta)$	Unit time transformation function
$P(\cdot)$	Probability
$p(\cdot)$	Probability density function
$\mathbf{f}_n$	Transition count matrix at cycle n
$f_n^{i,j}$	(i, j)-th element of transition count matrix at cycle n
$\mathbb{I}$	Indicator function
$\mathbf{u}$	Model input vector
$\mathbf{g}$	Model output vector
$\mathbf{e}$	Error term
$\mathbf{v}$	Vector of error parameters
$\boldsymbol{\mu}_\mathbf{e}$	Bias between model output and observations
$\boldsymbol{\Sigma}_\mathbf{e}$	Covariance matrix of error term
N_i	Dimension of model input vector
N_o	Dimension of model output vector
N_e	Dimension of error vector
d	Dimension of parameter vector

Symbol	Description
ψ_i	i-th candidate parameter for GSA
$\psi_{\sim i}$	Candidate parameters other than ψ_i
S_i^T	Total effects index of i-th candidate parameter ψ_i
$\mathbf{z}$	Joint state-parameter vector: $\mathbf{z} = (\boldsymbol{x}, \boldsymbol{\theta})$
$\mathcal{Z}$	$\mathbf{z}$-space
P_0	Conditional probability for SubSet simulation
m	Maximum number of simulation levels
ρ_{xy}	Chosen metric for ABC
$\eta(\cdot)$	Summary statistics
$\mathcal{B}_\epsilon(\mathcal{D})$	Metric ball of radius ϵ centered at $\mathcal{D}$
ϵ_j	Tolerance (metric distance) for j-th simulation level
$R^{(\tau)}$	Autocovariance of $h(\mathbf{z})$at lag τ
$R_j^{(\tau)}$	Autocov. of $h(\mathbf{z}_j)$ at lag τ for jth Subset simulation level
$q(\cdot\|\cdot)$	Proposal PDF
σ_q	Standard deviation for the proposal PDF
$\sigma_q^{(j)}$	Proposal st. dev. at the j-th simulation level
Σ_q	Covariance matrix for the proposal PDF level
r	Acceptance probability
$\bar{r}$	Acceptance ratio
γ	Autocorrelation factor
γ_j	Autocorrelation factor for j-th Subset simulation level
$R(\bar{l})$	Average stress perturbation function
$\mathbf{S}_0$	Compliance matrix of intact laminate
$Q_{i,j}$	(i, j)-th element of ply stiffness matrix
$\mathbf{A}^*$	Laminate stiffness matrix
$\mathbf{A}^k$	Stiffness matrix of k-th cracked ply (COD method)
$\boldsymbol{\beta}^{ik}$	k-th ply matrix of crack openings (COD method)
g_1	Micro-cracks density evolution model
g_2	Normalized longitudinal Young's modulus model

Symbol	SI	Description
$E_{x,0}$	[Pa]	Intact longitudinal Young's modulus
$E_x^{(\phi)}$	[Pa]	Sub-laminate longitudinal Young's modulus
E_x^*	[Pa]	Laminate effective Young's modulus
n_p	[-]	Number of plies in the laminate
ν^k	[-]	Poisson ratio of the k-th ply
t^k	[m]	Thickness of the k-th ply
ρ^k	$\frac{\text{\# cracks}}{m}$	matrix-cracks density of the k-th ply
$E_x^{(\phi)}$	[Pa]	Sublaminate longitudinal Young's modulus
$E_y^{(\phi)}$	[Pa]	Sublaminate tranvserse Young's modulus
$\nu_{xy}^{(\phi)}$	[-]	Sublaminate in-plane Poisson ratio
$G_{xy}^{(\phi)}$	[Pa]	Sublaminate in-plane shear modulus
$G_{yz}^{(\phi)}$	[Pa]	Sublaminate out-of-plane shear modulus

Symbol	SI	Description
h	[m]	Laminate half-thickness
B	[m]	Laminate half-width
t	[m]	Ply thickness
t_{90}	[m]	$[90^\circ]$-sublaminate half-thickness
t_0	[m]	$[0^\circ]$-sublaminate thickness
t_ϕ	[m]	$[\phi_{\frac{n_\phi}{2}}]$-sublaminate thickness
d_0	[m]	Interlaminar layer thickness
G_m	[m]	Interlaminar layer shear modulus
E_1	[Pa]	Ply longitudinal Young's modulus
E_2	[Pa]	Plytranvserse Young's modulus
ν_{12}	[-]	Ply in-plane Poisson ratio
ν_{23}	[-]	Ply out-of-plane Poisson ratio
G_{12}	[Pa]	Ply in-plane shear modulus
G_{23}	[Pa]	Ply out-of-plane shear modulus
R	[Pa]	Stress ratio
f	[Hz]	Frequency
σ_x	[Pa]	Applied axial tension
$\bar{l}$	[-]	Normalized half crack-spacing
ϕ	[rad]	Fibers direction
G	[J/m^2]	Energy release rate
ΔG	[J/m^2]	Increment in energy release rate
α	[-]	Paris' Law fitting parameter
A	[-]	Paris' Law fitting parameter
ξ	[-]	Shear lag parameter
ρ_n	$\frac{\#\text{ cracks}}{m}$	Normalized matrix-cracks density
D_n	[-]	Normalized effective Young's modulus
$\Gamma_{n_k}^{n_l}$	[-]	Damage sequence between cycles n_k and n_l
$\tilde{\Gamma}_{n_k}^{n_l}$	[-]	Simulated damage sequence between cycles n_k and n_l

Mathematics, rightly viewed, possesses not only truth, but supreme beauty - a beauty cold and austere, like that of sculpture, without appeal to any part of our weaker nature, without the gorgeous trappings of painting or music, yet sublimely pure, and capable of a stern perfection such as only the greatest art can show. The true spirit of delight, the exaltation, the sense of being more than Man, which is the touchstone of the highest excellence, is to be found in mathematics as surely as poetry

---

Mysticism and Logic and Other Essays
Bertrand Russell, 1919

Contents

List of Figures

List of Tables

List of Algorithms

Part I

INTRODUCTION

Uncertainty is not an accident of the scientific method, but its substance.

P. Høeg (1995)

1

Context and motivation

Fiber-reinforced polymer (FRP) composites are high performance materials used extensively in the construction of weight-critical engineering applications such as aeronautical or aerospace structures, which often require high reliability standards. These materials are well-known for their high strength-to-weight ratios, but also for being susceptible to fatigue degradation from the beginning of lifespan [2, 3]. Due to the direct impact on safety and cost, the fatigue behavior of composite materials has drawn close attention from industry and academia for decades, and still today, it is a partially understood problem and an active area of research.

The perception of the phenomenon of fatigue in composites has been typically associated with the behavior of isotropic, homogeneous, metallic materials and hence, there has been a strong tendency to study the fatigue behavior in composites as though they were metals [4–6]. As a consequence, a significant part of the composites fatigue literature deals with *life-time* models inspired by the well-known *S-N* curves (*S*: strength, *N*: lifespan) [5, 6]. These models, which are almost-entirely based on experimental fitting, do not take into account the actual damage mechanisms that govern the fatigue degradation in composites but predict the time at which fatigue failure occurs under specific testing conditions. This approach has typically led to oversized designs (after expensive experimental programs) and occasionally, to catastrophic failures [4].

Unlike metals, composites are inhomogeneous and anisotropic materials. They accumulate damage in several zones rather than a localized area, and failure does not generally occur by the propagation of a single macroscopic crack but for the degradation of macro-scale mechanical properties, such as strength or stiffness, as a consequence of the

densification and interaction of several fracture mechanisms at the micro-scale and meso-scale [3, 7]. These damage mechanisms, that include matrix micro-cracking, delamination, fibre breakage, etc., are noticeable from early stages of the lifecycle after only a few or a few hundred loading cycles, and their evolution and prevalences are highly influenced by material and testing conditions [2, 3, 8, 9]. Thus, modeling the progression of such internal damage mechanisms constitutes a more suitable approach for the study of the fatigue behavior and the lifecycle of the composite materials [5, 6].

But even under nominally identical testing and material conditions, the evolution of damage in composites can follow very different paths [3, 10, 11]. The onset and posterior growth of micro-scale fractures (e.g., micro-cracks and local delaminations) is a partially-understood process highly influenced by the random presence of manufacturing defects, such as voids, fiber waviness, etc. [12–15]. The inherent complexity of this process implies *uncertainty* in modeling, that comes not only from the random distribution of such defects and imperfections but also from the lack of knowledge about the physics of the damage process [16, 17]. It follows that if a deterministic model was chosen to make predictions about damage growth (even when using sophisticated approaches based on first physical principles), a limited fit to reality would be obtained due to the inherent uncertainty of the fatigue damage process. Notwithstanding, the vast majority of fatigue models in the composites literature are deterministic formulations valid for some specific testing and material conditions [5].

An alternative approach for this problem, that is adopted in this thesis, is to use data from the recorded fatigue response of the structure to *update* a given damage model so as to make more accurate predictions after assimilating the data, while accounting for the underlying modeling uncertainty. It is important to remark here that, in this thesis, a Cox-Jaynes [18, 19] reinterpretation of the Popperian paradigm [20, 21] is adopted, by which the experimental data is not intended to be used to validate or falsify a hypothesis/model for system response, but, instead, to estimate the *degree of belief* of such hypothesis/model for representing the observed system response given by the data.

In addition to the complexity of the problem due to the aforementioned uncertainty as a consequence of the variability in the damage response, there is another important source of uncertainty that should not be neglected when dealing with the prediction of the fatigue damage behavior in composite materials. It is the uncertainty coming from the selection of a particular *model class* [22] (e.g., the parameterized mathematical structure of the model for damage behavior) when several candidates model classes are available based on different hypothesis about the system. This modeling uncertainty is motivated by the fact that the model itself may not necessarily reproduce the real fatigue behavior of the structure, as a consequence of the aforementioned lack of knowledge about such fatigue behavior, but it is just an approximation [19, 23]. Several studies have attempted to deal with the uncertainty of fatigue behavior in composites focusing on the variability or scattering in the observed damage response, for example [10, 11, 24–26] to cite but a few; however most if not all of

these models neglect the modeling uncertainty coming from the adoption of a particular model class for fatigue behavior.

While the topic of modeling uncertainty has not been addressed in the composites fatigue literature (except for the author's publications derived from this thesis [16, 27]), methods for model class assessment have been developed and applied to a variety of engineering applications. For example, several methods based on classical statistics [28] and Bayesian statistics [22, 29] have been proposed, which address model uncertainty either by quantifying model error through a discrepancy function (for example, the Kennedy O' Hagan framework [30]) or by considering multiple competing models and quantifying the extent of support available for each of these models [22, 28, 29]. The latter approach, which is an extension of the so-called *Bayesian inverse problem* [19, 22, 31], is adopted in this thesis because multiple competing models are available for fatigue behavior in composite materials and Bayesian model assessment methods facilitates model ranking while simultaneously quantifying the uncertainty in these models. In addition, the Bayesian approach is best suited even in the presence of limited data, which is generally the case while studying the progression of fatigue damage in composites.

In particular, Bayesian methods have been previously applied for uncertainty quantification in fatigue modeling, albeit in the context of metals [17, 32–38]. For example, Cross *et al.* [33] and Sankararaman *et al.* [34] used Bayesian inference to estimate parameters underlying crack growth behavior. Sankararaman *et al.* [36] used dynamic Bayesian networks for model parameter estimation and calculated Bayes factors as a means to quantify model uncertainty. Therefore it seems reasonable to explore the applicability of these methods to the problem of fatigue damage modeling in composites materials, where the benefits of the Bayesian approach can be fully exploited due to the inherent complexity and the existence of multiple competing models.

In summary, the topic of uncertainty quantification in composites is slowly gaining interest and there is an evident need for the development of a rigorous treatment of the uncertainty as a consequence of the lack of knowledge about the physics of the fatigue damage process. The efficient and reliable use of composite materials in any application will require an adequate treatment of this modeling uncertainty. Instead of the commonly used deterministic approaches inherited from the metal fatigue experience, and, in addition to continue understanding the first physical principles that govern the fatigue damage evolution in composites, new probabilistic procedures are needed to accurately predict the fatigue behavior of the composite structures taking into account the uncertainty of the underlying damage process. In this context, the Bayesian inverse problem approach proposed in this thesis emerges as a powerful tool providing its ability and rigor for uncertainty management when dealing with several model clases and real data from the system response. This procedure has not been reported before, hence, it is the main contribution of this doctoral thesis.

It is unanimously agreed that statistics depends somehow on probability [...]. However there is a fundamental difference between frequentist and Bayesian interpretations that cannot be bridged.

Leonard J. Savage (1972)

2 Research objectives

Modeling the fatigue behavior of composite materials is a challenging problem due to the lack of knowledge about the multi-scale physics of the underlying damage process. As a result, several models have been proposed in the literature based on different assumptions about such damage process [5, 7]. The majority of these models are deterministic semi-empirical formulations calibrated for a particular material configuration under some specific testing conditions. Therefore, they not only neglect the modeling uncertainty coming from the adoption of single values for model parameters, but also from the selection of a particular model class (e.g., the parameterized mathematical structure of the model for the damage behavior) based on specified hypothesis about damage evolution. The use of Bayesian methods for model class assessment emerges as a rational way to select the model class or set of model classes that better predict the fatigue behavior of composite materials, while considering the underlying uncertainties. This is the central objective of the research presented in this thesis. To approach this objective, several concrete objectives are formulated on the basis of some research hypothesis which are listed and commented below.

1. Fatigue damage in composite materials is well-known as an irreversible memoryless process that can follow very different paths even under identical testing conditions [3, 10, 11, 39, 40]. Numerous fatigue models have been proposed [5, 41–43] and a large amount of data has been derived from expensive experimental programs. The vast majority of these models are deterministic approaches that do not account for the modeling uncertainty and the variability that is observed in the the fatigue damage process.

Recently, probabilistic damage models are emerging as a more suitable approach for fatigue in composite materials, but the extension of such methods is not as mature as the deterministic approach [5, 10, 11, 44].

Hypothesis 1: Damage progression in composites can be idealized as a Markovian-type stochastic process.

☛ **Research objective 1:** *Propose a modeling approach based on Markov chains to idealize the progression of fatigue damage along with a suitable parameterization strategy for the Markov chains to efficiently account for the non-stationarity of the damage process.*

2. Given that pure stochastic models need data to infer the values of the model parameters, they may capture excessive details from the data except when robust model parameterizations are employed [16, 22]. In contrast, physics-based models for damage evolution may be expected to accurately represent the fatigue damage process with much less training from the data. Several families of damage-mechanics models have been proposed in the composites fatigue literature [7]. These models deal with sophisticated formulations that address the connection between the internal damage mechanisms and their macro-scale manifestation based on physics-based first principles. Therefore, they can efficiently adapt to different systems (materials, testing conditions, etc.) although it may be at the expense of higher computational demand when these models are repeatedly evaluated in a stochastic simulation framework.

   Hypothesis 2: Physics-based models are expected to better represent the fatigue behavior of composites as compared to data-driven approaches.

   ☛ **Research objective 2:** *Propose a stochastic modeling approach based on physics-based damage models along with computational strategies to confer efficiency in their implementation, and compare them with the set of Markov chain damage models.*

3. After decades of research, a large variety of fatigue damage models has been proposed and hypothesized to simulate and predict the fatigue damage progression in composite materials [3, 5, 7]. Several model parameterizations and even physically different "families" of models may be formulated to represent an observed degradation process. From the perspective of forward modeling problems, more complex models are expected to better represent the complexity of the damage process. For inverse problems, i.e., when dealing with models informed by data, it may be at the cost of an excessive dependence on the data and input information that may lead to over-fitting of the data; therefore the model does not generalize well when making predictions. The information-theoretic interpretation of the Bayesian model selection problem [19, 22] shows that the posterior probability of each model class automatically enforces a quantitative expression of the Principle of Model Parsimony or Ockham's razor [19, 45], by which simpler models that are reasonably consistent with the data are to be preferred over more complex models that lead to slightly better agreement with the data.

Hypothesis 3: Simpler models for fatigue damage evolution in composites that agree reasonably well with the data are expected to overperform more sophisticated competing candidates.

☛ **Research objective 3:** *Provide discussion about the plausibility of candidate model classes using an information-theoretic approach for model class assessment.*

In the next section, the contributions of this thesis are outlined in the context of the research objectives described here.

Entities are not to be multiplied without necessity.

William of Ockham (1330)

3 Outline of contributions

This thesis intends to investigate the hypothesis and research objectives outlined in Chapter 2. The methods and experiments originally designed to this end are presented in this chapter along with an indication of where they appear in the text. Most of them have been already published in several journal articles, book chapters or conference proceedings as separated pieces of work. A list of related publications can be found in Appendix B.

Research objective 1:

Propose a modeling approach based on Markov chains to idealize the progression of fatigue damage along with a suitable parameterization strategy for the Markov chains to efficiently account for the non-stationarity of the damage process.

To deal with this objective, a new stochastic damage model is proposed based on the theory of Markov chains [46]. To efficiently account for the non-stationarity of the process, a new model parameterization is proposed for the Markov chain model based on a modification of the *time transformation-condensation method* first developed by Bogdanoff and Kozin [47]. Several model classes are further defined as a generalization of the proposed model parameterization strategy. The mathematical description of the proposed Markov chain model along with the set of modeling assumptions that are adopted are presented in **Chapter 5**. An illustrative example is also provided in Chapter 5, where the Markov chain model is used to simulate a set of highly-scattered fatigue damage sequences for quasi-isotropic GFRP laminates. This dataset, which is referred to as the Dataset 1, is summarized in **Chapter 8**, Section 8.1.

Research objective 2:

Propose a stochastic modeling approach based on physics-based damage models along with computational strategies to confer efficiency in their implementation, and compare them with the set of Markov chain damage models.

To investigate this twofold objective, a set of physics-based stochastic models is previously proposed based on several families of damage mechanics models (shear-lag, variational and crack opening displacement models [7]) that represent the relation between the macro-scale stiffness reduction and the micro-scale damage due to matrix-cracks. Each candidate model is subsequently embedded into the *modified Paris' law* [48], that is used in this research to model the propagation forward in time of the matrix-cracks density. The resulting models are previously parameterized by means of a Global Sensitivity Analysis (GSA) [49] and further embedded stochastically to define a set of (Bayesian) candidate model classes. The proposed modeling framework is presented in **Chapter 6** along with the methodology for model class definition based on stochastic embedding. This approach results in formulations which require the evaluation of multidimensional integrals parameterized by uncertain model parameters, thus leading to computationally-intensive problems when these models are evaluated repeatedly, as typically arises for inference purposes. To tackle this drawback, two computational strategies are proposed. First, the implementation of the stochastic damage models on the Graphics Processing Unit (GPU), utilizing the Compute Unified Device Architecture (CUDA) code from NVIDIA using Matlab®. The implementation scheme is presented in Chapter 6. On the other hand, the use of an Approximate Bayesian Computation (ABC) method to circumvent the evaluation of the likelihood function, since it conveys the heaviest part of the computational burden. A novel ABC algorithm based on Subset simulation [50] is proposed, which has demonstrated higher computational efficiency as compared to the most recent ABC algorithms in the literature. This algorithm, that was initially proposed as a side objective, has raised to one of the most significant contributions of this thesis. It is presented in **Chapter 7**.

Finally, the performance of the proposed physics-based model classes is compared with the performance of the (data-driven) Markov chain model classes defined in Chapter 5. The comparison is accomplished through probabilities that measure the extent of agreement of their overall predictions with the data using an extension of the methodology for Bayesian model class selection presented in **Chapter 4**. To perform the comparison, SHM data for micro-cracks density and stiffness loss is used from a CFRP cross-ply laminate, which is summarized in **Chapter 8**, Section 8.2. The results of the *model set assessment* together with the methodology proposed for the comparison are presented in **Chapter 11**.

Research objective 3:

Provide discussion about the plausibility of candidate model classes using an information-theoretic approach for model class assessment.

To explore this research objective, the model classes defined in Chapters 5 (for Markov chain models) and 6 (for damage-mechanics models) and compared and ranked between them based on the methodology for Bayesian model class assessment presented in Chapter 4. To this end, Bayes' Theorem [22, 31] is applied at two levels: first, to deal with the posterior information about the model parameters of a specific model class within a set of candidate model classes, and second, to assess the degree of plausibility of each model class within the set of candidates. This application of Bayes' Theorem automatically enforces a quantitative expression of the Ockham's razor that allows us to know an information-theoretic balance between the average goodness of fit and the model complexity of each model class.

The results for model class assessment are presented in **Chapter 9** for the set of Markov chain models using two nominally different sets of data: Dataset 1 for glass-epoxy quasi-isotropic laminates (Section 8.1), and Dataset 2 for carbon-epoxy cross-ply laminates (Section 8.2). For the set of damage mechanics models, the results for model class assessment are provided in **Chapter 10** in application to Dataset 2. The Metropolis-Hasting (M-H) algorithm presented in Chapter 4 (Section 4.1.2) is used for both case studies to numerically solve the inverse problem. For the case study using physics-based model classes, the assessment is exemplified using the ABC-SubSim algorithm and results are compared with those using M-H algorithm.

The essence of the present theory is that no probability, direct, prior, or posterior, is simply a frequency.

H. Jeffreys (1939)

4 Theoretical fundamentals

This chapter aims at supplying the theoretical basis about the Bayesian inverse problem, which will be extensively used over the course of this thesis. Section 4.1 exposes the fundamentals about Bayesian model parameter updating. In Section 4.2, the problem of Bayesian model class selection is presented as an extension of the Bayesian model parameter updating problem. Algorithms for both, Bayesian model updating and Bayesian model class selection are provided.

4.1 Bayesian inverse problem

Using a physical theory or model to predict the response of a system corresponds to solving a *forward modeling problem*. The reciprocal situation, i.e., using information from the system output (e.g. measurements) to find the model or set of models that are more consistent with the observations of the system corresponds to the *inverse modeling problem* or *system identification problem*.

Whereas the forward problem has commonly a unique solution, the inverse problem may have many solutions [31], i.e., there may be several models that are consistent with the same set of observations. It follows that estimating a deterministic single value for the model parameters of a particular *model class* (e.g. the parameterized mathematical structure of the model for system behavior) when reconstructing the system response has a limited meaning if one considers that the model class is just an idealization of reality and so, that several *model classes* can be hypothesized and formulated based on different modeling assumptions about the system [22]. To provide a suitable answer, probabilistic instead of deterministic

values for both model parameters and model classes should be provided, which carry information about the *degree of plausibility* of those model parameters and classes providing the observations of the system.

To deal with these issues, a rigorous probabilistic approach for inverse problems is available based on Bayesian inference [22, 31]. The goal of Bayesian inversion [19, 22] is to use Bayes' Theorem to investigate the plausibility of a given model parameterized by $\boldsymbol{\theta}$ belonging to a candidate model class $\mathcal{M}_j$, for representing the system based on (incomplete) information $\mathcal{D} \in \mathfrak{D}$ from the system output, where $\mathfrak{D} \subset \mathbb{R}^\ell$ is the region of all possible outcomes of the system. The focus is twofold, (1) to investigate the plausibility of model parameters $\boldsymbol{\theta}$ over the set $\boldsymbol{\Theta} \subset \mathbb{R}^d$ of possible values in the model class $\mathcal{M}_j$ given the information from the system response $\mathcal{D}$, namely, $p(\boldsymbol{\theta}|\mathcal{D}, \mathcal{M}_j)$; and (2), to investigate the plausibility of the overall model class $\mathcal{M}_j$ within the set $\mathbf{M} = \{\mathcal{M}_1, \ldots, \mathcal{M}_j, \ldots, \mathcal{M}_{N_M}\}$ of candidate model classes for representing the system, based on data $\mathcal{D}$ from the system response, i.e., $p(\mathcal{M}_j|\mathcal{D}, \mathbf{M})$. Consequently, the Bayesian approach to the inverse problem has the advantage of being able to quantify the uncertainties associated with (1) model parameters and (2) model choice for the system behavior, and therefore, to further make predictions about the system output that rigorously incorporate different types of modeling uncertainty in a quantitative manner.

A rigorous foundation for such approach, which is adopted in this thesis, is given by the Cox-Jaynes theory of probability as a multi-valued logic for plausible inference [51, 52]. According to such approach, commonly known as *Probability Logic* [19, 22], probability is interpreted as a multi-valued propositional logic that expresses the *degree of belief* of a proposition conditioned on given information [19, 22]. For example, in Probability Logic $P[A|B]$ is interpreted as the degree of plausibility of proposition A based on the information in proposition B. Therefore, in contrast to the typical subjective interpretation of probability in Bayesian inference, logical probabilities are objective (logical) relations between propositions or *states of information*; i.e., if B holds, then A holds with probability $P[A|B]$. In the extreme situation, i.e. if B implies A, then proposition B gives complete information about A, and thus $P[A|B] = 1$; otherwise, when B implies not A, then $P[A|B] = 0$.

Using this interpretation of probability, the PDF of model parameters $p(\boldsymbol{\theta}|\mathcal{D}, \mathcal{M}_j)$ is read as: *If model class $\mathcal{M}_j$ is adopted and information $\mathcal{D}$ from system response is available* (conditional proposition B), *then the model specified by $\boldsymbol{\theta}$ represents the system* (proposition A) *with probability* $p(\boldsymbol{\theta}|\mathcal{D}, \mathcal{M}_j)$. Bayes' Theorem gives the aforementioned PDF of model parameters as follows:

$$p(\boldsymbol{\theta}|\mathcal{D}, \mathcal{M}_j) = c^{-1} p(\mathcal{D}|\boldsymbol{\theta}, \mathcal{M}_j) p(\boldsymbol{\theta}|\mathcal{M}_j) \tag{4.1}$$

where c is a normalizing constant so that $p(\boldsymbol{\theta}|\mathcal{D}, \mathcal{M}_j)$ is a valid probability density function. That is:

$$\int_{\boldsymbol{\Theta}} p(\boldsymbol{\theta}|\mathcal{D}, \mathcal{M}_j) d\boldsymbol{\theta} = c^{-1} \int_{\boldsymbol{\Theta}} p(\mathcal{D}|\boldsymbol{\theta}, \mathcal{M}_j) p(\boldsymbol{\theta}|\mathcal{M}_j) d\boldsymbol{\theta} = 1 \tag{4.2}$$

Notice that Bayes' Theorem takes the initial quantification of the plausibility of each model specified by $\boldsymbol{\theta}$ in $\mathcal{M}_j$, which is expressed by the *prior* PDF $p(\boldsymbol{\theta}|\mathcal{M}_j)$, and *updates* this

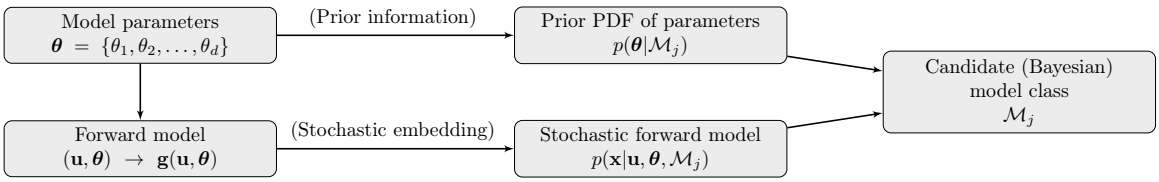

Figure 4.1: *Scheme for Bayesian model-class definition*

plausibility to obtain the *posterior* PDF $p(\boldsymbol{\theta}|\mathcal{D}, \mathcal{M}_j)$ by using information from the system output expressed through the PDF $p(\mathcal{D}|\boldsymbol{\theta}, \mathcal{M}_j)$, commonly known as the *likelihood function*. The likelihood function provides a measure about how likely the observed data $\mathcal{D}$ are reproduced if the model specified by $\boldsymbol{\theta}$ within model class $\mathcal{M}_j$ is adopted. It is obtained by evaluating the data $\mathcal{D}$ as the outcome of the stochastic forward model for the system behavior, expressed as $p(\boldsymbol{x}|\boldsymbol{\theta}, \mathcal{M}_j)$, where $\boldsymbol{x} \in \mathfrak{D}$ is the system output simulated by the model. The definition and further computation of the likelihood function constitutes one the major issues for the Bayesian model updating scheme presented here since it requires a large number of repetitive evaluations of the stochastic forward model; thus, specific details about likelihood computation are provided in the succeeding chapters in the context of the fatigue damage models discussed in this thesis.

From the above introduction, the following three important pieces of information can be highlighted for the proposed Bayesian approach for fatigue modeling:

$\mathcal{D}$: data set containing measurements of the system output.

$\mathcal{M}_j$: j-th Bayesian model class or candidate among alternative model classes hypothesized to idealize the system. This Bayesian model class is defined by two fundamental probability models [22]: the stochastic forward model $p(\boldsymbol{x}|\boldsymbol{\theta}, \mathcal{M}_j)$ and the prior probability distribution $p(\boldsymbol{\theta}|\mathcal{M}_j)$, that gives the initial relative plausibility of model parameters defining the stochastic forward model in the class $\mathcal{M}_j$ (see Figure 4.1).

$\boldsymbol{\theta}$: set of uncertain model parameters within model class $\mathcal{M}_j$ to be updated using Bayes' Theorem.

All the defined variables (output data $\mathcal{D}$, model parameters $\boldsymbol{\theta}$ or model classes $\mathcal{M}_j$) are defined to lie in manifolds $\mathfrak{D}$, $\mathbf{M}$ and $\boldsymbol{\Theta}$, respectively.

4.1.1 Model-class definition by stochastic embedding

As explained before, a stochastic forward model is required for the purpose of system identification. Most of the times, a forward model for system behavior is available in the form of a deterministic input-output relationship that does not allows for uncertainty management; notwithstanding, a stochastic forward model can be derived from a given deterministic forward model by means of *stochastic embedding* [22]. To this end, let us consider a candidate damage model defined by a deterministic relationship $\mathbf{g} = \mathbf{g}(\mathbf{u}, \mathbf{m}) : \mathbb{R}^{N_i} \times \mathbb{R}^{N_m} \rightarrow \mathbb{R}^{N_o}$ between the model input $\mathbf{u} \in \mathbb{R}^{N_i}$ and the model output $\mathbf{g} \in \mathbb{R}^{N_o}$, given a set of N_m uncertain parameters $\mathbf{m} \in \mathbb{R}^{N_m}$. This damage model can be "embedded" stochastically by

adding an error term $\mathbf{e} = \mathbf{e}(\mathbf{v}) : \mathbb{R}^{N_e} \to \mathbb{R}^{N_o}$ parameterized by $\mathbf{v} \in \mathbb{R}^{N_e}$, that represents the difference between the actual system output $\boldsymbol{x} \in \mathbb{R}^{N_o}$ and the model output $\mathbf{g}$, as follows:

$$\underbrace{\boldsymbol{x}}_{\text{system output}} = \underbrace{\mathbf{g}(\mathbf{u}, \mathbf{m})}_{\text{model output}} + \underbrace{\mathbf{e}(\mathbf{v})}_{\text{error}} \tag{4.3}$$

In the last equation, it is implicitly assumed that both measurement and model errors are subsumed into the error term $\mathbf{e}(\mathbf{v})$. Such assumption can be adopted when the measurement error is negligible as compared to the model error, or when an independent study about the measurement error is not available. In addition, the set $\mathbf{m}$ of parameters is augmented with the set $\mathbf{v}$ of error parameters, resulting in a set of model parameters defined as $\boldsymbol{\theta} = \{\mathbf{m}, \mathbf{v}\} \in \boldsymbol{\Theta} \subset \mathbb{R}^{d=N_m+N_e}$. This set of parameters is further updated through Bayes' Theorem using Equation 4.1.

It should be noted here that the probability model chosen for the error term $\mathbf{e}$ in Equation 4.3 determines the probability model for the system output $\boldsymbol{x}$. For example, if the error term is assumed to be modeled as a Gaussian distribution, i.e. $\mathbf{e} \sim \mathcal{N}(\boldsymbol{\mu}_\mathbf{e}, \boldsymbol{\Sigma}_\mathbf{e})$, then the system output $\boldsymbol{x}$ will be also distributed as a Gaussian, as follows:

$$\mathbf{e} = \boldsymbol{x} - \mathbf{g}(\mathbf{u}, \boldsymbol{\theta}) \sim \mathcal{N}(\boldsymbol{\mu}_e, \boldsymbol{\Sigma}_\mathbf{e}) \implies \boldsymbol{x} \sim \mathcal{N}(\mathbf{g}(\mathbf{u}, \boldsymbol{\theta}) + \boldsymbol{\mu}_\mathbf{e}, \boldsymbol{\Sigma}_\mathbf{e}) \tag{4.4}$$

where $\boldsymbol{\mu}_\mathbf{e} \in \mathbb{R}^{N_o}$ is a systematic bias between model output and the observed system output, and $\boldsymbol{\Sigma}_\mathbf{e} \in \mathbb{R}^{N_o \times N_o}$ is the covariance matrix of the error term. This assumption is supported by the Principle of Maximum Information Entropy (PMIE) [19], which enables a rational way to establish a probability model for the error term such that it produces the largest uncertainty (largest Shannon entropy). Thus, by adopting this assumption, a stochastic forward model for system behavior can be defined from any deterministic model as

$$p(\boldsymbol{x}|\mathbf{u}, \boldsymbol{\theta}, \mathcal{M}_j) = \left((2\pi)^{N_o}|\boldsymbol{\Sigma}_\mathbf{e}|\right)^{-\frac{1}{2}} \exp\left(-\frac{1}{2}(\boldsymbol{x} - \bar{\boldsymbol{x}})^T \boldsymbol{\Sigma}_\mathbf{e}^{-1}(\boldsymbol{x} - \bar{\boldsymbol{x}})\right) \tag{4.5}$$

where $\bar{\boldsymbol{x}} = \mathbf{g}(\mathbf{u}, \boldsymbol{\theta}) + \boldsymbol{\mu}_\mathbf{e}$ denotes the mean output of the stochastic forward model, and $\mathcal{M}_j$ represents the candidate Bayesian model class defined by the stochastic forward model and the prior PDF of model parameters, $p(\boldsymbol{\theta}|\mathcal{M}_j)$, as shown in Figure 4.1.

4.1.2 Markov Chain Monte Carlo simulation for Bayesian updating

While the power of the Bayesian inverse problem for model updating is well recognized, there are several computational issues during its implementation that need dedicated solutions. Specifically, the main difficulty when applying Bayes' Theorem is that normalizing constant c in Equation 4.1 cannot be evaluated analytically nor it is readily calculated by numerical integration methods, if the dimension d is not small [53]. To tackle this problem, Markov Chain Monte Carlo (MCMC) methods [54, 55] have been widely used for its ability to estimate the posterior PDF while avoiding the evaluation of constant c. In general, the

goal of these stochastic simulation methods is to generate samples that are distributed according to an arbitrary probability distribution, commonly known as the *target* PDF, which is known up to a scaling constant [56–59]. In the context of the Bayesian inverse problem proposed here, such target PDF corresponds to the posterior probability density function in Equation 4.1.

There are two required properties for the MCMC algorithms to obtain correct statistical estimations about the target: (1) *ergodicity*, which is concerned with whether the generated samples can populate the regions of significant probability of the target PDF; and (2) *stationarity*, which ensures that the forward samples of the Markov chain are equally distributed than the previous samples, provided that the later are distributed as the target PDF. Under the assumption of ergodicity, the samples generated from MCMC will converge to the target distribution (provided that a large amount of samples are used) even if the initial set of samples are simulated from a PDF different from the target. The theoretical demonstration of ergodicity and stationarity for MCMC is out of the scope of this work, but the interested reader is referred to [46] for a comprehensive theoretical treatment of Markov chains.

In the literature, several MCMC algorithms have been proposed after the celebrated paper by Metropolis *et al.* [60], such as the Metropolis-Hastings, Gibbs Sampler and Hybrid Monte Carlo algorithms, among others [57, 59]. In this thesis, the Metropolis-Hastings (M-H) algorithm is adopted for its versatility and implementation simplicity [60, 61]. This algorithm generates samples from a specially constructed Markov chain whose stationary distribution is the posterior PDF. In M-H, a candidate model parameter $\boldsymbol{\theta}'$ is sampled from a *proposal distribution* $q(\boldsymbol{\theta}'|\boldsymbol{\theta}^{(k-1)})$, given the state of the Markov chain at step $k-1$. At the next state of the chain k, the candidate parameter $\boldsymbol{\theta}'$ is accepted (i.e. $\boldsymbol{\theta}^{(k)} = \boldsymbol{\theta}'$) with probability $\min\{1, r\}$, and rejected ($\boldsymbol{\theta}^{(k)} = \boldsymbol{\theta}^{(k-1)}$) with probability $1 - \min\{1, r\}$, where r is calculated as:

$$r = \frac{p(\mathcal{D}|\boldsymbol{\theta}', \mathcal{M})p(\boldsymbol{\theta}'|\mathcal{M})q(\boldsymbol{\theta}^{(k-1)}|\boldsymbol{\theta}')}{p(\mathcal{D}|\boldsymbol{\theta}^{(k-1)}, \mathcal{M})p(\boldsymbol{\theta}^{(k-1)}|\mathcal{M})q(\boldsymbol{\theta}'|\boldsymbol{\theta}^{(k-1)})} \tag{4.6}$$

The process is repeated until N_s samples have been generated. An algorithmic description of this method is provided in Algorithm 1 below.

Algorithm 1 M-H algorithm

1. Initialize $\boldsymbol{\theta}^{(0)}$ by sampling from the prior: $\boldsymbol{\theta}^{(0)} \sim p(\boldsymbol{\theta}|\mathcal{M})$
for $k = 1$ to N_s **do**
   2. Sample from the proposal: $\boldsymbol{\theta}' \sim q(\boldsymbol{\theta}'|\boldsymbol{\theta}^{(k-1)})$
   3. Compute r from Eq. 4.6
   4. Generate a uniform random number: $\alpha \sim \mathcal{U}[0, 1]$
   if $r \geqslant \alpha$ **then**
      5. Set $\boldsymbol{\theta}^{(k)} = \boldsymbol{\theta}'$
   else
      6. Set $\boldsymbol{\theta}^{(k)} = \boldsymbol{\theta}^{(k-1)}$
   end if
end for

An important consideration is the specification of the variance σ_q^2 for the proposal distribution $q(\boldsymbol{\theta}'|\boldsymbol{\theta}^{(k-1)})$, which has a significant impact on the speed of convergence of the algorithm [61]. Small values tend to produce candidate samples that are accepted with high probability, but may result in highly dependent chains that explore the state space very slowly. In contrast, large values of the variance tend to produce large steps in the state space, but result in small acceptance rates. Thus, it is often worthwhile to select appropriate proposal variances by controlling the acceptance rate $\bar{r}$ (e.g., number of accepted samples over total amount of samples) in a certain range, depending on the dimension d of the proposal PDF, via some pilot runs [62, 63]. The interval $[20\% - 40\%]$ is suggested for the acceptance rate in low dimensional spaces, say $d \leqslant 10$ [63].

Modified Metropolis algorithm

The Modified Metropolis algorithm (MMA) [50] is a variant of the original Metropolis algorithm that differs from it in the way the candidate $\boldsymbol{\theta}'$ is generated in Step 2. A univariate proposal PDF is chosen for each component of the parameter vector such that the i-th component of the candidate vector $\boldsymbol{\theta}'$ is accepted or rejected separately, instead of drawing a full variable vector from a multi-dimensional PDF as in Algorithm 1. In this thesis, MMA is used in the context of SubSet simulation (introduced in Chapter 7), therefore the focus is to obtain samples from a conditional target PDF $p(\boldsymbol{\theta}|\mathcal{F})$, where $\mathcal{F}$ is a subset of the parameter space, i.e., $\mathcal{F} \subset \boldsymbol{\Theta}$. By means of Bayes' Theorem:

$$p(\boldsymbol{\theta}|\mathcal{F}) = \frac{\mathbb{I}_{\mathcal{F}}(\boldsymbol{\theta}) p(\boldsymbol{\theta}|\mathcal{M})}{P(\mathcal{F})} \tag{4.7}$$

where $\mathbb{I}_{\mathcal{F}}(\boldsymbol{\theta})$ is an indicator function for $\mathcal{F}$ so that $\mathbb{I}_{\mathcal{F}}(\boldsymbol{\theta}) = 1$ if $\boldsymbol{\theta} \in \mathcal{F}$, and 0 otherwise.

The univariate proposal PDF is denoted as $q_i(\theta_i|\theta_i')$, $i = 1, \ldots, d$ so that it has the symmetry property, i.e., $q_i(\theta_i|\theta_i') = q_i(\theta_i'|\theta_i)$. In MMA, it is assumed (with no loss of generality) that the prior information of the i-th component of model parameters (denoted here as $p_i(\theta_i|\mathcal{M})$) is independent from the rest, therefore $p(\boldsymbol{\theta}|\mathcal{M}) = \prod_{i=1}^{d} p_i(\theta_i|\mathcal{M})$.

To illustrate the MMA algorithm, let consider $\boldsymbol{\theta}^{(k-1)} = \left[\theta_1^{(k-1)}, \ldots, \theta_d^{(k-1)}\right] \sim p(\boldsymbol{\theta}|\mathcal{F})$. By sampling from the i-th univariate proposal PDF $q_i(\theta_i'|\theta_i^{(k-1)})$, $i = 1, \ldots, d$, a candidate sample $\boldsymbol{\theta}' = [\theta_1', \theta_2', \ldots, \theta_d']$ is generated based on the previous sample $\boldsymbol{\theta}^{(k-1)}$. Then a check is made whether $\boldsymbol{\theta}'$ belongs to $\mathcal{F}$ in which case it is accepted as the next state ($\boldsymbol{\theta}^{(k)} = \boldsymbol{\theta}'$); otherwise it is rejected, thus ($\boldsymbol{\theta}^{(k)} = \boldsymbol{\theta}^{(k-1)}$). A pseudocode implementation is provided below as Algorithm 2.

Au and Beck [50] demonstrated that MMA works well even in very high dimensions (e.g. $d = 10^3$-10^4), because the original M-H algorithm fails in this case (essentially all candidate samples from the proposal PDF are rejected). Later in [64], grouping of the variables was considered when constructing the proposal PDF to allow for the case where small groups of components in the variable vector are highly correlated when conditioned on $\mathcal{F}$.

Algorithm 2 MMA algorithm

1. Initialize $\boldsymbol{\theta}^{(0)}$ by sampling from the prior: $\boldsymbol{\theta}^{(0)} \sim p(\boldsymbol{\theta}|\mathcal{M})$

for $k = 1$ to N_s **do**

  for $i = 1$ to d **do**

    2. Generate $\theta_i' \sim q_i(\theta_i'|\theta_i^{(k-1)})$

    3. Compute the ratio $r = \frac{p_i(\theta_i'|\mathcal{M})}{p_i(\theta_i^{(k-1)}|\mathcal{M})}$

    4. Accept θ_i' by setting:

$$\theta_i' = \begin{cases} \theta_i' & \text{with probability } \min\{1, r\} \\ \theta_i^{(k-1)} & \text{with probability } 1 - \min\{1, r\} \end{cases}$$

  end for

  5. Set $\boldsymbol{\theta}^{(k)}$ as follows:

$$\boldsymbol{\theta}^{(k)} = \begin{cases} \boldsymbol{\theta}' & \text{if } \boldsymbol{\theta}' \in \mathcal{F} \\ \boldsymbol{\theta}^{(k-1)} & \text{if } \boldsymbol{\theta}' \notin \mathcal{F} \end{cases}$$

end for

4.2 Bayesian model-class assessment

As stated before, the probabilistic approach for model class selection is motivated by the fact that the model itself may not necessarily reproduce the observed system, but it is just an approximation [19, 23]. Therefore, there may exist not only different values for model parameters but physically different models classes that may be consistent with the observations of such system. The goal is then to use the available information from the system response $\mathcal{D}$ to asses the relative plausibility of the j-th candidate model class $\mathcal{M}_j$ for representing the system within a set of model classes $\mathbf{M} = \{\mathcal{M}_1, \ldots, \mathcal{M}_j, \ldots, \mathcal{M}_{N_M}\}$; namely, $p(\mathcal{M}_j|\mathcal{D}, \mathbf{M})$. As stated before with the posterior PDF of model parameters, Probability Logic enables us a rational interpretation of the posterior probability of a model class: given $\mathbf{M}$, a set of candidate model classes, and $\mathcal{D}$, data from the system response, then model class $\mathcal{M}_j$ represents the system with (posterior) probability $p(\mathcal{M}_j|\mathcal{D}, \mathbf{M})$.

The posterior probabilities can be obtained using Bayes' Theorem at the model class level [22], as:

$$p(\mathcal{M}_j|\mathcal{D}, \mathbf{M}) = \frac{p(\mathcal{D}|\mathcal{M}_j)p(\mathcal{M}_j|\mathbf{M})}{\sum_{i=1}^{N_M} p(\mathcal{D}|\mathcal{M}_i)p(\mathcal{M}_i|\mathbf{M})} \tag{4.8}$$

where $p(\mathcal{M}_j|\mathbf{M})$ is the prior probability of the j-th model class in the set $\mathbf{M}$, satisfying $\sum_{j=1}^{N_M} p(\mathcal{M}_j|\mathbf{M}) = 1$. This prior probability expresses the initial modeler's judgement on the relative degree of belief on $\mathcal{M}_j$ within the set $\mathbf{M}$. The factor $p(\mathcal{D}|\mathcal{M}_j)$ is the *evidence* (also called *marginal likelihood*) for the model class $\mathcal{M}_j$, and expresses how likely the observed system response is reproduced if model class $\mathcal{M}_j$ is adopted. The evidence is given by Total Probability Theorem as:

$$p(\mathcal{D}|\mathcal{M}_j) = \int_{\boldsymbol{\Theta}} p(\mathcal{D}|\boldsymbol{\theta}, \mathcal{M}_j)p(\boldsymbol{\theta}|\mathcal{M}_j)\mathrm{d}\boldsymbol{\theta} \tag{4.9}$$

where $p(\mathcal{D}|\boldsymbol{\theta}, \mathcal{M}_j)$ is the likelihood function and $p(\boldsymbol{\theta}|\mathcal{M}_j)$ is the prior PDF of model parameters, both of them introduced in Section 4.1. It is noted that the evidence is equal to the normalizing constant in establishing the posterior PDF in Equation 4.1.

Once the evidence for each model class is computed, their values allow us to rank the model classes according to the posterior probabilities given in Equation 4.8. However, the evaluation of the multi-dimensional integral in Equation 4.9 is nontrivial except for some cases where the Laplace's method of asymptotic approximation can be used [65]. In this thesis, a recent technique based on samples from the posterior is adopted to numerically solve this integral [66]. The details along with an algorithmic description of this method are provided below in Section 4.2.2.

4.2.1 Information-theory approach to model-class selection

From the perspective of forward modeling problems, more complex models may be preferred over simpler models because they are considered more realistic. For inverse problems, however, this may lead to over-fitting of the data where the model is unnecessarily adjusted to fit the given set of data. Then the model does not generalize well when making predictions since it depends too much on the details of data. The Bayesian approach to model class assessment shows that the evidence of each model class automatically enforces a quantitative expression of a Principle of Model Parsimony or Ockham's razor [19, 45], by which simpler models that are reasonably consistent with data should be preferred over more complex models that lead to only slightly better agreement with the data. In this context, Muto and Beck [58] proposed an information-theoretic interpretation of the evidence for a model class that is adopted in this thesis, as follows:

$$\begin{aligned}\log p(\mathcal{D}|\mathcal{M}_j) &= \int_{\boldsymbol{\Theta}} \left[\log p(\mathcal{D}|\boldsymbol{\theta}, \mathcal{M}_j)\right] p(\boldsymbol{\theta}|\mathcal{D}, \mathcal{M}_j) d\boldsymbol{\theta} - \int_{\boldsymbol{\Theta}} \left[\log \frac{p(\boldsymbol{\theta}|\mathcal{D}, \mathcal{M}_j)}{p(\boldsymbol{\theta}|\mathcal{M}_j)}\right] p(\boldsymbol{\theta}|\mathcal{D}, \mathcal{M}_j) d\boldsymbol{\theta} \\ &= \mathbb{E}[\log p(\mathcal{D}|\boldsymbol{\theta}, \mathcal{M}_j)] - \mathbb{E}\left[\log \frac{p(\boldsymbol{\theta}|\mathcal{D}, \mathcal{M}_j)}{p(\boldsymbol{\theta}|\mathcal{M}_j)}\right]\end{aligned} \tag{4.10}$$

where $\mathbb{E}$ is the expectation respect to the posterior $p(\boldsymbol{\theta}|\mathcal{D}, \mathcal{M}_j)$. This expression is obtained by strategically multiplying the logarithm of the evidence by a factor of one:

$$\log p(\mathcal{D}|\mathcal{M}_j) = \left(\log p(\mathcal{D}|\mathcal{M}_j)\right) \underbrace{\int_{\boldsymbol{\Theta}} p(\boldsymbol{\theta}|\mathcal{D}, \mathcal{M}_j) d\boldsymbol{\theta}}_{=1} \tag{4.11}$$

and then making substitutions according to Bayes' Theorem (Equation 4.1) to expand the evidence.

The first term of the right side of Equation 4.10 is the posterior mean of the log-likelihood function, which is a measure of the average goodness of fit (AGF) of the model class $\mathcal{M}_j$ to the data $\mathcal{D}$. This term accounts for the goodness of fit for different combinations of the model parameters, weighted by their posterior probabilities [22, 58]. The second term is the *relative*

entropy between the posterior and the prior PDFs, which measures the "difference" between those PDFs [67]. This term determines the expected information gained (EIG) about the model class $\mathcal{M}_j$ from the data and it is, by definition, always non-negative. It will usually be larger for more complex models with more parameters, therefore, the resulting log-evidence of a model class is comprised of a data-fit term and a term that provides a penalty against more complex model classes, that are those that extract more information from the data to update their prior information. This interpretation of the evidence allows us to find a correct trade-off between fitting accuracy and model complexity for a particular model class, and gives an intuitive understanding of why the computation of evidence automatically enforces a quantitative expression of the Principle of Model Parsimony or Ockham's razor [19].

4.2.2 Computation of the evidence of a model class

The calculation of the evidence given in Equation 4.9 is not a trivial task. In the case of globally identifiable model classes based on the data [68, 69], the posterior PDF in Equation 4.1 may be accurately approximated by a Gaussian distribution, and the evidence term can be obtained by Laplace's approximation [65, 68, 70]. In the more general case, where the posterior PDF may not be approximated by a Gaussian distribution, or if the amount of data is small [65] (as normally arises when dealing with fatigue damage modeling), stochastic simulation methods are required.

One straight-forward way to approximate the evidence is by considering the probability integral in Equation 4.9 as a mathematical expectation of the likelihood $p(\mathcal{D}|\boldsymbol{\theta}, \mathcal{M}_j)$ with respect to the prior $p(\boldsymbol{\theta}|\mathcal{M}_j)$. This approach leads to the direct Monte Carlo method as follows,

$$p(\mathcal{D}|\mathcal{M}_j) \approx \frac{1}{N_1} \sum_{k=1}^{N_1} p(\mathcal{D}|\boldsymbol{\theta}^{(k)}, \mathcal{M}_j) \tag{4.12}$$

where the $\boldsymbol{\theta}^{(k)}$ are N_1 samples drawn from the prior PDF. Although this calculation can be easily implemented, it results in a computationally inefficient method (large-variance estimator), since the region of high probability content of $p(\boldsymbol{\theta}|\mathcal{M}_j)$ is usually very different from the region where the likelihood $p(\mathcal{D}|\boldsymbol{\theta}, \mathcal{M}_j)$ has its largest values. To overcome this problem, some techniques for calculating the evidence based on samples from the posterior $p(\boldsymbol{\theta}|\mathcal{D}, \mathcal{M}_j)$ have received attention [71–76], although with known drawbacks of instability [73]. In this thesis, a recent stable technique based on an analytical approximation of the posterior is adopted [66]. The relevant details from [66] are presented here with special focus on the Metropolis-Hastings algorithm, which is the algorithm used in this thesis to generate samples from the posterior.

Let $K(\boldsymbol{\theta}|\boldsymbol{\theta}^*)$ be the transition PDF of any MCMC algorithm with stationary PDF $\pi(\boldsymbol{\theta}) = p(\boldsymbol{\theta}|\mathcal{D}, \mathcal{M}_j)$. The stationarity condition for the MCMC algorithm satisfies the following relation:

$$\pi(\boldsymbol{\theta}) = \int K(\boldsymbol{\theta}|\boldsymbol{\theta}^*)\pi(\boldsymbol{\theta}^*)d\boldsymbol{\theta}^* \tag{4.13}$$

A general choice of $K(\boldsymbol{\theta}|\boldsymbol{\theta}^*)$ that applies to many MCMC algorithms, can be defined as:

$$K(\boldsymbol{\theta}|\boldsymbol{\theta}^*) = T(\boldsymbol{\theta}|\boldsymbol{\theta}^*) + (1 - a(\boldsymbol{\theta}^*))\delta(\boldsymbol{\theta} - \boldsymbol{\theta}^*) \tag{4.14}$$

where $T(\boldsymbol{\theta}|\boldsymbol{\theta}^*)$ is a smooth function that does not contain delta functions and $a(\boldsymbol{\theta}^*)$ is the acceptance probability which must satisfy $a(\boldsymbol{\theta}^*) = \int T(\boldsymbol{\theta}|\boldsymbol{\theta}^*)d\boldsymbol{\theta} \leqslant 1$. By substituting Equation 4.14 into 4.13, an analytical approximation of the posterior results as follows:

$$\pi(\boldsymbol{\theta}) = p(\boldsymbol{\theta}|\mathcal{D}, \mathcal{M}_j) = \frac{\int T(\boldsymbol{\theta}|\boldsymbol{\theta}^*)\pi(\boldsymbol{\theta}^*)d\boldsymbol{\theta}^*}{a(\boldsymbol{\theta})} \approx \frac{1}{a(\boldsymbol{\theta})N_1}\sum_{k=1}^{N_1} T(\boldsymbol{\theta}|\boldsymbol{\theta}^{(k)}) \tag{4.15}$$

where the $\boldsymbol{\theta}^{(k)}$ are N_1 samples distributed according to the posterior. For the special case of the Metropolis-Hastings algorithm, $T(\boldsymbol{\theta}|\boldsymbol{\theta}^*) = r(\boldsymbol{\theta}|\boldsymbol{\theta}^*)q(\boldsymbol{\theta}|\boldsymbol{\theta}^*)$, where $q(\boldsymbol{\theta}|\boldsymbol{\theta}^*)$ is the proposal PDF, and $r(\boldsymbol{\theta}|\boldsymbol{\theta}^*)$ is given by:

$$r(\boldsymbol{\theta}|\boldsymbol{\theta}^*) = \min\left\{1, \frac{p(\mathcal{D}|\boldsymbol{\theta}, \mathcal{M}_j)p(\boldsymbol{\theta}|\mathcal{M}_j)q(\boldsymbol{\theta}^*|\boldsymbol{\theta})}{p(\mathcal{D}|\boldsymbol{\theta}^*, \mathcal{M}_j)p(\boldsymbol{\theta}^*|\mathcal{M}_j)q(\boldsymbol{\theta}|\boldsymbol{\theta}^*)}\right\} \tag{4.16}$$

Additionally, for this algorithm, the denominator in Equation 4.15 can be approximated by an estimator that uses samples from the proposal distribution as follows:

$$a(\boldsymbol{\theta}) = \int r(\tilde{\boldsymbol{\theta}}|\boldsymbol{\theta})q(\tilde{\boldsymbol{\theta}}|\boldsymbol{\theta})d\tilde{\boldsymbol{\theta}} \approx \frac{1}{N_2}\sum_{k=1}^{N_2} r(\tilde{\boldsymbol{\theta}}^{(k)}|\boldsymbol{\theta}) \tag{4.17}$$

where the $\tilde{\boldsymbol{\theta}}^{(k)}$ are N_2 samples from $q(\tilde{\boldsymbol{\theta}}|\boldsymbol{\theta})$, when $\boldsymbol{\theta}$ is fixed. Once the analytical approximation to the posterior in Equation 4.15 is set, then Equation 4.1 can be used to evaluate the evidence, as follows:

$$\log p(\mathcal{D}|\mathcal{M}_j) \approx \log p(\mathcal{D}|\boldsymbol{\theta}, \mathcal{M}_j) + \log p(\boldsymbol{\theta}|\mathcal{M}_j) - \underbrace{\log p(\boldsymbol{\theta}|\mathcal{D}, \mathcal{M}_j)}_{\text{Analytical approx.}} \tag{4.18}$$

The last expression is obtained by taking logarithms of Bayes' Theorem, explained earlier in Equation 4.1. Observe that, except for the posterior PDF $p(\boldsymbol{\theta}|\mathcal{D}, \mathcal{M}_j)$, whose information is based on samples, the rest of terms can be evaluated analytically for any $\boldsymbol{\theta} \in \boldsymbol{\Theta}$. Bayes' Theorem ensures that the last equation is valid for all $\boldsymbol{\theta} \in \boldsymbol{\Theta}$, so it is possible to use only one value for this parameter. However a more accurate estimate for the log-evidence can be obtained by averaging the results from Equation 4.18 using different values for $\boldsymbol{\theta}$ [16, 66]. The method is briefly summarized by the pseudocode given in Algorithm 3, which specifically focuses on the proposed implementation for the inverse problem based on the M-H algorithm.

Once the evidence is obtained, the data-fit term (AGF) in Equation 4.10 can also be estimated based on the N_1 samples from the posterior, and then the EIG term in this equation

Algorithm 3 Evidence computation by [66]

1.- Take $\left\{\boldsymbol{\theta}^{(k)}\right\}_{k=1}^{N_1}$ samples from $p(\boldsymbol{\theta}|\mathcal{D},\mathcal{M}_j)$
2.- Choose a model parameter vector $\boldsymbol{\theta} \in \boldsymbol{\Theta}$
for $k = 1$ to N_1 **do**
  3.- Evaluate $q(\boldsymbol{\theta}|\boldsymbol{\theta}^{(k)})$
  4.- Evaluate $r(\boldsymbol{\theta}|\boldsymbol{\theta}^{(k)})$ (Eq. 4.6)
end for
5.- Take $\left\{\boldsymbol{\theta}^{(\ell)}\right\}_{\ell=1}^{N_2}$ samples from $q(\cdot|\boldsymbol{\theta})$
for $\ell = 1$ to N_2 **do**
  6.-Evaluate $r(\boldsymbol{\theta}^{(\ell)}|\boldsymbol{\theta})$ (Eq. 4.6)
end for
7.- Obtain $p(\boldsymbol{\theta}|\mathcal{D},\mathcal{M}_j) \approx \frac{\frac{1}{N_1}\sum_{k=1}^{N_1} q(\boldsymbol{\theta}|\boldsymbol{\theta}^{(k)}) r(\boldsymbol{\theta}|\boldsymbol{\theta}^{(k)})}{\frac{1}{N_2}\sum_{\ell=1}^{N_2} r(\boldsymbol{\theta}^{(\ell)}|\boldsymbol{\theta})}$
8.- Evaluate $\log p(\mathcal{D}|\mathcal{M}_j)$ (Eq. 4.18)

can be approximated by:

$$\mathbb{E}\left[\log \frac{p(\boldsymbol{\theta}|\mathcal{D},\mathcal{M}_j)}{p(\boldsymbol{\theta}|\mathcal{M}_j)}\right] \approx \frac{1}{N_1}\sum_{k=1}^{N_1} \log p(\mathcal{D}|\boldsymbol{\theta}^{(k)},\mathcal{M}_j) - \log p(\mathcal{D}|\mathcal{M}_j) \tag{4.19}$$

4.2.3 Robust prediction and model class averaging

In addition to select the best ranked model class among candidates using Equation 4.8, a *robust* [22] stochastic forward model can be obtained as a outcome of the proposed Bayesian framework, by using the information encapsulated in the posterior PDF of model parameters for the chosen model class $\mathcal{M}_j$. It is accomplished by Total Probability Theorem, as:

$$p(\boldsymbol{x}|\mathcal{D},\mathcal{M}_j) = \int_{\boldsymbol{\Theta}} p(\boldsymbol{x}|\boldsymbol{\theta},\mathcal{M}_j) p(\boldsymbol{\theta}|\mathcal{D},\mathcal{M}_j) d\boldsymbol{\theta} \tag{4.20}$$

The last multidimensional integral can be readily estimated as a mathematical expectation of the stochastic forward model $p(\boldsymbol{x}|\boldsymbol{\theta},\mathcal{M}_j)$ with respect to the posterior $p(\boldsymbol{\theta}|\mathcal{D},\mathcal{M}_j)$, leading to the standard MC method:

$$p(\boldsymbol{x}|\mathcal{D},\mathcal{M}_j) = \frac{1}{N_s}\sum_{k=1}^{N_s} p(\boldsymbol{x}|\boldsymbol{\theta}^{(k)},\mathcal{M}_j) \tag{4.21}$$

where $\boldsymbol{\theta}^{(k)}$ are samples from the posterior PDF $p(\boldsymbol{\theta}|\mathcal{D},\mathcal{M}_j)$. In certain cases, more than one model class may have significant posterior probability in comparison with the rest of model classes in the set $\mathbf{M}$. Then, an *hyper-robust* [22, 77] stochastic forward model can be obtained by using the posterior information from the complete set of models classes in $\mathbf{M}$. To this end, Total Probability Theorem is applied at the model class level, as follows

$$p(\boldsymbol{x}|\mathcal{D},\mathbf{M}) = \sum_{j=1}^{N_m} p(\boldsymbol{x}|\mathcal{D},\mathcal{M}_j) p(\mathcal{M}_j|\mathcal{D},\mathbf{M}) \tag{4.22}$$

with $p(\boldsymbol{x}|\mathcal{D}, \mathcal{M}_j)$ the robust stochastic forward model presented before (Equation 9.4). Note that the last equation constitutes in fact a weighted model averaging formula [22, 77], where the "weights" are the posterior probabilities $p(\mathcal{M}_j|\mathcal{D}, \mathbf{M})$ of the candidate model classes in the set $\mathbf{M}$. Therefore, this formula provides a rational way to account for the overall posterior uncertainty related to both, model parameters and model choice, when predicting the system response.

Part II

THEORETICAL CONTRIBUTIONS

Probability theory is nothing but common sense reduced to calculation.

Laplace (1819)

5 Markov chain damage model

In this chapter, a new stochastic model for damage accumulation is proposed based on the theory of Markov chains. A novel parameterization is proposed to efficiently account for the non-stationarity of the damage process with a reduced set of model parameters. The model is based on solid statistical grounds and can be applied to a wide range of problems related with cumulative damage degradation. In Section 5.2, the mathematical definition and the modeling assumptions of the Markov chain model are presented. Section 5.3 provides the bases for the formulation of the likelihood function using the proposed Markov chain model. To demonstrate the suitability of the proposed approach, an illustrative example is provided in Section 5.4 in application to fatigue damage data for quasi-isotropic glass-fiber laminates.

5.1 Introduction and state-of-art

Throughout decades of investigation, numerous fatigue models have been proposed for composite materials and a large amount of data has been derived from experimental programs. Earlier reviews about fatigue modeling can be found in [5, 41, 43, 78, 79], while a more recent review for spectrum loadings is presented in Post *et al.* [80]. The majority of these models are deterministic approaches and hardly ever account for the large variability observed in data. Several studies have reported and quantified the uncertainty in fatigue damage modeling in composites, some of the most relevant can be found in [10, 11, 24–26, 39, 40, 81, 82]. Among them, cumulative damage models based on the theory of Markov chains [83] are found of major interest due to their versatility and efficiency to deal with complex cumulative damage processes.

A stochastic damage model based on Markov chains was first applied to fatigue modeling in composites by Rowatt and Spanos [10], as an extension of the pioneering work of Bogdanoff and Kozin [47]. By embedding this model within laminate plate theory, the evolutionary probability of failure was derived based on the *critical element* approach [84]. Ganesan [24] discussed the limitations of the Weibull model in favor of Markov chain models to describe the damage accumulation in composites, and provided an analytical expression for the evolutionary PDF of damage based on the Principle of Maximum Information Entropy [23, 85]. In Pappas *et al.* [86], the results of several fatigue tests for both organic and ceramic matrix composite materials were presented and an algorithmic description for the Markov chain calibration was provided. More recently, Wei *et al.* [11] propose a Markov chain model to describe the progression of fatigue damage from infrared thermography measurements. In that work, a novel procedure to generate stochastic *S-N* curves using previously calibrated Markov chain models is also provided. Later, Johnson *et al.* [87] extend the aforementioned work of Wei *et al.* to describe the accumulation of damage in single-lap shear joints for composites laminates. More applications of Markov chain damage models are found in [88–100], most of them for metals, and theoretical insight about them is found in [101, 102]. As a general comment, most of the proposed models are based on lifetime data instead of non-destructive damage data along the lifespan, which provides better information of the process being modeled.

In this chapter, a new Markov chain model is proposed to idealize the evolution of damage in composite materials. The key contribution is a new model parameterization for the Markov chains to efficiently account for the nonstationarity of the damage process with a reduced set of model parameters. This is achieved by introducing a spline transformation over an unit time scale as a generalization of the *time transformation-condensation method* first developed by Bogdanoff and Kozin [47]. However, the proposed modeling approach is subjected to modeling uncertainty that comes from the adoption of a particular model parameterization. This uncertainty may be explicitly accounted for using the Bayesian approach presented in Chapter 4. In this chapter, a methodology is provided to define several (Bayesian) model classes for the proposed Markov chain damage model, with special focus on the computation of the likelihood function for the subsequent Bayesian model class selection.

The proposed approach confers an efficient way to make inference for damage evolution using an optimum set of model parameters and, in general, to treat cumulative damage processes in composites in a robust sense.

5.2 Modeling approach

Fatigue damage in composites is revealed as a progressive or sudden degradation of the macro-scale mechanical properties from the virgin or no damage state up to the final failure of the material, as a consequence of growing fracture modes at the micro and meso-scale [2, 3]. For the proposed modeling approach, damage is defined as a scalar variable, $x_{ij}(n) \in$

$[0, 1]$ acting at a certain fatigue cycle n as a macro-scale relative stiffness reduction at one specific point, section or element:

$$x_{ij}(n) = \frac{A^*_{ij}(0) - A^*_{ij}(n)}{A^*_{ij}(0)}; \;\; n \in \mathbb{N} \tag{5.1}$$

where $A^*_{ij}(n)$ is the (i, j) component of the effective stiffness matrix $\mathbf{A}^*$ at the fatigue cycle n. This definition of damage has been adopted by several authors in the literature [103–107] and may be motivated from the linear elasticity theory coupled with the concept of *effective stress* from Continuum Damage Mechanics, under the hypothesis of *strain equivalence* [108, 109]. However, the methodology proposed in this chapter is general enough to be applied to other suitable definitions of damage [110, 111].

As stated by Equation 5.1, a complete characterization of damage accumulation would require the evaluation of x_{ij} for all independent components of the stiffness matrix. For simplicity but no loss of generality, the proposed modeling approach is presented here for a particular component selection (i, j), so the notation x_n is adopted instead of $x_{ij}(n)$. For this component, we define $\mathcal{X} = [0, 1] \subset \mathbb{R}$ as the set of possible values of damage x_n so for each n, $x_n \in \mathcal{X}$. The uncertainty in the fatigue damage process is modeled as a stochastic process $\{x_n, n \in \mathbb{N}\}$ taking values in $\mathcal{X}$, with the adoption of the following description items:

1. The damage space $\mathcal{X}$ is partitioned into a discrete set of events or *damage states* $\mathcal{X}_i$, where $i \in I = \{0, \ldots, s\} \subset \mathbb{N}$ such that $\mathcal{X} = \cup_{i=0}^{s} \mathcal{X}_i$. Each damage state $\mathcal{X}_i \subset \mathcal{X}$ is a subinterval represented by its center $\bar{x}^i_n = \frac{2i+1}{2s+2}$ such that $p^i_n \triangleq p(\bar{x}^i_n) \triangleq P\left[x_n \in \mathcal{X}_i\right] \geqslant 0$. The no-damage state corresponds to $i = 0$.
2. The evolution of fatigue damage is modeled by a Markov chain, so the *Markov property* [83] holds, which states that the future of the process is conditionally independent of the past states, given the present. In mathematical terms: $p(\bar{x}^k_{n+1}|\bar{x}^i_0, \ldots, \bar{x}^j_n) = p(\bar{x}^k_{n+1}|\bar{x}^j_n) \triangleq p^{j,k}_n; \;\; i, j, k \in I$.
3. We can define a duty cycle (DC) as an appropriate fixed amount of fatigue cycles in which damage is accumulated. By means of this, the fatigue cycles can be divided into a discrete set of regularly scheduled duty cycles: $\mathcal{T} = \{1, \ldots, n, \ldots, N\} \subset \mathbb{N}$.
4. During duty cycle n, damage may go from a certain damage state $\bar{x}^i_n$ to the next $\bar{x}^{i+1}_{n+1}$ with probability $p(\bar{x}^{i+1}_{n+1}|\bar{x}^i_n) = p^{i,i+1}_n$, and remain in the same state with a probability $p(\bar{x}^i_{n+1}|\bar{x}^i_n) = p^{i,i}_n = 1 - p^{i,i+1}_n$. Then damage is described by a *cumulative stochastic process*.
5. There exists an *absorbing state* $\mathcal{X}_s$ defined such that $p(\bar{x}^s_{n+1}|\bar{x}^s_n) = p^{s,s}_n = 1$. In other words, once the damage process has reached this state it is impossible to leave it. Consequently, the absorbing state corresponds to the final state of the process.
6. A set of K experimental sequences of fatigue damage from K nominally-identical specimens, $\mathcal{D} = \{Y^{(1)}_{n_N}, \ldots, Y^{(j)}_{n_N}, \ldots, Y^{(K)}_{n_N}\}$ where $Y^{(j)}_{n_N} = \{y^{(j)}_{n_1}, \ldots, y^{(j)}_{n_k}, \ldots, y^{(j)}_{n_N}\}$, is assumed to be available at a discrete set of regularly scheduled or even opportunistically staggered duty cycles $\mathcal{T}_\mathcal{D} = \{n_1, \ldots, n_k, \ldots, n_N\}$, such that $\mathcal{T}_\mathcal{D} \subseteq \mathcal{T}$.

5.2.1 *Model formulation*

The probability of damage to follow a certain sequence of states $i, j, \ldots, k, l \in I$ from an arbitrary duty cycle n to $m > n$ is, under the Markov hypothesis, given by:

$$\begin{aligned} p(\bar{x}_n^i, \bar{x}_{n+1}^j, \ldots, \bar{x}_{m-1}^k, \bar{x}_m^l) &= p(\bar{x}_n^i) p(\bar{x}_{n+1}^j | \bar{x}_n^i) \cdots p(\bar{x}_m^l | \bar{x}_{m-1}^k) \\ &= p_n^i p_n^{i,j} \cdots p_{m-1}^{k,l} \end{aligned} \tag{5.2}$$

By Total Probability Theorem, the probability of damage to be in a certain state l at DC m given it was in damage state i at DC n, can be obtained by summing over all possible damage paths from n to m as,

$$p_m^l = \sum_{i=0}^{s} \sum_{j=0}^{s} \cdots \sum_{k=0}^{s} p_n^i p_n^{i,j} \cdots p_{m-1}^{k,l} \tag{5.3}$$

From the last equation, the probability density function of damage discretized by the set of states $\{\bar{x}_m^0, \bar{x}_m^1 \ldots, \bar{x}_m^s\}$ with corresponding probabilities $\{p_m^0, p_m^1 \ldots, p_m^s\}$ can be written in a formal mathematical fashion using the Dirac delta function as:

$$p(x_m) = \sum_{i=0}^{s} p_m^i \cdot \delta(x_m - \bar{x}_m^i); \;\; i \in I \tag{5.4}$$

The PDF $p(x_m)$ in the last equation denotes in practice a discrete probability mass function (PMF) of damage at DC m, that can be easily expressed by the row vector $\mathbf{p}_m = \left(p_m^0, p_m^1, \ldots, p_m^s\right)$. Here, we use bold $\mathbf{p}_m$ for vectors to distinguish from the PDF $p(x_m)$. By recognizing that Equation 5.3 can be obtained as a matrix multiplication, the PMF of damage at DC $m = n + 1$ can be written as:

$$\mathbf{p}_{n+1} = \mathbf{p}_n \cdot \mathbf{P}_n \tag{5.5}$$

with $\mathbf{P}_n$ the "one-step" *probability transition matrix* for duty cycle n. For general m, the probability mass function of damage at DC $m > n$ corresponding to Equation 5.3 can be written as:

$$\mathbf{p}_m = \mathbf{p}_n \cdot \prod_{j=n}^{m-1} \mathbf{P}_j; \;\; j \in \mathbb{N} \tag{5.6}$$

where $\{\mathbf{P}_j\}_{j=n}^{m-1}$ is the set of all probability transition matrices from duty cycle n to $m-1$.

For a certain DC n, the matrix $\mathbf{P}_n$ stores in its $(i+1, j+1)$ element the conditional probability of transition $p(\bar{x}_{n+1}^j | \bar{x}_n^i) = p_n^{i,j}$ from state $\bar{x}_n^i$ to $\bar{x}_{n+1}^j$ in one DC. Modeling assumptions (4) and (5) restrict the structure of $\mathbf{P}_n$ to a bi-diagonal $(s+1) \times (s+1)$ matrix with $p_n^{s,s} = 1$, then:

$$\mathbf{P}_n = \begin{pmatrix} p_n^{0,0} & p_n^{0,1} & & & \\ & p_n^{1,1} & p_n^{1,2} & & \\ & & \ddots & \ddots & \\ & & & p_n^{s-1,s-1} & p_n^{s-1,s} \\ & & & & 1 \end{pmatrix} \tag{5.7}$$

where

$$p_n^{i,i} + p_n^{i,i+1} = 1; \;\; i \in \{0, \ldots, s-1\} \tag{5.8}$$

If the transition probabilities $p_n^{i,j}$ do not depend on the duty cycle of transition n, then $\mathbf{P}_n = \mathbf{P} \;\; \forall n \in \mathbb{N}$ and the process is termed as *conditionally stationary* or simply *stationary*. Otherwise, in the more general case (assumed here) where the transition probabilities may change with time, the process is named *conditionally non-stationary* or *non-stationary*.

As stated by Equation 5.6, the cumulative damage process described by a Markov chain model can be characterized by the family of transition matrices $\{\mathbf{P}_j\}_{j=n}^{m-1}$ and the starting probability distribution of damage $\mathbf{p}_n$. When the fatigue process starts from the no-damage state then $p_n^0 = 1$, and the probability distribution of the starting damage is known, i.e. $\mathbf{p}_n = [1, 0, \ldots, 0]$. In this case, the set of matrices $\{\mathbf{P}_j\}_{j=n}^{m-1}$ is sufficient to completely characterize the process from DC n to m requiring $s \cdot (m-n)$ parameters to be determined. More details about Markov chain models of cumulative damage are found in [47].

5.2.2 *Parameterization for non-stationarity*

For the purpose of model inference from data, a parameterization strategy is proposed here to avoid a high dimensional problem for characterizing the non-stationary Markov chain model described above. The strategy consists of adopting the same value for the one-step probability of transition for every duty cycle n and for every state $i \in \{0, \ldots, s-1\}$, except for the absorbing state in which $p_n^{s,s} = 1$. This allows us to have a single probability transition matrix, now called $\mathbf{Q}$, that remains invariant during the process, defined as:

$$\mathbf{Q} = \begin{pmatrix} 1-p & p & & & \\ & 1-p & p & & \\ & & \ddots & \ddots & \\ & & & 1-p & p \\ & & & & 1 \end{pmatrix} \tag{5.9}$$

To account for the non-stationarity, an *ad-hoc* modification of the "natural" time scale n into a transformed time scale $n' = g'(n)$ is introduced such that any probability transition matrix from step n to step m can be calculated as $\mathbf{Q}^{g'(m)-g'(n)}$, satisfying:

$$\prod_{j=n}^{m-1} \mathbf{P}_j = \mathbf{Q}^{g'(m)-g'(n)}; \;\; m, n \in \mathbb{N} \tag{5.10}$$

where $g'(n)$ is a nonlinear function of n, that is given below. This procedure is based on the *time transformation-condensation method* (TTCM) first proposed by Bogdanoff and Kozin [47] by using undefined polynomials. Instead, we express $g'(n)$ in terms of a continuous monotonic function $g(\theta) : [0, 1] \to [0, 1]$ as follows:

$$g'(n) = N \cdot \left(g(n/N)\right) \tag{5.11}$$

where function g is suitably defined as an interpolating monotonic cubic spline [112] for a given set of $j \in \mathbb{N}$ interpolation points $\{\theta_1, \theta_1', \ldots, \theta_j, \theta_j'\}$, and N is a sufficiently large amount of duty cycles along which damage is completely developed. See Figure 5.1 for illustration. Here, N is chosen as the maximum duty cycle of the observed sequences of damage. Notice that to maintain the matrix structure of the model, the exponent $g'(m) - g'(n)$ in Equation 5.10 must be an integer after the transformation, to which an approximation to the nearest integer is applied; otherwise a condensation technique as proposed in [47] must be considered.

The transformation in Equation 5.11 distorts the natural time scale by using a nonlinear mapping over the unit interval, which has the double benefit over the TTCM of (1) having a bounded and defined searching space, and (2) keeping a fixed number of parameters. Each interpolation point is defined by its cartesian coordinates (θ_j, θ_j') in the unit time scale. Figure 5.1 illustrates this concept.

The coordinates of the overall interpolation points together with the probability of transition p, define the set of parameters $\boldsymbol{\theta} = \{\theta_1, \theta_1', \ldots, \theta_j, \theta_j', p\}$ that allows for a complete description of the proposed Markov chain damage model. Thus, this model can be reformulated by replacing Equation 5.6 with:

$$\mathbf{p}_m = \mathbf{p}_n \cdot \mathbf{Q}^{g'(m)-g'(n)} \tag{5.12}$$

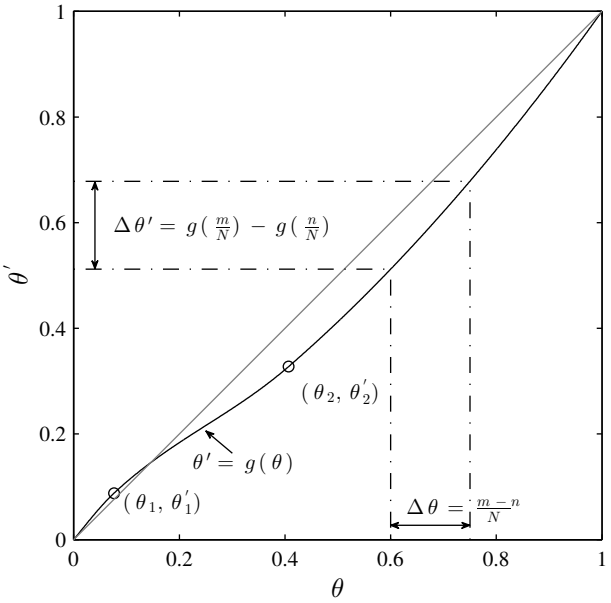

Figure 5.1: *Spline transformation $\theta' = g(\theta)$ of the unit time scale θ controlled by the set of interpolation points $\{(0,0), (\theta_1, \theta_1'), \ldots (\theta_j, \theta_j'), (1,1)\}$; $\theta_j > \theta_{j-1}$ and $\theta_j' > \theta_{j-1}'$; $j > 1$. The grey line would correspond to a stationary process in which the time transformation does not take place, so $\theta' = \theta$; instead the darker curve corresponds to a non-stationary damage process.*

5.2.3 *Model class definition*

According to the Markov chain parameterization detailed in Section 5.2.2, the model proposed is prescribed by the definition of the set of model parameters $\boldsymbol{\theta} = \{\theta_1, \theta_1^{'}, \ldots, \theta_j, \theta_j^{'}, p\}$. Then, we can denote by $\mathcal{M}_j$ the j-th Bayesian model class [22] that incorporates the Markov chain forward model with $\boldsymbol{\theta}_\mathbf{j} = \{\theta_1, \theta_1^{'}, \ldots, \theta_j, \theta_j^{'}, p\} \in \boldsymbol{\Theta}_\mathbf{j}$ as model parameters along with the prior PDF $p(\boldsymbol{\theta}_\mathbf{j}|\mathcal{M}_j)$, that gives the initial relative plausibility of each value of $\boldsymbol{\theta}_\mathbf{j}$ before the information from measurements is incorporated. Observe that the parameter vector $\boldsymbol{\theta}$ depends on the model class $\mathcal{M}_j$ even thought it is not reflected with the subscript j, since the conditioning on $\mathcal{M}_j$ is sufficient to indicate which parameter vector is being considered.

Based on this definition, a discrete set of possible candidate model classes $\mathbf{M} = \{\mathcal{M}_j,\ j : 1, 2, \ldots, N_M\}$, $N_M \in \mathbb{N}$, can be obtained by adding the coordinates of j interpolation points for the definition of model class $\mathcal{M}_j$. See Table 5.1 for a clarification of the parameterization of the set of model classes $\mathbf{M}$.

Model Class	Parameters							
$\mathcal{M}_1$	θ_1	$\theta_1^{'}$	-	-	-	-	-	p
$\mathcal{M}_2$	θ_1	$\theta_1^{'}$	θ_2	$\theta_2^{'}$	-	-	-	p
$\vdots$					$\ddots$			
$\mathcal{M}_{N_M}$	θ_1	$\theta_1^{'}$	θ_2	$\theta_2^{'}$	$\ldots$	θ_{N_M}	$\theta_{N_M}^{'}$	p

Table 5.1: *Parameterization scheme for the set of N_m Markov chain model classes*

5.3 Formulation of likelihood function

The Bayesian approach for inverse problem presented in Section 4.1 allows to adequately treat uncertainties for both, model parameters and model classes, based on the Cox-Jaynes [19, 51, 52] interpretation of probability that is adopted in this thesis. In this approach, the *likelihood function* $p(\mathcal{D}|\boldsymbol{\theta}, \mathcal{M}_j)$ is a fundamental probability model for both problems, model parameter estimation and model class selection, which express the information of idealized relationship between data $\mathcal{D}$ and model parameters $\boldsymbol{\theta}$ in a model class $\mathcal{M}_j$. In other words, it provides a meassure of how good the model is in explaining the data.

In general, data $\mathcal{D}$ may consist of a set of K experimental sequences of fatigue-based damage from K nominally-identical specimens, as defined in Section 5.2, item 6. A correspondence between an observed damage sequence $Y_{n_N}^{(k)} = \{y_{n_1}^{(k)}, y_{n_2}^{(k)}, \ldots, y_{n_N}^{(k)}\}$ and the latent sequence of damage states $\{\bar{x}_{n_1}^{i,(k)}, \bar{x}_{n_2}^{j,(k)}, \ldots, \bar{x}_{n_N}^{l,(k)}\}$, with $i, j \ldots, l \in I$, can be established based on the defined set $\{\bar{x}_n^0, \bar{x}_n^1, \ldots, \bar{x}_n^s\}$ in Section 5.2.1, by taking $\bar{x}_n^{i,(k)}$ when $y_n^{(k)} \in \mathcal{X}_i$. See Figure 5.2 for further details. Then, the likelihood function can be formulated as follows: First, the probability to observe a sequence of damage states $\{\bar{x}_{n_1}^{i,(k)}, \bar{x}_{n_2}^{j,(k)}, \ldots, \bar{x}_{n_N}^{l,(k)}\}$ in the k-th specimen at the given set of duty cycles $\mathcal{T}_\mathcal{D} = \{n_1, n_{2,} \ldots, n_N\}$, $\mathcal{T}_\mathcal{D} \subseteq \mathcal{T}$, is modeled as a

Markov chain parameterized by $\boldsymbol{\theta}$ in the model class $\mathcal{M}_j$. By means of the Markov property, this probability can be obtained as

$$p(\bar{x}^i_{n_1}, \bar{x}^j_{n_2}, \ldots, \bar{x}^l_{n_N}|\boldsymbol{\theta}) = p(\bar{x}^i_{n_1}|\boldsymbol{\theta})p(\bar{x}^j_{n_2}|\bar{x}^i_{n_1}, \boldsymbol{\theta}) \cdots p(\bar{x}^l_{n_N}|\bar{x}^k_{n_{N-1}}, \boldsymbol{\theta}) \tag{5.13}$$

where the superscript (k) denoting the k-th specimen is not used in the last equation, and furthermore, the conditioning on the model class $\mathcal{M}_j$ is omitted for simper notation. The likelihood function is then the product of probabilities as in Equation 5.13 over all K specimen test sequences.

The structure of this likelihood function can be clarified by introducing the matrix $\mathbf{f}_{n_h}$, called the *transition count matrix*, that accounts for the number of observed transitions $\bar{x}^i_{n_h} \rightarrow \bar{x}^j_{n_{h+1}}$, i.e., the number of times for which the damage reaches the state j at DC n_{h+1}, given that it previously was in state i at DC n_h [113, 114]. In mathematical terms, the (i, j) element of this matrix can be expressed as:

$$f^{i,j}_{n_h} = \sum_{k=1}^{K} \sum_{i^*, j^*=0}^{s} \mathbb{I}\left(\bar{x}^{i^*=i,(k)}_{n_h}, \bar{x}^{j^*=j,(k)}_{n_{h+1}}\right) \tag{5.14}$$

with $\bar{x}^{i(k)}_{n_h}$ the damage state i at duty cycle n_h, for the k-th specimen. In the last expression, $\mathbb{I}\left(\bar{x}^{i^*=i,(k)}_{n_h}, \bar{x}^{j^*=j,(k)}_{n_{h+1}}\right)$ is an indicator function which assigns the value of 1 when the transition $\bar{x}^i_{n_h} \rightarrow \bar{x}^j_{n_{h+1}}$ holds, and 0 otherwise. In Figure 5.2, a detailed example about the construction of $\mathbf{f}_{n_h}$ is provided considering two hypothetical curves of stiffness reduction. In this figure, damage states are represented on the vertical axis while the set of DC are represented on the horizontal axis. Observe that a transition between states 1 (for $n = n_3$) and 3 (for $n = n_4$) occurs in specimen 1, so $f^{1,3}_{n=n_4} = 1$. Notice that in specimen 2, damage remains in the same state for $n = n_3$ and $n = n_4$, so $f^{1,1}_{n=n_4} = 1$. See the example transition count matrix $\mathbf{f}_{n=n_4}$ in the upper-left side of this figure.

The likelihood function can then be formulated as:

$$p(\mathcal{D}|\boldsymbol{\theta}, \mathcal{M}_j) = p(\bar{x}^i_{n_1}|\boldsymbol{\theta}) \prod_{n_h=n_1}^{n_{N-1}} \prod_{i,j=0}^{s} \left(p(\bar{x}^j_{n_{h+1}}|\bar{x}^i_{n_h}, \boldsymbol{\theta})\right)^{f^{i,j}_{n_h}} \tag{5.15}$$

where $p(\bar{x}^j_{n_{h+1}}|\bar{x}^i_{n_h}, \boldsymbol{\theta})$ is the probability transition between damage states i and j at DC n_h and n_{h+1} respectively, corresponding to the $(i+1, j+1)$ element of the matrix $\mathbf{Q}^{g'(n_{h+1})-g'(n_h)}$, which is obtained by the model parameterization $\boldsymbol{\theta} \in \mathcal{M}_j$.

Finally, it is remarked that in constructing the likelihood function in Equation 5.15, any measurement error when assigning the i-th damage state based on the observed value $y_n \in \mathcal{X}_i$ at duty cycle n is subsumed by the uncertainty in the damage states described by the Markov chain model, and so it is not explicitly modeled.

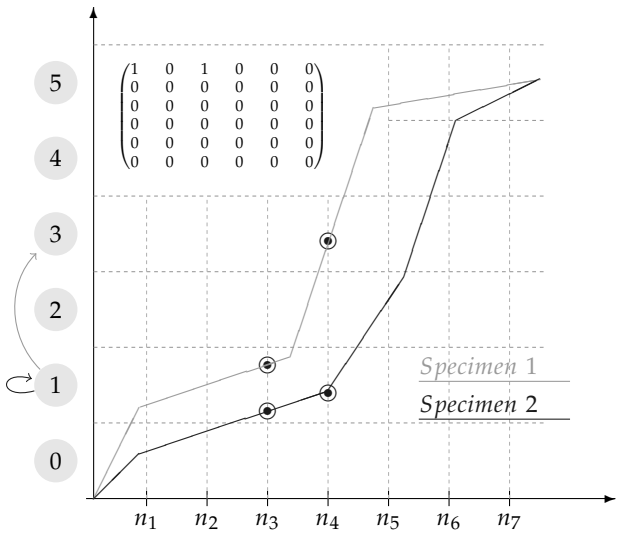

Figure 5.2: *Toy example for obtaining the transition count matrix when a Markov chain with 6-states is adopted with data from two specimens.*

5.4 Illustrative example

To demonstrate the suitability of the stochastic model proposed in this chapter, an illustrative example is provided in this section using experimental damage data for GFRP quasi-isotropic laminates, which corresponds to Dataset 1 in Chapter 8 (Section 8.1). For this example, a set of five parameters $\boldsymbol{\theta} = \{\theta_1, \theta_1', \theta_2, \theta_2', p\}$ is used for the Markov chain parameterization, which involves two anchor points to define the spline function that distorts the natural time scale (see Figure 5.1), as explained in Section 5.2.2. Some pilot tests revealed that the most suitable value for duty cycle DC for this dataset is 500 load cycles with a Markov chain assembly of $s = 30$ states. Hence, the total number of duty cycles is $N = {}^{213900}/_{500} = 428$. To estimate an optimal value for model parameters, a simple approach of matching the model-based cumulative distribution functions (CDFs) and empirical CDFs is proposed, that is sufficient to demonstrate the suitability of the fatigue model proposed. It is summarized below.

Let $F(y_{n_h})$ be the empirical CDF of damage at a certain duty cycle $n_h \in \mathcal{T}_\mathcal{D}$, defined as

$$F(y_{n_h}) = \frac{1}{K} \sum_{j=1}^{K} \mathbb{I}_{[0, y_{n_h}]}(y_{n_h}^{(j)}), \quad y_{n_h}^{(j)} \in \mathcal{D} \tag{5.16}$$

where K is the number of experimental damage sequences in $\mathcal{D}$, and $\mathbb{I}_{[0, y_{n_h}]}(y)$ is the indicator function for the interval $[0, y_{n_h}]$. Let $F(x_{n_h}|\boldsymbol{\theta})$ be the CDF of damage at the same duty cycle n_h, obtained by the Markov chain model parameterized by $\boldsymbol{\theta}$:

$$F(x_{n_h}|\boldsymbol{\theta}) = \sum_{i=0}^{s} \sum_{j=0}^{i} p_{n_h}^{j} \cdot \delta(x_{n_h} - \bar{x}_{n_h}^{i}), \quad x_{n_h} \in \mathcal{X}, \;\; i, j \in I \tag{5.17}$$

Then a reasonable estimator of $\boldsymbol{\theta}$ is a value $\boldsymbol{\theta}^* \in \boldsymbol{\Theta} \subseteq \mathbb{R}^d$ that minimizes any function $\mathcal{C}$ of the distance between (5.16) and (5.17) for every duty cycle at which damage measurements

are available. Mathematically:

$$\boldsymbol{\theta}^* = \arg\min_{\boldsymbol{\theta}\in\boldsymbol{\Theta}} \mathcal{C}\left(d\Big(F(y_{n_h}), F(x_{n_h}|\boldsymbol{\theta})\Big)\right);\ \ \forall n_h \in \mathcal{T}_{\mathcal{D}} \tag{5.18}$$

A distance between $F(y_{n_h})$ and $F(x_{n_h}|\boldsymbol{\theta})$ for a particular DC $n_h \in \mathcal{T}_{\mathcal{D}}$, can be defined as [115, 116]:

$$d\Big(F(y_{n_h}), F(x_{n_h}|\boldsymbol{\theta})\Big) = \int_{\mathcal{X}} \Big(F(y_{n_h}) - F(x_{n_h}|\boldsymbol{\theta})\Big)^2 \,\mathrm{d}x_{n_h} \tag{5.19}$$

For each n_h, the distance defined in Equation 5.19 can be stored within a *residual vector* $\mathbf{r}$:

$$\mathbf{r}(\boldsymbol{\theta}) = \Big[d\Big(F(y_{n_h}), F(x_{n_h}|\boldsymbol{\theta})\Big)\Big]_{h=1}^{N} \tag{5.20}$$

Finally the function $\mathcal{C} : \mathbb{R}^N \to \mathbb{R}$, named the *cost functional*, can be defined as the ℓ_2 norm of the residual vector $\mathbf{r}$:

$$\mathcal{C}(\boldsymbol{\theta}) = \|\mathbf{r}(\boldsymbol{\theta})\|_2 \tag{5.21}$$

The inference problem is then defined as the problem of finding $\boldsymbol{\theta}^* \in \boldsymbol{\Theta}$ that satisfies:

$$\boldsymbol{\theta}^* = \arg\min_{\boldsymbol{\theta}\in\boldsymbol{\Theta}} \mathcal{C}(\boldsymbol{\theta}) \tag{5.22}$$

The minimization problem defined in Equation 5.22 can be numerically solved using genetic algorithms (GA) [117, 118]. The optimal model parameters found by GA for the experimental dataset used in this example are $\boldsymbol{\theta}^* = \{0.104, 0.082, 0.226, 0.298, 0.884\}$. From these parameters, CDFs of damage are obtained at the set $\mathcal{T}_{\mathcal{D}}$ of monitored duty cycles and compared with the corresponding experimental CDFs in Figure 5.3.

In addition, a set of $T = 1000$ simulated Markov chains of damage $\{X_{n_N}^{(1)}, \ldots, X_{n_N}^{(t)}, \ldots, X_{n_N}^{(T)}\}$ has been drawn using the Markov chain model specified by the set of parameters $\boldsymbol{\theta}^*$. To this end, the standard procedure of conditional sampling [119] is adopted: first sample using the initial state probability distribution, then successively sample states from the transition probability distributions (conditional on the previous state sample). Mathematically, each simulated sequence is defined as $X_{n_N}^{(t)} = \{\bar{x}_0^i, \bar{x}_1^j|\bar{x}_0^i, \cdots, \bar{x}_n^l|\bar{x}_{n-1}^k, \cdots, \bar{x}_{n_N}^s|\bar{x}_{n_{N-1}}^r\}$, where the conditional sample $\bar{x}_n^l|\bar{x}_{n-1}^k$ is obtained by sampling from the k-th row of the probability transition matrix $\mathbf{P}_{n-1}$, so:

$$\bar{x}_n^l|\bar{x}_{n-1}^k \sim \mathbf{P}_{n-1}(k,:) \tag{5.23}$$

Finally, the simulation of the calibrated Markov chain model is represented in Figure 5.4 where it is compared with the experimental damage realizations from the dataset $\mathcal{D}$.

The performance of the model classes presented in this chapter is investigated in Chapter 9 using damage data for both, CFRP and GFRP laminates.

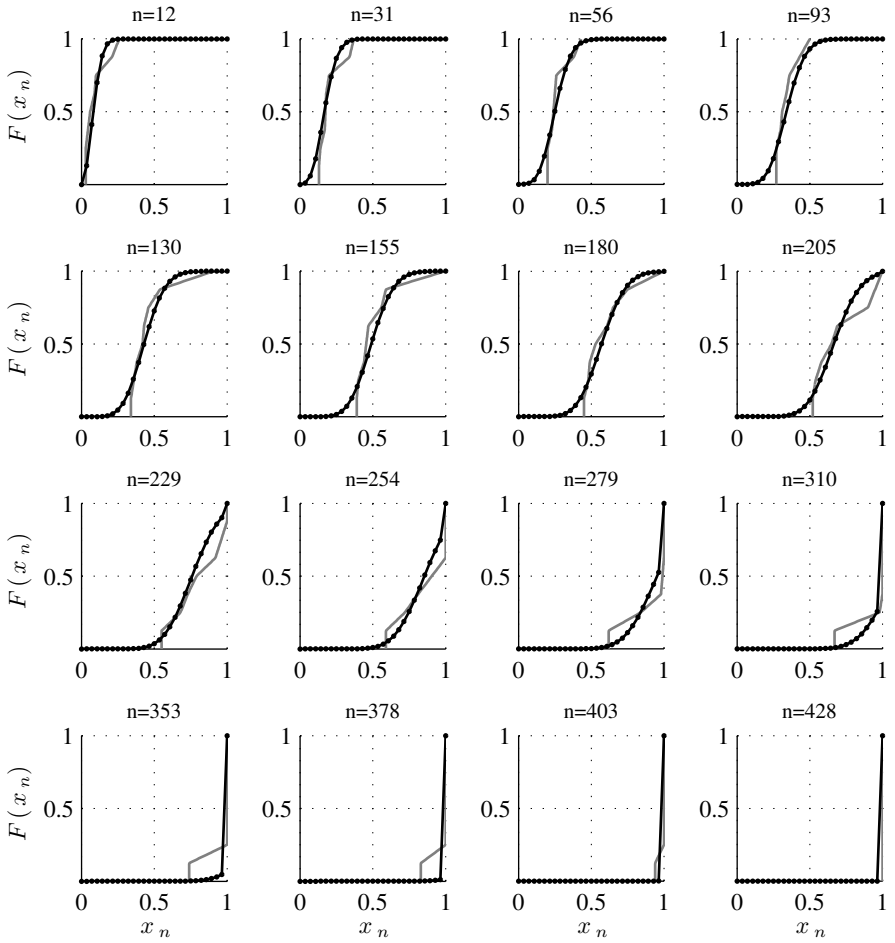

Figure 5.3: *CDFs of damage obtained by the the Markov chain model for θ^* at a increasing series of duty cycles in comparison with the corresponding experimental CDFs obtained from Dataset 1. Dotted black line: Modeled CDFs of damage. Solid grey line: experimental CDFs of damage.*

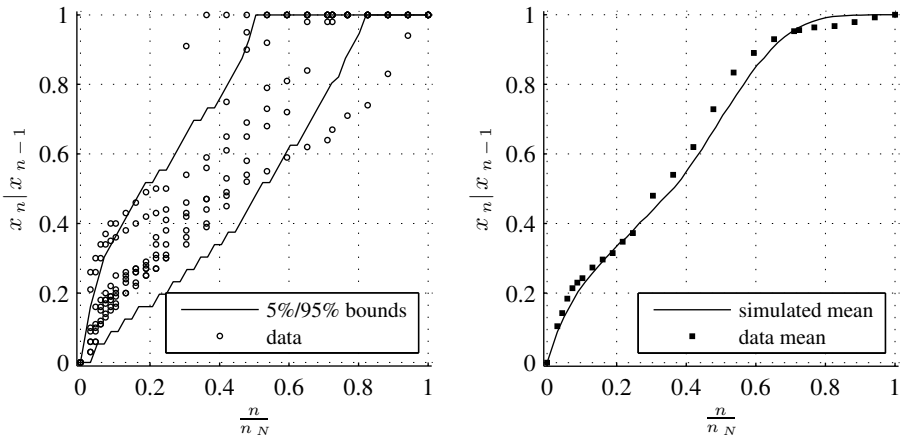

Figure 5.4: *Simulation of the Markov chain damage model by conditional sampling. Left side, the 5% and 95% bounds together with the experimental sequences. Right part, the mean of the simulated damage sequences $\{X_{n_N}^{(1)}, X_{n_N}^{(2)}, \ldots, X_{n_N}^{(1000)}\}$ in comparison with the mean of experimental sequences. The mean of simulations is in good agreement with data mean. Also the 0.05/0.95 simulated bounds cover well the experimental realizations, except some outliers.*

All truths are easy to understand once they are discovered; the point is to discover them.

Galileo Galilei (1564–1642)

6

Physics-based modeling framework

This chapter aims at providing the mathematical basis to quantify the modeling uncertainty of a set of damage-mechanics models through a full Bayesian approach that simultaneously estimates the plausibility of each individual model class along with the uncertainty of the underlying model parameters. In Section 6.2, the proposed physics-based modeling approach is presented. The methodology for the definition of the candidate model classes is provided in Section 4.1.1. In Section 6.4, the formulation of the likelihood function is presented for the proposed damage mechanics models. An scheme of implementation using a Graphics Processing Unit is also provided. Finally, in Section 6.5, a methodology for model parameterization using Global Sensitivity Analysis is presented.

6.1 Introduction and state of art

Fatigue in composites is governed by a complex multi-scale damage process driven by several internal fracture events that leads to the alteration of the macro-scale mechanical properties of the material. The inherent complexity of this process implies uncertainty in modeling, that not only includes the uncertainty in model parameters but also the uncertainty arising from the choice of a particular *model class* (e.g., the parameterized mathematical structure of the model for predicting damage behavior).

In the literature, there is an increasing number of researchers that have started investigating the role of uncertainties in modeling the behavior of composites materials. For example, Sriramula and Chryssanthopoulos [120] reviewed and discussed different stochastic modeling approaches for analyzing uncertainties at the ply-level, coupon-level and component-level. Uncertainty quantification methods have also been used to assess the uncertainty in

the material properties [121, 122] and extended to study a variety of phenomena such as elastic response [123, 124], aeroelastic behavior [125, 126], and failure [127, 128], among others. In particular, the Bayesian approach has been successfully applied for uncertainty quantification in fatigue, albeit in the context of metals [17, 32–38]. For example, Cross *et al.* [33] and Sankararaman *et al.* [34] used Bayesian inference to estimate parameters underlying crack growth behavior. Sankararaman *et al.* [36] used dynamic Bayesian networks for model parameter estimation and calculated Bayes factors to quantify model uncertainty. However, the application of Bayesian methods remains very limited in the composites fatigue literature, precisely where the benefits of the Bayesian approach can be fully exploited due to the inherent complexity of the fatigue process and the existence of multiple competing models.

In this chapter, a set of five model classes pertaining to three families of damage mechanics models [7] (i.e., shear-lag, variational and crack opening displacement (COD)) is proposed to represent the relation between the macro-scale stiffness reduction and the micro-scale damage, due to matrix-cracks. Damage mechanics models are preferred over other analytical approaches (e.g. continuum damage mechanics models or synergistic damage mechanics models [7]) due to their efficiency in relation to the assumptions adopted, and for being well connected with the physics of the underlying damage process. Moreover, these models have the ability to adapt to different systems (specimen, materials, loading conditions, etc.) without much training and furthermore, they can incorporate structural health monitoring data.

Each candidate damage mechanics model is subsequently embedded into the *modified Paris' law* [48], that is used here to represent the propagation forward in time of the matrix-cracks density. This two-level modeling approach results in a large number of uncertain parameters, leading to a computationally-intensive inference problem. To reduce the dimensionality of the problem without significantly altering the underlying uncertainty in the model output, a model input tuning is carried out by means of a Global Sensitivity Analysis (GSA) [49]. This allows to determine in advance the subset of inputs that are most "sensitive" to the model output uncertainty, which are further used as model parameters.

The results of the assessment are provided in Chapter 10 in application to data for micro-cracks density and stiffness loss for carbon-epoxy cross-ply laminates (Dataset 8.2, Section 8.2).

6.2 Candidate damage mechanics models

Typically, fatigue damage is perceived as a progressive or sudden change of the macro-scale mechanical properties, such as stiffness or strength, as a consequence of several fracture modes (matrix cracking, delamination, etc.) that evolve at the micro-scale along the lifespan of the structure [3]. For the modeling approach proposed in this chapter, longitudinal stiffness loss is chosen as the macro-scale damage variable. In contrast to the strength, the stiffness loss can be measured through non-destructive methods during operation, which is of key importance for the model-updating approach proposed. At the micro-scale level,

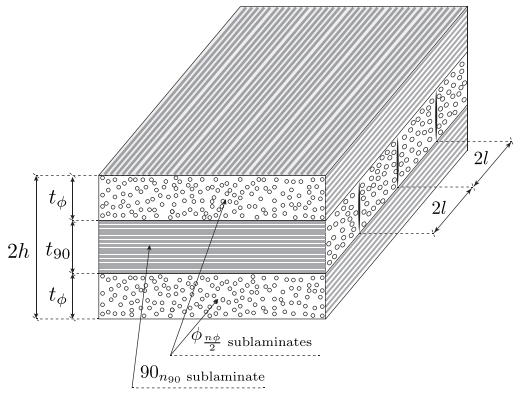

Figure 6.1: *Illustration for internal damage in* $\left[\phi_{\frac{n_\phi}{2}}/90_{n_{90}}/\phi_{\frac{n_\phi}{2}}\right]$ *laminate along with basic geometrical parameters.*

matrix cracking [129] is hypothesized as the dominant damage mode for the early stage of the fatigue process. Matrix cracks usually initiate from internal defects in 90° plies (transverse to the loading direction) during first loading cycles, and grow rapidly along fibers direction spanning the entire width of the specimen [129]. Continued loading leads to formation of new cracks between the already formed cracks thereby progressively increasing the matrix-cracks density of the ply until saturation. This saturated state, usually termed as *characteristic damage state* [2], is long recognized as a precursor of more severe fracture modes in adjacent plies, such as delamination and fiber breakage [130, 131], which may subsequently lead to the final failure of the laminate. In addition, matrix micro-cracking may itself constitute failure of the design when micro-cracks induced degradation in properties exceeds the predefined threshold.

To accurately represent the relation between this micro-scale damage mode and its macro-scale manifestation, several families of *micro-damage mechanics* models have been proposed in the literature [7]. These models, that are grounded on first principles of admissible ply stress fields in presence of damage, can be roughly classified into 1) computational methods, 2) semi-analytical methods and 3) analytical methods. Among them, computational and semi-analytical methods have been shown to be promising approaches, however they are computationally intensive; hence a large number of repeated evaluations in a simulation-based inference procedure is computationally prohibitive. Therefore, the set of analytical models is chosen here to address the relationship between stiffness loss and micro-crack density. Three types of analytical models are considered: *shear-lag* models [9, 132], *variational* models [133], and *crack opening displacement* based models [134, 135].

Shear-lag models use one-dimensional approximations of the stress field to derive expressions for stiffness properties of the cracked laminate. They assume basically that, in the position of matrix cracks, axial load is transferred to uncracked plies by the axial shear stresses. These models have received the most attention in the literature and thus, a vast number of modifications and extensions of that analysis can be found. However, as stated

by Talreja and Singh [7], all the one-dimensional shear-lag models are virtually identical, except for the choice of the *shear-lag parameter*, as explained later in this section.

Variational models are based on a two-dimensional approximation of the equilibrium stress field, that in contrast to shear-lag analysis, is obtained from the Principle of Minimum Complementary Energy [136, 137].

Finally, COD-based models use a 3-D homogenization procedure derived from the study of the average crack-face opening displacement of a single matrix crack as a function of the applied load, that can be calculated either analytically [134] or numerically [135, 138, 139]. While shear-lag and variational models are applicable mostly to cross-ply laminates (i.e. those with stacking sequence $\left[0_{\frac{n_0}{2}}/90_{n_{90}}/0_{\frac{n_0}{2}}\right]$, where $n_{0,90}$ = total number of plies at 0° and 90°, respectively), COD-based models are applicable to general laminates with an arbitrary distribution of matrix cracks. The reader is referred to the recent work of Talreja and Singh [7] for a detailed overview of these models, but for the sake of clarity, the key formulation is appropriately reproduced here with a uniform notation.

6.2.1 Shear-lag and variational models

Following the unifying formulation by Joffe and Varna [140], the effective longitudinal Young's modulus E_x^* can be calculated in $\left[\phi_{\frac{n_\phi}{2}}/90_{n_{90}}/\phi_{\frac{n_\phi}{2}}\right]$ laminates (where $\phi \in [-90^\circ, 90^\circ]$) as a function of the crack-spacing in 90° layers for both shear-lag and variational models as follows:

$$E_x^* = \frac{E_{x,0}}{1 + a\frac{1}{2\bar{l}}R(\bar{l})} \tag{6.1}$$

In the last equation, $E_{x,0}$ is the longitudinal Young's modulus, $\bar{l} = \frac{l}{t_{90}}$ is the half crack-spacing normalized with the 90° sub-laminate thickness, $R(\bar{l})$ is the average stress perturbation function, and a is a known function of laminate properties (defined in Appendix A). It should be noted that matrix-cracks density is usually defined as $\rho = \frac{1}{2l}$, so that the normalized half crack-spacing $\bar{l}$ can be expressed as a function of ρ as $\bar{l} = \frac{1}{2\rho t_{90}}$. The function $R(\bar{l})$ takes different expressions depending on the approach considered:

$$R(\bar{l}) = \frac{2}{\xi}\tanh(\xi\bar{l}) \qquad \text{(Shear-Lag)} \tag{6.2a}$$

$$R(\bar{l}) = \frac{4\alpha_1\alpha_2}{\alpha_1^2+\alpha_2^2}\frac{\cosh(2\alpha_1\bar{l}) - \cos(2\alpha_2\bar{l})}{\alpha_2\sinh(2\alpha_1\bar{l}) + \alpha_1\sin(2\alpha_2\bar{l})} \qquad \text{(Variational)} \tag{6.2b}$$

where ξ is the shear-lag parameter, and α_1, α_2 are known functions dependent on ply and laminate properties, as described in Appendix A. Depending on the choice of parameter ξ, different shear-lag models, that have been proposed in the literature, can be obtained [7].

In this thesis three candidate shear-lag models are selected, namely, the "classical" shear-lag model [132, 141] and two of its modifications: interlaminar shear-lag model [9], and bi-dimensional shear-lag model [142, 143]. The main difference between the classical approach and the interlaminar approach is that the later assumes that shear stresses develop within

a resin rich region near the interfaces between adjacent plies, whose thickness d_0 and shear modulus G_m are uncertain. The bi-dimensional shear-lag approach is essentially equivalent to the classical approach except for that it introduces a minor correction to account for the Poisson's effect [7, 144]. See [7] for further discussion about shear-lag analysis.

The shear-lag parameter of each candidate model can be obtained as a function of the ply and laminate properties (see Appendix A for nomenclature description), as follows:

$$\xi^2 = G_{23}\left(\frac{1}{E_2} + \frac{1}{\lambda E_x^{(\phi)}}\right) \qquad \text{(classical)} \tag{6.3a}$$

$$\xi^2 = \frac{G_m}{d_0} t_{90}\left(\frac{1}{E_2} + \frac{1}{\lambda E_x^{(\phi)}}\right) \qquad \text{(interlaminar)} \tag{6.3b}$$

$$\xi^2 = \frac{\frac{1}{Q_{22}} + \frac{1}{\lambda Q_{xx}^{(\phi)}}}{\frac{1}{3G_{23}} + \frac{\lambda}{3G_{xz}^{(\phi)}}} \qquad \text{(bi-dimensional)} \tag{6.3c}$$

where Q_{22} in Equation 6.3c is the $(2,2)$-th element of the on-axis (local coordinates) ply stiffness matrix, defined as $Q_{22} = \frac{E_2}{1-\nu_{12}^2 E_2/E_1}$, and $Q_{xx}^{(\phi)}$ is the $(1,1)$-th element of the stiffness matrix of the $\left[\phi_{\frac{n_\phi}{2}}\right]$ sub-laminate. Given the ply stiffness matrix, which can be straightforwardly obtained from basic ply properties, the stiffness matrix of the total laminate or any sub-laminate can be obtained using the classical laminates theory [145].

6.2.2 Crack opening displacement model

For the COD-based model, the formulation of Gudmundson and Weilin [134] is adopted, which uses a closed-form expression for the average COD to derive expressions for the effective longitudinal Young's modulus in laminates with general layup, as:

$$E_x^* = \frac{1}{\left((\mathbf{S}_0)^{-1} - \sum_{k=1}^{n_p} \nu^k t^k \rho^k (\mathbf{A}^k)^T \sum_{i=1}^{n_p} \boldsymbol{\beta}^{ik} \mathbf{A}^i\right)^{-1}_{(1,1)}} \tag{6.4}$$

In the last equation, $\mathbf{S}_0$ is the in-plane compliance matrix of the intact laminate, n_p is the number of plies and, ν^k, t^k and ρ^k stand for the volume fraction, the thickness and the matrix-cracks density of the k-th ply, respectively. $\mathbf{A}^k$ is a matrix defined by the compliance matrix and the unit normal vector on the crack surfaces of the k-th ply, and $\boldsymbol{\beta}^{ik}$ is a matrix associated with the average crack opening displacements and tractions of the surface of transverse cracks. Both are detailed in Appendix A. The subscript $(1,1)$ at the denominator of Equation 6.4 denotes the first component of the resulting matrix.

6.2.3 Micro-cracks density evolution model

Having identified the candidate models to express the relationship between effective stiffness and micro-cracks density, the next step is to address the time evolution of the micro-cracks density. To this end, the previously explained micro-damage mechanics models are used to obtain the energy released per unit crack area due to the formation of a new crack

between two existing cracks, denoted here as G. This energy, known as energy release rate (ERR), can be calculated as [146, 147]:

$$G = \frac{\sigma_x^2 h}{2\rho t_{90}} \left(\frac{1}{E_x^*(2\rho)} - \frac{1}{E_x^*(\rho)} \right) \tag{6.5}$$

where σ_x is the applied axial tension, and h and t_{90} are the laminate and 90°-sublaminate half-thickness, respectively. The result of the energy calculation is further introduced into the modified Paris' law [48], that gives the evolution of matrix-cracks density as a function of fatigue cycle n, as shown below:

$$\frac{d\rho}{dn} = A(\Delta G)^\alpha \tag{6.6}$$

where A and α are fitting parameters, and ΔG is the increment in ERR for a specific stress amplitude: $\Delta G = G(\sigma_{x,max}) - G(\sigma_{x,min})$. Note that a closed-form solution for Equation 6.6 is difficult to obtain due to the complexity of the expression for ΔG, which involves the underlying micro-damage mechanics models for the computation of $E_x^*(\rho)$. To overcome this drawback, the resulting differential equation can be solved by approximating the derivative using "unit-time" finite differences, as follows:

$$\rho_n = \rho_{n-1} + A\left(\Delta G(\rho_{n-1})\right)^\alpha \tag{6.7}$$

To summarize, five micro-damage mechanics models, namely shear-lag (×3), variational and COD models, are selected to compute $E_x^*(\rho)$, i.e. the relationship between the effective stiffness (macro-scale) and the matrix-cracks density (micro-scale). The evolution of matrix-cracks density is modeled by the modified Paris' law in Equation 6.7, that uses one of the candidate damage mechanics models to evaluate the increment in ERR. Therefore, for this study, five candidate models are considered to investigate the overall damage progression at both micro-scale and macro-scale.

6.3 Stochastic embedding for deterministic damage models

For the purpose of Bayesian model selection and parameter estimation, a probability-based description of the deterministic damage models described in Section 6.2 is required. To this end, the stochastic embedding methodology explained in Section 4.1.1 is applied here. Given a deterministic damage model defined by the relationship $\mathbf{g} = \mathbf{g}(\mathbf{u}, \mathbf{m}) : \mathbb{R}^{N_i} \times \mathbb{R}^{N_m} \rightarrow \mathbb{R}^{N_o}$ between the model input $\mathbf{u} \in \mathbb{R}^{N_i}$ and the model output $\mathbf{g} \in \mathbb{R}^{N_o}$, provided a set of N_m model parameters $\mathbf{m} \in \mathbb{R}^{N_m}$, a stochastic damage model can be obtained by adding an error term $\mathbf{e} = \mathbf{e}(\mathbf{v}) : \mathbb{R}^{N_e} \rightarrow \mathbb{R}^{N_o}$ parameterized by $\mathbf{v} \in \mathbb{R}^{N_e}$, that represents the difference between the measured output $\boldsymbol{x} \in \mathbb{R}^{N_o}$ and the model output $\mathbf{g}$, as follows:

$$\underbrace{\boldsymbol{x}}_{\text{system output}} = \underbrace{\mathbf{g}(\mathbf{u}, \mathbf{m})}_{\text{model output}} + \underbrace{\mathbf{e}(\mathbf{v})}_{\text{error}} \tag{6.8}$$

As discussed in Section 6.2, the progression of fatigue damage in composites is studied at every fatigue cycle n by focusing on two of its output manifestations: the matrix-cracks density, ρ_n, and the normalized effective stiffness, defined as $D_n = \frac{E_x^*}{E_{x,0}}$. Then, according to Equation 6.8, the overall system response can be represented by:

$$x_{1,n} = \rho_n = \underbrace{g_1(\rho_{n-1}, \mathbf{u}, \boldsymbol{\theta})}_{\text{Eq. 6.7}} + e_1 \tag{6.9a}$$

$$x_{2,n} = D_n = \underbrace{g_2(\rho_n, \mathbf{u}, \boldsymbol{\theta})}_{\text{Eq. 6.1 \& 6.4}} + e_2 \tag{6.9b}$$

where subscripts 1 and 2 denote the corresponding damage subsystems: matrix-crack density and normalized effective stiffness, respectively.

From Equations 6.9a and 6.9b, the three main elements defining the stochastic forward model for system behavior (recall Equation 4.5) can be identified: (1) the system output $\boldsymbol{x}_n = (\rho_n, D_n) \in \mathbb{R}^2$, (2) the model output $\mathbf{g} = (g_1, g_2) \in \mathbb{R}^2$, and (3) the corresponding error term $\mathbf{e} = (e_1, e_2) \in \mathbb{R}^2$. A key concept here is the consideration of errors e_1 and e_2 as stochastically independent (i.e., not correlated) *a priori*, even though models g_1 and g_2 are mathematically related, as shown in Section 6.2. This means that the covariance operator $\boldsymbol{\Sigma}_\mathbf{e}$ is a diagonal matrix, i.e. $\boldsymbol{\Sigma}_\mathbf{e} = diag(\sigma_{e_1}^2, \sigma_{e_2}^2)$ and therefore, the stochastic forward model of damage can be readily expressed as a product of univariate Gaussians, as follows:

$$p(\boldsymbol{x}_n|\mathbf{u}, \boldsymbol{\theta}, \mathcal{M}) = p(\rho_n|\rho_{n-1}, \mathbf{u}, \boldsymbol{\theta}, \mathcal{M}) p(D_n|\rho_n, \mathbf{u}, \boldsymbol{\theta}, \mathcal{M}) \tag{6.10}$$

where

$$p(\rho_n|\rho_{n-1}, \mathbf{u}, \boldsymbol{\theta}, \mathcal{M}) = \mathcal{N}\big(g_1(\rho_{n-1}, \mathbf{u}, \boldsymbol{\theta}) + \mu_{e_1}, \sigma_{e_1}^2\big) \tag{6.11a}$$

$$p(D_n|\rho_n, \mathbf{u}, \boldsymbol{\theta}, \mathcal{M}) = \mathcal{N}\big(g_2(\rho_n, \mathbf{u}, \boldsymbol{\theta}) + \mu_{e_2}, \sigma_{e_2}^2\big) \tag{6.11b}$$

and where $(\mu_{e_1}, \sigma_{e_1})$ and $(\mu_{e_2}, \sigma_{e_2})$ are the parameters (mean, standard deviation) of the error terms e_1 and e_2, respectively; i.e., $\mathbf{v} = \{\mu_{e_1}, \sigma_{e_1}, \mu_{e_2}, \sigma_{e_2}\}$. See Figure 6.2 for illustration.

The same assumption of stochastic independency made for error parameters $\mathbf{v}$ can also be adopted for the rest of model parameters in $\boldsymbol{\theta}$. Under this assumption, the prior PDF of model parameters is defined as the unconditional product of the individual priors $p(\theta_i|\mathcal{M}), i = 1, \ldots, d$; i.e., $p(\boldsymbol{\theta}|\mathcal{M}) = \prod_{i=1}^{d} p(\theta_i|\mathcal{M})$. Note that this assumption is not an assertion that no correlations actually exist in model parameters, but is only a description of the available prior information about such correlations. If they existed, they would become apparent after Bayesian updating and therefore, they would be considered in subsequent forward model simulations.

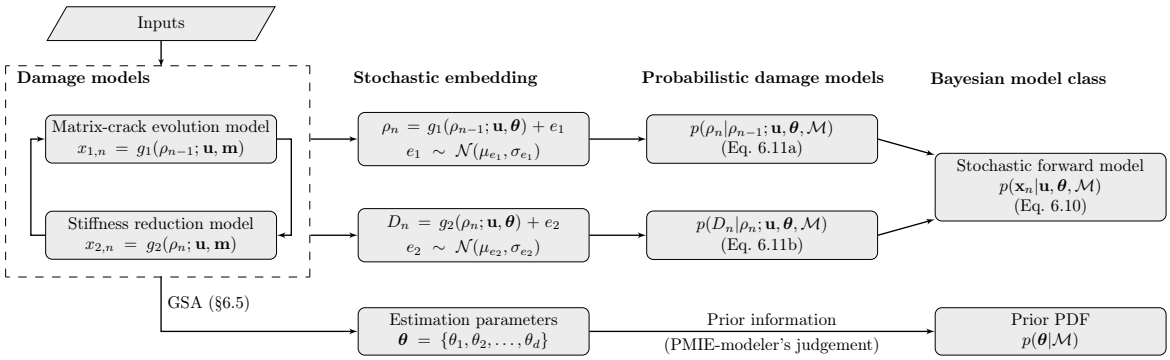

Figure 6.2: *Scheme of stochastic embedding for deterministic damage models*

6.4 Formulation of the likelihood function

In this study, data $\mathcal{D}$ consists of an experimental sequence of N fatigue damage measurements $\mathcal{D} = \{\mathbf{y}_1, \ldots, \mathbf{y}_n, \ldots, \mathbf{y}_N\}$ defined over a set of fatigue cycles $\mathcal{T} = \{1, \ldots, n, \ldots, N\} \subset \mathbb{N}$, where $\mathbf{y}_n = (\rho_n, D_n)$. The likelihood function is then computed as the probability of predicting the experimental sequence $\mathcal{D}$ by the stochastic model defined in Equation 6.10 under the parameterization specified by $\boldsymbol{\theta}$ within the model class $\mathcal{M}$, as follows:

$$p(\mathcal{D}|\boldsymbol{\theta}, \mathcal{M}) = \prod_{n=1}^{N} p(\mathbf{y}_n|\mathbf{u}, \boldsymbol{\theta}, \mathcal{M}) \tag{6.12}$$

By substituting Equation 6.10 into Equation 6.12, the likelihood function can be finally expressed as:

$$p(\mathcal{D}|\boldsymbol{\theta}, \mathcal{M}) = \prod_{n=1}^{N} p(D_n|\rho_n, \mathbf{u}, \boldsymbol{\theta}, \mathcal{M}) p(\rho_n|\rho_{n-1}, \mathbf{u}, \boldsymbol{\theta}, \mathcal{M}) \tag{6.13}$$

Note that when data are given over a set of non-regularly scheduled cycles $\mathcal{T}_D = \{n_k, n_l, \ldots, n_N\}$, $\mathcal{T}_D \subset \mathcal{T}$, the likelihood function defined in Equation 6.13 cannot be evaluated due to the "one-step" description of the matrix-cracks evolution model, as is defined in Equation 6.9a. A proposed solution is to use Total Probability Theorem to bridge the missing damage path between two non-subsequent measurements of matrix-cracks density. For example, for general cycles n_k and n_l, such that $n_l = n_k + \Delta n$ with $\Delta n \in \mathbb{N} \geqslant 1$, the probability $p(\rho_{n_l}|\rho_{n_k}, \mathbf{u}, \boldsymbol{\theta}, \mathcal{M})$ in Equation 6.13 can be calculated as:

$$p\left(\rho_{n_l}|\rho_{n_k}, \boldsymbol{\theta}\right) = \int p\left(\rho_{n_l}|\Gamma_{n_k}^{n_l}, \rho_{n_k}, \boldsymbol{\theta}\right) p\left(\Gamma_{n_k}^{n_l}|\rho_{n_k}, \boldsymbol{\theta}\right) d\Gamma_{n_k}^{n_l} \tag{6.14}$$

where $\Gamma_{n_k}^{n_l}$ represents the missing damage sequence between the observed data ρ_{n_k} and ρ_{n_l}, i.e., $\Gamma_{n_k}^{n_l} = \{\rho_{n_k+1}, \rho_{n_k+2}, \ldots, \rho_{n_l-1}\}$. Note that, for the sake of clarity, the conditioning on model class $\mathcal{M}$ and model inputs $\mathbf{u}$ is dropped. The high dimensional probability integral in Equation 6.14 can be readily estimated as a mathematical expectation using the direct

Monte Carlo method, as:

$$p\left(\rho_{n_l}|\rho_{n_k},\boldsymbol{\theta}\right) \approx \frac{1}{T}\sum_{i=1}^{T} p\big(\rho_{n_l}|\tilde{\Gamma}_{n_k}^{n_l,(i)},\rho_{n_k},\boldsymbol{\theta}\big) \tag{6.15}$$

where $\tilde{\Gamma}_{n_k}^{n_l,(i)} = \{\tilde{\rho}_{n_k+1}^{(i)},\tilde{\rho}_{n_k+2}^{(i)},\ldots,\tilde{\rho}_{n_l-1}^{(i)}\}$ is the i-th simulated sequence of damage growth between cycles n_k and n_l, $i = 1,\ldots,T$. It can be obtained by conditional sampling from the stochastic matrix-cracks evolution model given in Equation 6.11a as follows: first sample $\tilde{\rho}_{n_k+1}^{(i)}$ using the aforementioned evolution model conditional on the initial observed state ρ_{n_k}, i.e. $\tilde{\rho}_{n_k+1}^{(i)} \sim p(\cdot|\rho_{n_k},\boldsymbol{\theta})$; then sample the next state conditional on the previous sample, i.e. $\tilde{\rho}_{n_k+2}^{(i)} \sim p(\cdot|\tilde{\rho}_{n_k+1}^{(i)},\boldsymbol{\theta})$; finally, repeat the same process until the final damage state in $\tilde{\Gamma}_{n_k}^{n_l,(i)}$ is reached.

By the Markovian type of evolution of the matrix-cracks density, inherited from the definition of the crack evolution model in Equation 6.9a, the probability of any future damage state is conditionally independent of the past history given the immediately previous state, thus $p(\rho_{n_l}|\Gamma_{n_k}^{n_l},\boldsymbol{\theta}) = p(\rho_{n_l}|\rho_{n_l-1},\boldsymbol{\theta})$. Then Equation 6.15 can be rewritten as:

$$p(\rho_{n_l}|\rho_{n_k},\boldsymbol{\theta}) \approx \frac{1}{T}\sum_{i=1}^{T} p(\rho_{n_l}|\tilde{\rho}_{n_l-1}^{(i)},\boldsymbol{\theta}) \tag{6.16}$$

where $\tilde{\rho}_{n_l-1}^{(i)}$ is the last damage state in the simulated sequence $\tilde{\Gamma}_{n_k}^{n_l,(i)}$. The probability estimate obtained from Equation 6.16 is further inserted in Equation 6.13 to calculate the overall likelihood of the damage model specified by $\boldsymbol{\theta}$ in model class $\mathcal{M}$. Figure 6.3 provides further clarification about the calculation of the likelihood along with details for its computational implementation, as will be shown further below.

6.4.1 Computation of likelihood function using a GPU

As explained in Section 4.1.2, the computation of each MCMC step requires the evaluation of the overall likelihood function $p(\mathcal{D}|\boldsymbol{\theta},\mathcal{M})$, which (recall Equation 6.13) involves the evaluation of multi-dimensional integrals such as those defined by Equation 6.14. The Monte Carlo method can be applied to numerically solve these integrals, as shown in Equation 6.15, however it requires the simulation of T (large enough) damage growth sequences $\big\{\tilde{\Gamma}_{n_k}^{n_l,(i)}\big\}_{i=1}^{T}$, which increases the computational complexity dramatically.

To speed up these computations, the evaluation of the heaviest part of the likelihood is carried out in parallel on the Graphics Processing Unit (GPU), utilizing the Compute Unified Device Architecture (CUDA) code from NVIDIA using Matlab®. Figure 6.3 provides a scheme of the MH algorithm implementation using the GPU. Observe that the simulation of the T damage growth sequences, $\big\{\tilde{\Gamma}_{n_k}^{n_l,(i)}\big\}_{i=1}^{T}$, together with the evaluation of the PDFs $\big\{p(\rho_{n_l}|\tilde{\rho}_{n_l-1}^{(i)},\boldsymbol{\theta})\big\}_{i=1}^{T}$ (recall Equation 6.16), are performed using the GPU. The summation of the individual probability density values of Equation 6.16 together with the remaining part of the likelihood function are handled by the CPU. The CPU also takes charge of the

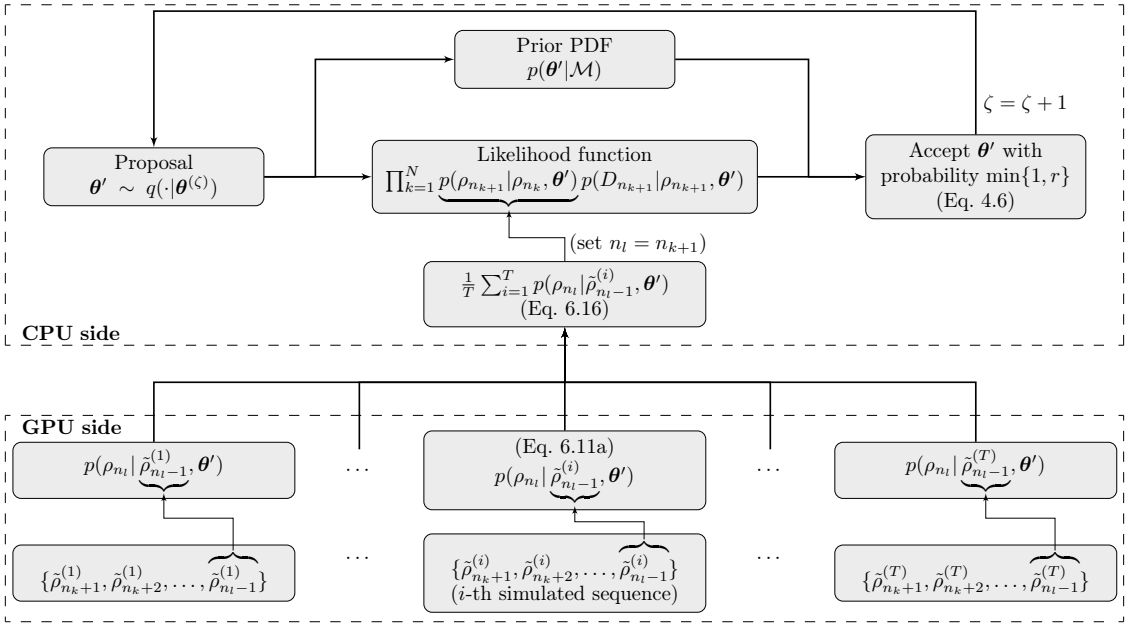

Figure 6.3: *Implementation scheme of M-H algorithm using the GPU to accelerate the computation of likelihood function. Note that M-H runs serially on the CPU, while the GPU executes part of the likelihood in parallel.*

rest of the MH steps. An averaged speed-up factor of up to 900, compared to an equivalent serial computation on the CPU, is observed while updating each model class using a GPU NVIDIA GeForce GTX 680 (1536 CUDA cores) and a 3.2 GHz CPU system.

6.5 Model parameterization through Global Sensitivity Analysis

The Bayesian approach to model parameter estimation and model class selection involves an inference problem defined over a multi-dimensional parameter space $\boldsymbol{\Theta} \subset \mathbb{R}^d$. It is clear that the higher d, the higher the complexity and computational cost of the updating process. At the same time, adopting a predetermined set of model parameters may lead to an unjustified uncertainty reduction [148]. Sankararaman *et al.* [36] addressed this issue for fatigue crack growth prediction in metals, where GSA was used to select the model parameters that were further updated using Bayes' Theorem. A similar approach has recently been adopted by Gobbato *et al.* [38] for fatigue crack growth prediction in metals by using partial-derivatives for sensitivity analysis. In this section, a variance-based approach for GSA is adopted following the approach by [36], i.e. simplify the model parameterization by identifying the subset of parameters that can be fixed at any given value (e.g., the mean or nominal value) of their range of variation without affecting the uncertainty of the model output.

For the sake of illustration, let us consider the model $\mathbf{g} : \mathbf{g}(\boldsymbol{\pi})$ defined in Section 4.1.1 as a function of the set of parameters $\boldsymbol{\pi} = \{\mathbf{u}, \mathbf{m}\} = \{\psi_1, \ldots, \psi_i, \ldots, \psi_{N_p}\} \subset \mathbb{R}^{N_p = N_i + N_m}$. Each component ψ_i is defined over a nonnull range of variation or uncertainty determined by the prior PDF. The goal is to identify $\mathbf{u} \subset \boldsymbol{\pi}$, as the subset of noninfluential parameters. As stated by Saltelli *et al.* [49, 148], the necessary and sufficient condition for parameter ψ_i to be

noninfluential is that $S_i^T = 0$, where S_i^T is the *total effects index* of parameter ψ_i, which can be computed as [49]:

$$S_i^T = \frac{\mathbb{E}_{\psi_{\sim i}}(V_{\psi_i}(\mathbf{g}|\psi_{\sim i}))}{V(\mathbf{g})} \tag{6.17}$$

with $S_i^T \in [0,1]$ and $\sum_{i=1}^{N_p} S_i^T \geqslant 1$. The numerator of the right hand side of Equation 6.17 can be evaluated using double-loop MC sampling, although single-loop MC sampling approaches have also been discussed in the literature [49]. In the inner loop, the conditional variance $V_{\psi_i}(\mathbf{g}|\psi_{\sim i})$ is calculated by evaluating the model considering random variations in ψ_i, when the parameters other than ψ_i (denoted by $\psi_{\sim i}$) are fixed at a random value sampled from the associated prior PDFs. The outer loop considers random variations in $\psi_{\sim i}$ and computes the expectation of the aforementioned variance. Finally, the result is divided by $V(\mathbf{g})$, the unconditional variance of the model response, which can be readily obtained by evaluating the model using samples from the joint prior PDF of the complete set parameters $\boldsymbol{\pi}$. As stated before, the lower the total effects index of a particular parameter ψ_i, the smaller its influence for Bayesian updating. Therefore, parameters with low sensitivity are left out of the updating procedure, thereby reducing the dimensionality of the problem.

This procedure is applied for each candidate damage model and, as a result, a subset $\mathbf{m} \subseteq \boldsymbol{\pi}$ of model parameters arises for each model class. The rest of non-influential parameters are then used as deterministic input parameters $\mathbf{u}$, hence they can be fixed anywhere within their range of variation. As stated in Section 4.1.1, the vector $\mathbf{m}$ of model parameters is augmented with the set of error parameters $\mathbf{v}$, resulting in a set of model parameters for Bayesian updating defined by $\boldsymbol{\theta} = \{\mathbf{m}, \mathbf{v}\} \in \boldsymbol{\Theta} \subset \mathbb{R}^{d=N_m+N_e}$.

More insight and numerical results for GSA are found in Chapter 10, where the performance of the model classes presented in this chapter is investigated using damage data for CFRP laminates.

[...] I believe it to be most important to open people's eyes to the number of superfluous hypotheses they are making, and would rather exaggerate the opposite view, if need be, than proceed along these false lines.

H. von Helmholtz (1868)

7

Approximate Bayesian Computation by SubSet Simulation

In this chapter, a new Approximate Bayesian Computation (ABC) algorithm for Bayesian updating is proposed by combining the ABC principles with the technique of *Subset Simulation* for efficient rare-event simulation, first developed in S.K. Au and J.L. Beck [50]. It has been named ABC-SubSim. The methodology for ABC is introduced and reviewed in Section 7.1. In Section 7.2, the Subset Simulation technique is summarized. The methodology for ABC-SubSim algorithm is presented in Section 7.3. Finally, the efficiency of the algorithm is demonstrated in Section 7.4 for two examples using synthetic data.

7.1 Introduction and state of art

As explained in Section 4.1, the main goal of Bayesian inverse problem is to update the *a priori* information about the set of parameters $\boldsymbol{\theta} \in \boldsymbol{\Theta} \subset \mathbb{R}^d$ for a parameterized model class $\mathcal{M}_j$, based on the information contained in a given set of data $\mathcal{D} \in \mathfrak{D} \subset \mathbb{R}^\ell$. Then, Bayes' Theorem yields the posterior PDF $p(\boldsymbol{\theta}|\mathcal{D}, \mathcal{M}_j)$ of the model specified by $\boldsymbol{\theta}$ in the model class $\mathcal{M}_j$, as

$$p(\boldsymbol{\theta}|\mathcal{D}, \mathcal{M}_j) = c^{-1} p(\mathcal{D}|\boldsymbol{\theta}, \mathcal{M}_j) p(\boldsymbol{\theta}|\mathcal{M}_j) \tag{7.1}$$

where c is a normalizing constant such that

$$\int_{\boldsymbol{\Theta}} p(\boldsymbol{\theta}|\mathcal{D}, \mathcal{M}_j) d\boldsymbol{\theta} = c^{-1} \int_{\boldsymbol{\Theta}} p(\mathcal{D}|\boldsymbol{\theta}, \mathcal{M}_j) p(\boldsymbol{\theta}|\mathcal{M}_j) d\boldsymbol{\theta} = 1 \tag{7.2}$$

However, there are situations where Bayesian model updating is conducted with a likelihood function $p(\mathcal{D}|\boldsymbol{\theta}, \mathcal{M}_j)$ that is not completely known or it is difficult to compute, perhaps because it requires the evaluation of an intractable multi-dimensional integral over a latent vector, such as in hidden Markov models or dynamic state-space models, or because the normalization in the likelihood over the output space $\mathfrak{D}$ involves an intractable integral parameterized by $\boldsymbol{\theta}$ [149].

Approximate Bayesian Computation (ABC) was conceived with the aim of evaluating the posterior PDF in those cases where the likelihood function is intractable or computational unaffordable [150, 151], although it also avoids the problem of the intractable integral in Equation 7.2. In the Bayesian literature, such method is also found as *likelihood-free computation algorithms*, which refers to the main aim of circumventing the explicit evaluation of the likelihood function by using a stochastic simulation approach. In this section, the method ABC is briefly described and the body of ABC literature is summarized.

Let $\boldsymbol{x} \in \mathfrak{D} \subset \mathbb{R}^{\ell}$ denote a simulated outcome from $p(\boldsymbol{x}|\boldsymbol{\theta}, \mathcal{M})$, the stochastic forward model for model class $\mathcal{M}$ parameterized by $\boldsymbol{\theta}$. ABC aims at evaluating the posterior $p(\boldsymbol{\theta}|\mathcal{D}, \mathcal{M}) \propto p(\mathcal{D}|\boldsymbol{\theta}, \mathcal{M})p(\boldsymbol{\theta}|\mathcal{M})$ by applying Bayes' Theorem to the pair $(\boldsymbol{\theta}, \boldsymbol{x}) \in \boldsymbol{\Theta} \times \mathfrak{D} \subset \mathbb{R}^{d+\ell}$:

$$p(\boldsymbol{\theta}, \boldsymbol{x}|\mathcal{D}) \propto p(\mathcal{D}|\boldsymbol{x}, \boldsymbol{\theta})p(\boldsymbol{x}|\boldsymbol{\theta})p(\boldsymbol{\theta}) \tag{7.3}$$

In the last equation, the conditioning on model class $\mathcal{M}$ has been omitted for clarity, given that the theory is valid for any specific model class. The basic form of the algorithm to generate samples from the posterior in Equation 7.3, is a rejection algorithm that consists of generating jointly $\boldsymbol{\theta} \sim p(\boldsymbol{\theta})$ and $\boldsymbol{x} \sim p(\boldsymbol{x}|\boldsymbol{\theta})$, and accepting them conditional on fulfilling the equality $\boldsymbol{x} = \mathcal{D}$. This is due to the fact that the function $p(\mathcal{D}|\boldsymbol{x}, \boldsymbol{\theta})$ in Equation 7.3 gives higher densities for the posterior in those regions where $\boldsymbol{x}$ is close to $\mathcal{D}$. Of course, obtaining the sample $\boldsymbol{x} = \mathcal{D}$ is unlikely in most applications, and it is only feasible if $\mathfrak{D}$ consists of a finite set of values rather than a continuous region in $\mathbb{R}^{\ell}$. Two main approximations have been conceived in ABC theory to address the above difficulty [152]: a) replace the equality $\boldsymbol{x} = \mathcal{D}$ by the approximation $\boldsymbol{x} \approx \mathcal{D}$ and introduce a tolerance parameter ϵ that accounts for how close they are through some type of metric ρ_{xy}; and b) introduce a low-dimensional vector of summary statistics $\eta(\cdot)$ that permits a comparison of the closeness of $\boldsymbol{x}$ and $\mathcal{D}$ in a weak manner. Through this approach, the posterior $p(\boldsymbol{\theta}, \boldsymbol{x}|\mathcal{D})$ in Equation 7.3 is approximated by $p_{\epsilon}(\boldsymbol{\theta}, \boldsymbol{x}|\mathcal{D})$, which assigns higher probability density to those values of $(\boldsymbol{\theta}, \boldsymbol{x}) \in \boldsymbol{\Theta} \times \mathfrak{D}$ that satisfy the condition $\rho_{xy}\big(\eta(\boldsymbol{x}), \eta(\mathcal{D})\big) \leqslant \epsilon$.

The standard version of the ABC algorithm defines an approximate likelihood function as[1] $P_{\epsilon}(\mathcal{D}|\boldsymbol{\theta}, \boldsymbol{x}) = P(\boldsymbol{x} \in \mathcal{B}_{\epsilon}(\mathcal{D})|\boldsymbol{\theta}, \boldsymbol{x})$, where $\mathcal{B}_{\epsilon}(\mathcal{D})$ is a region of $\mathfrak{D}$ defined as:

$$\mathcal{B}_{\epsilon}(\mathcal{D}) = \big\{\boldsymbol{x} \in \mathfrak{D} : \rho_{xy}\big(\eta(\boldsymbol{x}), \eta(\mathcal{D})\big) \leqslant \epsilon\big\} \tag{7.4}$$

[1] In what follows, $P(\cdot)$ is adopted to denote probability whereas $p(\cdot)$ denotes a PDF.

Thus, from Bayes' Theorem, the approximate posterior $p_\epsilon(\boldsymbol{\theta}, \boldsymbol{x}|\mathcal{D})$ is given by:

$$p_\epsilon(\boldsymbol{\theta}, \boldsymbol{x}|\mathcal{D}) \propto P(\boldsymbol{x} \in \mathcal{B}_\epsilon(\mathcal{D})|\boldsymbol{x}, \boldsymbol{\theta}) p(\boldsymbol{x}|\boldsymbol{\theta}) p(\boldsymbol{\theta}) \tag{7.5}$$

where $P(\boldsymbol{x} \in \mathcal{B}_\epsilon(\mathcal{D})|\boldsymbol{x}, \boldsymbol{\theta}) = \mathbb{I}_{\mathcal{B}_{\epsilon(\mathcal{D})}}(\boldsymbol{x})$, an indicator function for the set $\mathcal{B}_\epsilon(\mathcal{D})$ that assigns the value 1 when $\rho_{xy}\big(\eta(\boldsymbol{x}), \eta(\mathcal{D})\big) \leqslant \epsilon$, and 0 otherwise. It follows that the approximate posterior $p_\epsilon(\boldsymbol{\theta}, \boldsymbol{x}|\mathcal{D})$ can be readily calculated as:

$$p_\epsilon(\boldsymbol{\theta}, \boldsymbol{x}|\mathcal{D}) \propto p(\boldsymbol{x}|\boldsymbol{\theta}) p(\boldsymbol{\theta}) \mathbb{I}_{\mathcal{B}_{\epsilon(\mathcal{D})}}(\boldsymbol{x}) \tag{7.6}$$

Since the ultimate interest of Bayesian inverse problem is typically the posterior of model parameters $p_\epsilon(\boldsymbol{\theta}|\mathcal{D})$, it can be obtained by marginalizing the approximate posterior PDF in Equation 7.6:

$$p_\epsilon(\boldsymbol{\theta}|\mathcal{D}) \propto p(\boldsymbol{\theta}) \int_{\mathfrak{D}} p(\boldsymbol{x}|\boldsymbol{\theta}) \mathbb{I}_{\mathcal{B}_{\epsilon(\mathcal{D})}}(\boldsymbol{x}) d\boldsymbol{x} = P(\boldsymbol{x} \in \mathcal{B}_\epsilon(\mathcal{D})|\boldsymbol{\theta}) p(\boldsymbol{\theta}) \tag{7.7}$$

This integration need not be done explicitly since samples from this marginal PDF are obtained by taking the $\boldsymbol{\theta}$-component of samples from the joint PDF in Equation 7.6 [153]. A pseudocode to generate K samples by the standard version of ABC algorithm is given in Algorithm 4.

Algorithm 4 Standard ABC algorithm

for $k = 1$ to K **do**
  repeat
    1.- Simulate $\boldsymbol{\theta}'$ from the prior $p(\boldsymbol{\theta}|\mathcal{M})$
    2.- Generate $\boldsymbol{x}'$ from the stochastic forward model $p(\boldsymbol{x}|\boldsymbol{\theta}', \mathcal{M})$
  until $\rho_{xy}\big(\eta(\boldsymbol{x}'), \eta(\mathcal{D})\big) \leqslant \epsilon$
  Accept $(\boldsymbol{\theta}', \boldsymbol{x}')$ as $(\boldsymbol{\theta}^{(k)}, \boldsymbol{x}^{(k)})$
end for

Notice that the quality of the posterior approximation in Equations 7.6 and 7.7 depends on a suitable selection of the metric ρ_{xy}, the tolerance parameter ϵ and, of special importance, the summary statistic $\eta(\cdot)$ [154]. The choice of the tolerance parameter ϵ is basically a matter of the amount of computational effort that the modeler wishes to expend, but a possible guiding principle is described later in Section 7.3. For ϵ sufficiently small $\eta(\boldsymbol{x}') \to \eta(\mathcal{D})$, and so all accepted samples corresponding to Equation 7.7 come from the closest approximation to the required posterior density $p(\boldsymbol{\theta}|\mathcal{D})$, where the exactness is achieved when $\eta(\cdot)$ is a sufficient statistic. This desirable fact is at the expense of a high computational effort (usually prohibitive) to get $\eta(\boldsymbol{x}') = \eta(\mathcal{D})$ under the stochastic forward model $p(\boldsymbol{x}|\boldsymbol{\theta}, \mathcal{M})$. On the contrary, as $\epsilon \to \infty$, all accepted simulations $\boldsymbol{x}^{(k)}$ come from the prior. So, the choice of tolerance parameter ϵ reflects a trade-off between computability and accuracy.

In the literature, several computational improvements have been proposed addressing this trade-off. In those cases where the probability content of the posterior is concentrated

over a small region in relation to a diffuse prior, the use of MCMC methods (introduced in Section 4.1.2) has been demonstrated to be efficient [152]. In fact, the use of a proposal PDF $q(\boldsymbol{\theta}'|\boldsymbol{\theta}^{(k-1)})$ over the parameter space allows a new parameter $\boldsymbol{\theta}'$ to be proposed based on a previous accepted one $\boldsymbol{\theta}^{(k-1)}$, targeting the stationary distribution $p_\epsilon(\boldsymbol{\theta}|\mathcal{D})$. The resulting algorithm, commonly called ABC-MCMC, is similar to the standard one (Algorithm 4) with the main exception being the acceptance probability, which in this case is influenced by the MCMC acceptance probability. A pseudocode is provided in Algorithm 5.

Algorithm 5 ABC-MCMC algorithm

1.- Initialize $(\theta^{(0)}, \boldsymbol{x}^{(0)})$ from $p_\epsilon(\boldsymbol{\theta}, \boldsymbol{x}|\mathcal{D})$; e.g. use Algorithm 4.
for $k = 1$ to K **do**
  2.- Generate $\boldsymbol{\theta}' \sim q(\boldsymbol{\theta}|\boldsymbol{\theta}^{(k-1)})$ and $\boldsymbol{x}' \sim p(\boldsymbol{x}|\boldsymbol{\theta}')$
  3.- Accept $(\boldsymbol{\theta}', \boldsymbol{x}')$ as $(\boldsymbol{\theta}^{(k)}, \boldsymbol{x}^{(k)})$ with probability:
  $r = \min\left\{1, \frac{P_\epsilon(\mathcal{D}|\boldsymbol{x}', \boldsymbol{\theta}')p(\boldsymbol{\theta}')q(\boldsymbol{\theta}^{(k-1)}|\boldsymbol{\theta}')}{P_\epsilon(\mathcal{D}|\boldsymbol{x}^{(k-1)}, \boldsymbol{\theta}^{(k-1)})p(\boldsymbol{\theta}^{(k-1)})q(\boldsymbol{\theta}'|\boldsymbol{\theta}^{(k-1)})}\right\}$
  else set $(\boldsymbol{\theta}^{(k)}, \boldsymbol{x}^{(k)}) = (\boldsymbol{\theta}^{(k-1)}, \boldsymbol{x}^{(k-1)})$
end for

It should be noted that when the likelihood function is approximated as $P_\epsilon(\mathcal{D}|\boldsymbol{x}, \boldsymbol{\theta}) = \mathbb{I}_{\mathcal{B}_{\epsilon(\mathcal{D})}}(\boldsymbol{x})$ as in our case, the acceptance probability r (Step 3, Algorithm 5) is decomposed into the product of the MCMC acceptance probability and the indicator function as follows:

$$r = \min\left\{1, \frac{p(\boldsymbol{\theta}')q(\boldsymbol{\theta}^{(k-1)}|\boldsymbol{\theta}')}{p(\boldsymbol{\theta}^{(k-1)})q(\boldsymbol{\theta}'|\boldsymbol{\theta}^{(k-1)})}\right\}\mathbb{I}_{\mathcal{B}_{\epsilon(\mathcal{D})}}(\boldsymbol{x}') \tag{7.8}$$

Equation 7.8 clearly shows that the dependence upon ϵ in the indicator function may lead to an inefficient algorithm for a good approximation of the true posterior. In fact, given that r can only be non-zero if $\mathbb{I}_{\mathcal{B}_{\epsilon(\mathcal{D})}}(\boldsymbol{x}') = 1$ (i.e., $\rho_{xy}\big(\eta(\boldsymbol{x}'), \eta(\mathcal{D})\big) \leqslant \epsilon$), the Markov chain may persist in distributional tails for long periods of time if ϵ is sufficiently small, due to the acceptance probability being zero in Step 3 of Algorithm 5.

Some modifications to the ABC-MCMC scheme have been proposed [155] that provide a moderate improvement in the simulation efficiency. See [156] for a complete tutorial about ABC-MCMC. More recently, a branch of computational techniques have emerged in the context of ABC-MCMC to obtain high accuracy ($\epsilon \to 0$) with a feasible computational cost by combining sequential sampling algorithms [157] adapted for ABC. These techniques share a common principle of achieving computational efficiency by learning about intermediate target distributions determined by a decreasing sequence of tolerance levels $\epsilon_1 > \epsilon_2 > \ldots > \epsilon_m = \epsilon$, where the last is the desired tolerance ϵ. Table 7.1 lists the main contributions to the literature on this topic. In this chapter, a new algorithm is proposed in this direction, which makes use of the technique of Subset Simulation [50, 64, 158] to achieve computational efficiency in a sequential way. This algorithm, that has been named ABC-SubSim, is presented in Section 7.3. Before that, the methodology for Subset Simulation is summarized in Section 7.2.

Paper	Algorithm	Year	Notes
S.A. Sisson *et al.* [159]	ABC-PRC	2007	Requires forward and a backward kernels to perturb the particles. Uses a SMC sampler. Induces bias.
T. Toni *et al.* [160]	ABC-SMC	2009	Does not require resampling steps in [159]. Based on sequential importance sampling. Induces bias.
S.A. Sisson *et al.* [161]	ABC-PRC	2009	This version incorporates an improved weight updating function. Outperforms original in [159].
M.A. Beaumont *et al.* [162]	ABC-PMC	2009	Does not require a backward kernel as in the preceding works [159, 161].
M. Baragatti *et al.* [163]	ABC-PT	2011	Based on MCMC with exchange moves between chains. Capacity to exit from distribution tails.
C.C. Drovanti *et al.* [164]	Adaptive ABC-SMC	2011	Outperforms original in [160]. Automatic determination of the tolerance sequence $\epsilon_j, j = \{1, \ldots, m\}$ and the proposal distribution of the MCMC kernel.
P. Del Moral *et al.* [165]	Adaptive ABC-SMC	2012	More efficient than ABC-SMC [160, 164]. Automatic determination of the tolerance sequence $\epsilon_j, j = \{1, \ldots, m\}$.

PRC: Partial Rejection Control, SMC: Sequential Monte Carlo, PT: Parallel Tempering,

PMC: Population Monte Carlo.

Table 7.1: *Bibliography synoptic table about ABC with sequential algorithms. Papers ordered by increasing date of publication.*

7.2 Subset Simulation method

Subset Simulation is a simulation approach originally proposed to compute small failure probabilities in the context of reliability analysis (e.g. [50, 64, 166]). Strictly speaking, it is a method for progressively generating conditional samples distributed over a nested sequence of subsets that correspond to specified levels of a performance function. This general aspect makes Subset Simulation applicable to a broad range of areas of science where the simulation/prediction of unprovable events is required. For illustration purposes, the Subset Simulation method is presented in this section using its primary aim on small failure probabilities estimation (later, it will be specialized for ABC).

Let $\mathcal{F}$ be the failure region in the $\mathbf{z}$-space of states, $\mathbf{z} \in \mathcal{Z}$, corresponding to exceedance of the performance function g above some specified threshold b:

$$\mathcal{F} = \{\mathbf{z} \in \mathcal{Z} : g(\mathbf{z}) > b\} \tag{7.9}$$

For simpler notation, the identity $P(\mathcal{F}) \triangleq P(\mathbf{z} \in \mathcal{F})$ is adopted. In addition, $\mathcal{F}$ is assumed to be defined as the intersection of m regions $\mathcal{F} = \bigcap_{j=1}^{m} \mathcal{F}_j$, such that $\mathcal{F}_1 \supset \mathcal{F}_2 \ldots \supset \mathcal{F}_{m-1} \supset \mathcal{F}_m = \mathcal{F}$, where $\mathcal{F}_j = \{\mathbf{z} \in \mathcal{Z} : g(\mathbf{z}) > b_j\}$, with $b_{j+1} > b_j$. The PDF of $\mathbf{z}$ conditional to the event $\mathcal{F}_j$ can be expressed as $p(\mathbf{z}|\mathcal{F}_j)$, so that $p(\mathbf{z}|\mathcal{F}_j) \propto p(\mathbf{z})\mathbb{I}_{\mathcal{F}_j}(\mathbf{z})$, $j = 1, \ldots, m$. The term $p(\mathbf{z})$ denotes the stochastic forward model for $\mathbf{z}$. Because of the way the subsets $\mathcal{F}_j$ are

arranged, it is clear that when the event $\mathcal{F}_j$ holds, then the set of events $\{\mathcal{F}_{j-1}, \ldots, \mathcal{F}_1\}$ also hold, and hence $P(\mathcal{F}_j|\mathcal{F}_{j-1}, \ldots, \mathcal{F}_1) = P(\mathcal{F}_j|\mathcal{F}_{j-1})$, so it follows that:

$$P(\mathcal{F}) = P\left(\bigcap_{j=1}^{m} \mathcal{F}_j\right) = P(\mathcal{F}_1) \prod_{j=2}^{m} P(\mathcal{F}_j|\mathcal{F}_{j-1}) \tag{7.10}$$

where $P(\mathcal{F}_j|\mathcal{F}_{j-1}) \triangleq P(\mathbf{z} \in \mathcal{F}_j|\mathbf{z} \in \mathcal{F}_{j-1})$, is the conditional failure probability at the $(j-1)$-th conditional level. Notice that although the probability $P(\mathcal{F})$ can be relatively small, by choosing the intermediate regions appropriately, the conditional probabilities involved in Equation 7.10 can be made large, so that the simulation of low probability events is avoided.

In the last equation, the conditional probabilities cannot be efficiently estimated by the standard Monte Carlo method (MC) because of the conditional sampling involved, especially at higher intermediate levels. Therefore, in Subset Simulation only the first probability $P(\mathcal{F}_1)$ is estimated by MC:

$$P(\mathcal{F}_1) \approx \bar{P}_1 = \frac{1}{K} \sum_{k=1}^{K} \mathbb{I}_{\mathcal{F}_1}(\mathbf{z}_0^{(k)}), \qquad \mathbf{z}_0^{(k)} \overset{\text{i.i.d.}}{\sim} p(\mathbf{z}_0) \tag{7.11}$$

When $j \geqslant 2$, sampling from the PDF $p(\mathbf{z}_{j-1}|\mathcal{F}_{j-1})$ can be achieved by using MCMC at the expense of generating K dependent samples, giving:

$$P(\mathcal{F}_j|\mathcal{F}_{j-1}) \approx \bar{P}_j = \frac{1}{K} \sum_{n=1}^{K} \mathbb{I}_{\mathcal{F}_j}(\mathbf{z}_{j-1}^{(k)}), \qquad \mathbf{z}_{j-1}^{(k)} \sim p(\mathbf{z}_{j-1}|\mathcal{F}_{j-1}) \tag{7.12}$$

where $\mathbb{I}_{\mathcal{F}_j}(\mathbf{z}_{j-1}^{(k)})$ is the indicator function for the region $\mathcal{F}_j$, $j = 1, \ldots, m$, that assigns a value of 1 when $g(\mathbf{z}_{j-1}^{(k)}) > b_j$, and 0 otherwise. Observe that the Markov chain samples that are generated at the $(j-1)$-th level and that lie in $\mathcal{F}_j$, are distributed as $p(\mathbf{z}|\mathcal{F}_j)$. Thus, they act as "seeds" for the subsequent samples according to $p(\mathbf{z}|\mathcal{F}_j)$ by using MCMC sampling with no burn-in required. As described further below, $\mathcal{F}_j$ is defined in an automated manner based on the samples $\{\mathbf{z}_{j-1}^{(k)}, k = 1, \ldots, K\}$ from $p(\mathbf{z}|\mathcal{F}_{j-1})$, in such a way that there are exactly KP_0 of these seed samples in $\mathcal{F}_j$ $\left(\text{so } \bar{P}_j = P_0 \text{ in Equation 7.12}\right)$. Then a further amount of $(1/P_0 - 1)$ samples are generated from $p(\mathbf{z}|\mathcal{F}_j)$ by MCMC starting at each seed, giving a total of K samples in $\mathcal{F}_j$. Repeating this process, the conditional probabilities of the higher-conditional levels can be computed until the final region $\mathcal{F}_m = \mathcal{F}$ is reached.

To draw samples from the target PDF $p(\mathbf{z}|\mathcal{F}_j)$ using the Metropolis algorithm, a suitable proposal PDF must be chosen. In the original version of Subset Simulation [50], a modified Metropolis algorithm (MMA) was proposed that works well even in very high dimensions (e.g. 10^3-10^4), because the original M-H algorithm fails in this case (essentially all candidate samples from the proposal PDF are rejected. See the analysis in [50]). In MMA, a univariate proposal PDF is chosen for each component of the parameter vector and each component

candidate is accepted or rejected separately, instead of drawing a full parameter vector candidate from a multi-dimensional PDF, as in the original algorithm. Later in [64], grouping of the parameters was considered when constructing a proposal PDF to allow for the case where small groups of components in the parameter vector are highly correlated when conditioned on any $\mathcal{F}_j$. An appropriate choice for the proposal PDF for ABC-SubSim is introduced in the next section.

It is important to remark that in Subset Simulation, an inadequate choice of the b_j-sequence may lead to the conditional probability $P(\mathcal{F}_j|\mathcal{F}_{j-1})$ being very small (if the difference $b_j - b_{j-1}$ is too large), which will lead to a rare-event simulation problem. If, on the contrary, the intermediate threshold values were chosen too close so that the conditional failure probabilities were very high, the algorithm would take a large total number of simulation levels m (and hence large computational effort) to progress to the target region of interest $\mathcal{F}$. A rational choice that strikes a balance between these two extremes is to choose the b_j-sequence adaptively [50], so that the estimated conditional probabilities are equal to a fixed value P_0 (e.g. $P_0 = 0.2$). For convenience, P_0 is chosen so that KP_0 and $1/P_0$ are positive integers. For a specified value of P_0, the intermediate threshold value b_j defining $\mathcal{F}_j$ is obtained in an automated manner as the $[(1-P_0)K]$-th largest value among the values $g(\mathbf{z}_{j-1}^{(k)})$, $k = 1, \ldots, K$, so that the sample estimate of $P(\mathcal{F}_j|\mathcal{F}_{j-1})$ in Equation 7.12 is equal to P_0.

7.3 The ABC-SubSim algorithm

In this section, a new efficient sampler for the inference of rare events is proposed by just specializing the Subset Simulation method described in Section 7.2 to ABC. To this end, let us define the joint state-parameter vector $\mathbf{z} = (\boldsymbol{x}, \boldsymbol{\theta}) \in \mathcal{Z} \subset \mathbb{R}^{\ell+d}$, where $\boldsymbol{x}$ are simulated outcomes from the model class parameterized by $\boldsymbol{\theta}$, so that $p(\mathbf{z}) = p(\boldsymbol{x}|\boldsymbol{\theta})p(\boldsymbol{\theta})$. Let also $\mathcal{F}_j$ in Section 7.2 be replaced by a nested sequence of regions $\mathcal{Z}_j$, $j = 1 \ldots, m$, in $\mathcal{Z}$ defined by:

$$\mathcal{Z}_j = \Big\{(\boldsymbol{\theta}, \boldsymbol{x}) : \rho_{xy}\big(\eta(\boldsymbol{x}), \eta(\mathcal{D})\big) \leqslant \epsilon_j\Big\} \tag{7.13}$$

where $\mathcal{Z}_1 \ldots \supset \mathcal{Z}_j \supset \mathcal{Z}_{j+1} \ldots \supset \mathcal{Z}_m = \mathcal{Z}$, and ρ_{xy} a metric on the set $\big\{\eta(x), \eta(\mathcal{D})\big\}$. The sequence of tolerances $\epsilon_1, \ldots, \epsilon_j, \ldots, \epsilon_m$, with $\epsilon_{j+1} < \epsilon_j$, will be chosen adaptively as described in Section 7.2, where the number of levels m is chosen so that $\epsilon_m \leqslant \epsilon$, a specified tolerance.

As stated by Equation 7.6, an ABC algorithm aims at evaluating the sequence of intermediate posteriors $p(\boldsymbol{\theta}, \boldsymbol{x}|\mathcal{Z}_j)$, $j = 1, \ldots, m$, where by Bayes' Theorem:

$$p(\boldsymbol{\theta}, \boldsymbol{x}|\mathcal{Z}_j) = \frac{P(\mathcal{Z}_j|\boldsymbol{\theta}, \boldsymbol{x})p(\boldsymbol{x}|\boldsymbol{\theta})p(\boldsymbol{\theta})}{P(\mathcal{Z}_j)} \propto \mathbb{I}_{\mathcal{Z}_j}(\boldsymbol{\theta}, \boldsymbol{x})p(\boldsymbol{x}|\boldsymbol{\theta})p(\boldsymbol{\theta}) \tag{7.14}$$

Here, $\mathbb{I}_{\mathcal{Z}_j}(\boldsymbol{\theta}, \boldsymbol{x})$ is the indicator function for the set $\mathcal{Z}_j$. Notice that when $\epsilon \to 0$, $\mathcal{Z}_m$ represents a small closed region in $\mathcal{Z}$ and hence $P(\mathcal{Z}_m)$ will be very small under the model

$p(\boldsymbol{\theta}, \boldsymbol{x}) = p(\boldsymbol{x}|\boldsymbol{\theta})p(\boldsymbol{\theta})$. In this situation, using MCMC sampling directly is not efficient due to difficulties in initializing the chain and in achieving convergence to the stationary distribution. This is the point at which the efficiency of Subset Simulation is exploited for ABC, given that such a small probability $P(\mathcal{Z}_m)$ is converted into a sequence of larger conditional probabilities, as stated in Equations 7.10, 7.11 and 7.12.

Algorithm 6 provides a pseudocode implementation of ABC-SubSim that is intended to be sufficient for most situations. The algorithm is implemented such that a maximum allowable number of simulation levels (m) is considered in case the specified ϵ is too small. The choice of ϵ is discussed in Section 7.3.2.

Algorithm 6 Pseudocode implementation for ABC-SubSim

Inputs:

$P_0 \in [0, 1]$ {gives percentile selection, chosen so that $KP_0, 1/P_0 \in \mathbb{Z}^+$; $P_0 = 0.2$ is recommended}.
K, {number of samples per intermediate level}; m, {maximum number of simulation levels}

Algorithm:

Sample $\left[(\boldsymbol{\theta}_0^{(1)}, \boldsymbol{x}_0^{(1)}), \ldots, (\boldsymbol{\theta}_0^{(k)}, \boldsymbol{x}_0^{(k)}), \ldots, (\boldsymbol{\theta}_0^{(K)}, \boldsymbol{x}_0^{(K)})\right]$, where $(\boldsymbol{\theta}, \boldsymbol{x}) \sim p(\boldsymbol{\theta})p(\boldsymbol{x}|\boldsymbol{\theta})$
for $j : 1, \ldots, m$ **do**
  for $k : 1, \ldots, K$ **do**
    Evaluate $\rho_{xy,j}^{(k)} = \rho_{xy}\left(\eta(\boldsymbol{x}_{j-1}^{(k)}), \eta(\mathcal{D})\right)$
  end for
  Renumber $\left[(\boldsymbol{\theta}_{j-1}^{(k)}, \boldsymbol{x}_{j-1}^{(k)}), k : 1, \ldots, K\right]$ so that $\rho_{xy,j}^{(1)} \leqslant \rho_{xy,j}^{(2)} \leqslant \ldots \rho_{xy,j}^{(K)}$
  Fix $\epsilon_j = \frac{1}{2}\left(\rho_{xy,j}^{(KP_0)} + \rho_{xy,j}^{(KP_0+1)}\right)$
  for $k = 1, \ldots, KP_0$ **do**
    Select as a seed $(\boldsymbol{\theta}_j^{(k),1}, \boldsymbol{x}_j^{(k),1}) = (\boldsymbol{\theta}_{j-1}^{(k)}, \boldsymbol{x}_{j-1}^{(k)}) \sim p\left(\boldsymbol{\theta}, \boldsymbol{x}|(\boldsymbol{\theta}, \boldsymbol{x}) \in \mathcal{Z}_j\right)$
    Run Modified Metropolis Algorithm [50] to generate $1/P_0$ states of a Markov chain lying in $\mathcal{Z}_j$ (Eq. 7.13): $\left[(\boldsymbol{\theta}_j^{(k),1}, \boldsymbol{x}_j^{(k),1}), \ldots, (\boldsymbol{\theta}_j^{(k),1/P_0}, \boldsymbol{x}_j^{(k),1/P_0})\right]$
  end for
  Renumber $\left[(\boldsymbol{\theta}_j^{(k),i}, \boldsymbol{x}_j^{(k),i}) : k = 1, \ldots, KP_0;\ i = 1, \ldots, 1/P_0\right]$ as
  $\left[(\boldsymbol{\theta}_j^{(1)}, \boldsymbol{x}_j^{(1)}), \ldots, (\boldsymbol{\theta}_j^{(K)}, \boldsymbol{x}_j^{(K)})\right]$
  if $\epsilon_j \leqslant \epsilon$ **then**
    End algorithm
  end if
end for

7.3.1 Choice of intermediate tolerance levels

In Algorithm 6, the ϵ_j values are chosen adaptively as in Subset Simulation [50], so that the sample estimate $\bar{P}_j$ of $P(\mathcal{Z}_j|\mathcal{Z}_{j-1})$ satisfies $\bar{P}_j = P_0$. By this way, the intermediate tolerance value ϵ_j can be simply obtained as the $100P_0$ percentile of the set of distances $\rho_{xy}\left(\eta(\boldsymbol{x}_{j-1}^{(k)}), \eta(\mathcal{D})\right)$, $k = 1, \ldots, K$, arranged in increasing order. Additionally, for convenience of implementation, P_0 is chosen such that KP_0 and $1/P_0$ are integers, and so the size of the subset of samples generated in $\mathcal{Z}_{j-1}$ that lie in $\mathcal{Z}_j$ is known in advance and equal to KP_0. These KP_0 samples in $\mathcal{Z}_j$ are used as seeds for KP_0 Markov chains of length $1/P_0$, where

the new $(1/p_0 - 1)$ samples in $\mathcal{Z}_j$ in each chain are generated by MMA [50]. Hence the total number of samples of $(\boldsymbol{\theta}, \boldsymbol{x})$ lying in $\mathcal{Z}_j$ is K, but KP_0 of them were generated at the $(j-1)$-th level. Because of the way the seeds are chosen, ABC-SubSim exhibits the benefits of *perfect sampling* [153, 167], which is an important feature to avoid wasting samples during a burn-in period, in contrast to ABC-MCMC.

7.3.2 Choosing ABC-SubSim control parameters

The important control parameters to be chosen in Algorithm 6 are P_0 and $\sigma_q^{(j)}$, the standard deviation in the Gaussian proposal PDF in MMA at the j-th level. In this section, recommendations for the choice of these control parameters are provided.

In the literature, the optimal variance of a local proposal PDF for a MCMC sampler has been studied due to its significant impact on the speed of convergence of the algorithm [62, 63]. ABC-SubSim has the novelty of incorporating the Subset Simulation procedure in the ABC algorithm, so the same optimal adaptive scaling strategy is used as in Subset Simulation. To avoid duplication of literature for this technique but conferring a sufficient conceptual framework, the method for the optimal choice of the $\sigma_q^{(j)}$ is presented in a brief way. The reader is referred to the recent work of [167], where optimal scaling is addressed for Subset Simulation and a brief historical overview is also given for the topic.

Suppose that the reason for wanting to generate posterior samples is that we wish to calculate the posterior expectation of a quantity of interest which is a function $h : \boldsymbol{\theta} \in \boldsymbol{\Theta} \rightarrow \mathbb{R}$. To evaluate the quality of $\bar{h}$ as an estimator of h, the estimate of its expectation with respect to the samples generated in each of the j-th levels, is considered:

$$\bar{h}_j = \mathbb{E}_{p_\epsilon(\boldsymbol{\theta}|\mathcal{Z}_j)}\left[h(\boldsymbol{\theta})\right] \approx \frac{1}{K}\sum_{k=1}^{K} h(\boldsymbol{\theta}_j^{(k)}) \tag{7.15}$$

where $\boldsymbol{\theta}_j^{(k)}, k = 1, \ldots, K$ are dependent samples drawn from K_c Markov chains generated at the j-th conditional level. An expression for the variance of the estimator can be written as follows [50]:

$$\mathrm{Var}(\bar{h}_j) = \frac{R_j^{(0)}}{K}(1 + \gamma_j), \tag{7.16}$$

with

$$\gamma_j = 2\sum_{\tau=1}^{K_s-1}\left(\frac{K_s - \tau}{K_s}\right)\frac{R_j^{(\tau)}}{R_j^{(0)}} \tag{7.17}$$

In the last equation $K_s = 1/p_0$ is the length of each of the Markov chains, which are considered probabilistically equivalent [50]. The term $R_j^{(\tau)}$ is the autocovariance of $h(\boldsymbol{\theta})$ at lag τ given by $R_j^{(\tau)} = \mathbb{E}\left[h(\boldsymbol{\theta}_j^{(1)})h(\boldsymbol{\theta}_j^{(\tau+1)})\right] - \bar{h}_j^2$, which can be estimated using the Markov chain samples $\left\{\boldsymbol{\theta}_j^{(l),i} : l = 1, \ldots, K_c;\ i = 1, \ldots, K_s\right\}$ as:

$$R_j^{(\tau)} \approx \tilde{R}_j^{(\tau)} = \left[\frac{1}{K - \tau K_c}\sum_{l=1}^{K_c}\sum_{i=1}^{K_s-\tau} h(\boldsymbol{\theta}_j^{(l),i})h(\boldsymbol{\theta}_j^{(l),\tau+i})\right] - \bar{h}_j^2 \tag{7.18}$$

where $K_c = KP_0$, so that $K = K_c K_s$.

Given that the efficiency of the estimator $\bar{h}_j$ is reduced when γ_j is high, the optimal standard deviation for the proposal $\sigma_q^{(j)}$ for simulation level j is chosen adaptively by minimizing γ_j, which gives an acceptance rate $\bar{r}$ for each simulation level in the range of 0.2-0.4 [167]. This is supported by the numerical experiments performed with the examples in the next section, which leads to the following recommendation for ABC-SubSim: *Adaptively choose the standard deviation $\sigma_q^{(j)}$ of the j-th intermediate level so that the monitored acceptance rate $\bar{r}_j \in [0.2, 0.4]$ based on an initial chain sample of small length (e.g. 10 states).*

Note that the conditional probability P_0 influences the number of simulation levels required by the algorithm. The higher P_0 is, the higher the number of simulation levels employed by the algorithm to reach the specified tolerance ϵ, for a fixed number of model evaluations (K) per simulation level. At the same time, the smaller P_0 is, the lower the quality of the posterior approximation, that is, the larger the values of γ_j in Equation 7.16. The choice of P_0 therefore requires a trade-off between computational efficiency and the quality of the ABC posterior approximation.

To examine this fact, let us take a fixed total number of samples, i.e. $K_T = mK$, where m is the number of levels required to reach the target tolerance value ϵ, a tolerance for which $R_m^{(0)} \approx \text{Var}\,[h(\boldsymbol{\theta})]$. The value of m depends on the choice of P_0, which can be optimally set by minimizing the variance of the estimator $\bar{h}_m$ for the last simulation level:

$$\text{Var}(\bar{h}_m) = \frac{R_m^{(0)}}{K_T/m}(1+\gamma_m) \propto m(1+\gamma_m) \tag{7.19}$$

Notice that γ_m also depends upon P_0, although it is not explicitly denoted, as it is shown later in Section 7.4 (Figure 7.3). In the original version of Subset Simulation by [50], $P_0 = 0.1$ was recommended, and more recently in [167], the range $0.1 \leqslant P_0 \leqslant 0.3$ was suggested after a sensitivity study, although the optimality in [167] is related to the coefficient of variation of the failure probability estimate. The value $P_0 = 0.2$ for ABC-SubSim is also supported by the numerical experiments performed with the examples in the next section, where the variance in Equation 7.19 is minimized as a function of P_0, which leads to the recommendation: *For ABC-SubSim, set the conditional probability $P_0 = 0.2$.*

Finally, it is important to remark that an appropriate final tolerance ϵ may be difficult to specify a priori. For these cases, one recommendation is to select ϵ adaptively so that the posterior samples give a stable estimate $\bar{h}_m$ of $\mathbb{E}_{p_\epsilon(\boldsymbol{\theta}|\mathcal{Z}_m)}[h(\boldsymbol{\theta})]$ (Equation 7.15), i.e. a further reduction in ϵ does not change $\bar{h}_m$ significantly.

The performance of ABC-SubSim algorithm dealing with a complex case study in the context of the (fatigue damage) inverse modeling problem proposed in this thesis is investigated in Chapter 10, Section 10.3.

7.4 Illustrative examples

In this section the performance of ABC-SubSim algorithm is illustrated with two different examples: 1) a moving average process of order $d = 2$, MA(2), previously considered in [149]; 2) a single degree-of-freedom (SDOF) linear oscillator subject to white noise excitation, which is an application to a state-space model. Both examples are input-output type problems, in which the notation $\mathcal{D} = \{y_1, \ldots, y_l, \ldots, y_\ell\}$ and $\boldsymbol{x} = \{x_1, \ldots, x_l, \ldots, x_\ell\}$ is adopted for the measured system output sequence and simulated system output respectively, both with length ℓ. The objective of these examples is to illustrate the ability of the proposed algorithm to be able to sample from the ABC posterior for small values of ϵ. In the MA(2) example, the quadratic distance between the two first autocovariances is taken for the metric, as in [149]:

$$\rho_{xy}\big(\eta(\boldsymbol{x}), \eta(\mathbf{y})\big) = \sum_{q=1}^{2} (\tau_{\mathcal{D},q} - \tau_{\boldsymbol{x},q})^2 \tag{7.20}$$

In the last equation, the terms $\tau_{\mathcal{D},q}$ and $\tau_{\boldsymbol{x},q}$ are the autocovariances of $\mathcal{D}$ and $\boldsymbol{x}$, respectively, which are used as summary statistics. They are obtained as $\tau_{\mathcal{D},q} = \sum_{k=q+1}^{\ell} y_k y_{k-q}$ and $\tau_{\boldsymbol{x},q} = \sum_{k=q+1}^{\ell} x_k x_{k-q}$, respectively. The Euclidean distance of $\boldsymbol{x}$ from $\mathcal{D}$ is considered as the metric for the oscillator example:

$$\rho_{xy} = \left[\sum_{l=1}^{\ell} (y_l - x_l)^2\right]^{1/2} \tag{7.21}$$

To evaluate the quality of the posterior, we study the variance of the mean estimator of a quantity of interest $h : \boldsymbol{\theta} \in \boldsymbol{\Theta} \to \mathbb{R}$, defined as follows (see Section 7.3.2):

$$h(\boldsymbol{\theta}) = \sum_{i=1}^{d} \left(\boldsymbol{\theta}_i\right)^2 = \|\boldsymbol{\theta}\|_2^2, \tag{7.22}$$

7.4.1 Example 1: Moving Average (MA) model

Consider a MA(2) stochastic process, with x_l, $l = 1, \ldots, \ell$, the state variable defined by:

$$x_l = e_l + \sum_{i=1}^{d} \theta_i e_{l-i} \tag{7.23}$$

with $d = 2$, $\ell = 100$ or 1000. Here e is a sequence of i.i.d random variables distributed as standard Gaussians $\mathcal{N}(0,1)$: $e = \{e_{-d+1}, \ldots, e_0, e_1 \ldots e_l, \ldots, e_\ell\}$. To avoid unnecessary difficulties, a standard identifiability condition is imposed on this model [149], namely that the roots of the polynomial $f(\lambda) = 1 - \sum_{i=1}^{d} \theta_i \lambda^i$ are outside the unit circle in the complex plane. In this example, $d = 2$, thus this condition is fulfilled when the region $\boldsymbol{\Theta}$ is defined as all $\boldsymbol{\theta} = (\theta_1, \theta_2)$ that satisfy: $-2 < \theta_1 < 2; \theta_1 + \theta_2 > -1; \theta_1 - \theta_2 < 1$. The prior PDF is taken as a uniform distribution over $\boldsymbol{\Theta}$.

Note that, in principle, this example does not need ABC methods given that the likelihood is a multidimensional Gaussian with zero mean and a covariance matrix of order ℓ that depends on (θ_1, θ_2), but its evaluation requires a considerable computational effort when ℓ

is large [168]. This example was also used to illustrate the ABC method in [149] where it was found that the performance is rather poor if the metric is the one in Equation 7.21 (which uses the "raw" data), but ABC gave satisfactory performance when the metric in Equation 7.20 was used. For comparison with Figure 1 in [149], the latter is also chosen here.

For this illustrative example, synthetic data is used for $\mathcal{D}$ by generating it from Equation 7.23 considering $\boldsymbol{\theta}_{true} = (0.6, 0.2)$. The chosen values of the control parameters for ABC-SubSim are shown in Table 7.2. The ABC-SubSim results are presented in Figure 7.2, which shows that the mean estimate of the "approximate" posterior samples at each level is close to $\boldsymbol{\theta}_{true}$ for both $\ell = 100$ and $\ell = 1000$ cases. Figure 7.2a shows the case $\ell = 100$ which can be compared with Figure 1 in [149]. In Figure 7.2a, a total of 3000 samples were used to generate 1000 samples to represent the posterior, whereas in [149], 1,000,000 samples were used to generate 1000 approximate posterior samples using the standard ABC algorithm that was called Algorithm 4 in Section 7.1. The ABC-SubSim posterior samples give a more compact set that is better aligned with the exact posterior contours given in Figure 1 of [149]. Figure 7.2b shows that for the case $\ell = 1000$, ABC-SubSim used 4000 samples to generate 1000 samples representing the much more compact posterior that corresponds to ten times more data.

model	sample size	cond. prob.	proposal std. dev.				sim. levels
	(K)	(P_0)	$(\sigma_q^{(2)})$	$(\sigma_q^{(2)})$	$(\sigma_q^{(2)})$	$(\sigma_q^{(2)})$	(m)
MA(2) ($\ell = 100$)	$1000^{(*)}$	0.2	0.4	0.2	0.1	$--$	3
MA(2) ($\ell = 1000$)	$1000^{(*)}$	0.2	0.4	0.2	0.1	0.04	4
Oscillator	$2000^{(*)}$	0.2	0.35	0.1	0.05	0.001	4

(*): per simulation level

Table 7.2: *Parameter configuration of ABC-SubSim algorithm for the MA(2) and SDOF linear oscillator examples. The information shown in the first and second rows correspond to the MA(2) example with $\ell = 100$ and $\ell = 1000$, respectively. The values shown from 4-th to 7-th column correspond to the optimal values for the proposal standard deviation per simulation level for both examples*

A preliminarily sensitivity study was done to corroborate the choice of the algorithm control parameters described in Section 7.3.2 and the results are shown in Figure 7.3. As described in Section 7.3.2, the optimal value of P_0 is the one that minimizes $m(1 + \gamma_m)$ for fixed tolerance ϵ. As an exercise, a final tolerance $\epsilon = 1.12 \cdot 10^4$ is considered.[2] The results in Figure 7.3 show that $P_0 = 0.2$ is optimal since then $m(1 + \gamma_m) = 3(1 + 2.8) = 11.4$; whereas for $P_0 = 0.5$ and $P_0 = 0.1$, it is $7(1 + 0.86) = 13.1$ and $2(1 + 5.1) = 12.2$, respectively. These results are consistent with those for rare event simulation in [167]. Observe also that the optimal standard deviation $\sigma_q^{(j)}$ for the Gaussian proposal PDF at the j-th level that minimizes γ_j occurs when the acceptance rate $\bar{r}_j$ in MMA lies in the range 0.2-0.4, which is also consistent with that found in [167] (except for the case of very low acceptance rate where the process is mostly controlled by the noise).

[2]It is unlikely that one or more values from the ϵ-sequence obtained using different P_0 values coincide exactly. Hence, the nearest value to the final tolerance is consider for this exercise.

7.4.2 *Example 2: Linear oscillator*

Consider the case of a SDOF oscillator subjected to white noise excitation as follows:

$$m\ddot{\zeta} + c\dot{\zeta} + k\zeta = f(t) \tag{7.24}$$

where $\zeta = \zeta(t) \in \mathbb{R}$ [m], m [Kg], k [N⁄m] and c [N s⁄m] are the displacement, mass, stiffness and damping coefficient, respectively. To construct synthetic input, a discrete-time history of input force f [N] modeled by Gaussian white noise with spectral intensity $S_f = 0.0048$ [N^2 · s], is used. The time step used to generate the input data is 0.01 [s], which gives an actual value for the variance of the discrete input force $\sigma_f^2 = 3$ [N] [169, 170].

The probability model that gives the likelihood function of this example is Gaussian and so, it can be written explicitly although its evaluation requires the computation of a high dimensional matrix inverse [171]. Repeated evaluations of the likelihood function for thousands of times in a simulation-based inference process is computationally prohibitive for large-size datasets. However it is easy to simulate datasets from this model after some trivial manipulations of Equation 7.24 [171]. Therefore, this example is particularly suited for the use of ABC methods.

The mechanical system is assumed to have known mass $m = 3$ [Kg] and known input force giving the excitation. For the state-space simulation, denote the *state vector* by $s(t) = \left[\zeta(t), \dot{\zeta}(t)\right]^T$. Equation 7.24 can be rewritten in state-space form as follows:

$$\dot{s}(t) = \mathbf{A}_c s(t) + \mathbf{B}_c f(t) \tag{7.25}$$

where $\mathbf{A}_c \in \mathbb{R}^{2\times 2}$, $\mathbf{B}_c \in \mathbb{R}^{2\times 1}$ are obtained as:

$$\mathbf{A}_c = \begin{pmatrix} 0 & 1 \\ -m^{-1}k & -m^{-1}c \end{pmatrix} \qquad \mathbf{B}_c = \begin{pmatrix} 0 \\ m^{-1} \end{pmatrix} \tag{7.26}$$

By approximating the excitation as constant within any interval, i.e. $f(l\triangle t + \tau) = f(l\triangle t), \forall \tau \in [0, \triangle t)$, Equation 7.25 can be discretized to a difference equation: $\forall l \geqslant 1$,

$$s_l = \mathbf{A} s_{l-1} + \mathbf{B} f_{l-1} \tag{7.27}$$

with $s_l \equiv s(l\triangle t)$, $f_l \equiv f(l\triangle t)$, $l = 0, 1, 2, \ldots, \ell$, and $\mathbf{A}$ and $\mathbf{B}$ are matrices given by:

$$\begin{aligned} \mathbf{A} &= e^{(\mathbf{A}_c \triangle t)} \\ \mathbf{B} &= \mathbf{A}_c^{-1} \left(\mathbf{A} - \mathbf{I}_2\right) \mathbf{B}_c \end{aligned} \tag{7.28}$$

where $\mathbf{I}_2$ is the identity matrix of order 2. The use of discrete-time input and output data here is typical of the electronically-collected data available from modern instrumentation on mechanical or structural systems.

In this example, $\boldsymbol{\theta} = (k, c)$ is adopted as the unknown model parameters while y_l and x_l denote the actual and predicted response measurements at each $\triangle t$. Samples of x_l for a given input force time history $\{f_l\}$ and $\boldsymbol{\theta}$, can be readily generated by the underlying state-space model:

$$s_l = \mathbf{A}s_{l-1} + \mathbf{B}f_{l-1} + e_l \tag{7.29a}$$

$$x_l = s_l + e'_l \tag{7.29b}$$

where e_l and e'_l are error terms to account for model prediction error and measurement noise, respectively. Since in reality these errors would be unknown, the Principle of Maximum Information Entropy [19, 22, 172] is adopted to choose e_l and e'_l as i.i.d. Gaussian variables, $e_l \sim \mathcal{N}(0, \sigma_e^2 \mathbf{I}_2)$, $e'_l \sim \mathcal{N}(0, \sigma_{e'}^2 \mathbf{I}_2)$ and so they can be readily sampled. For simplicity, the values $\sigma_e^2 = 10^{-2}$ and $\sigma_{e'}^2 = 10^{-6}$ are adopted for this example, taking them as known. The dataset is defined as $\mathcal{D} = \{y_1, \ldots, y_l, \ldots, y_\ell\}$, being collected during a total period of time $t = \ell \triangle t$, starting from known initial conditions $s_0 = [0.01, 0.03]^T$ (units expressed in [m] and [m/s] respectively). In this example, the noisy measurements y_l are synthetically generated from Equation 7.29 for the given input force history and for model parameters $\boldsymbol{\theta}_{true} = (k = 4\pi, c = 0.4\pi)$. A sampling rate for the resulting output signal of 100 [Hz] ($\triangle t = 0.01$[s]) is also adopted during a sampling period of $t = 3$[s], hence $\ell = 300$. In addition, a uniform prior is chosen over the parameter space $\boldsymbol{\Theta}$ defined by the region $0 < \theta_i \leqslant 3$; $i \in \{1, 2\}$. Table 7.2 provides the information for the algorithm configuration.

The results shown in Figure 7.4 are very satisfactory in the sense that ABC-SubSim can reconstruct the true signal with high precision with only a moderate computational cost. The posterior samples show that in Bayesian updating using noisy input-output data, the stiffness parameter $k = 4\pi\theta_1$ is identified with much less uncertainty that the damping parameter $c = 0.4\pi\theta_2$. The normalized mean value over the set of posterior samples corresponding to the smallest value of ϵ is $\bar{\boldsymbol{\theta}} = (1.00, 1.03)$, which is very close to the normalized true value $\boldsymbol{\theta}_{true} = (1.0, 1.0)$, (even if the exact likelihood was used, the equality $\bar{\boldsymbol{\theta}} = \boldsymbol{\theta}_{true}$ would not be expected because of the noise in the synthetic data $\mathcal{D}$).

7.5 Comparison with recent ABC algorithms

In this section, ABC-SubSim is compared with a selection of recent versions of sequential ABC algorithms: ABC-SMC [165], ABC-PMC [162] and ABC-PT [163], which are listed in Table 7.1 (see Section 7.1). The same number of evaluations per simulation level are adopted for all algorithms, corresponding to 1000 and 2000 for the MA(2) and SDOF model, respectively. The sequence of tolerance levels obtained by ABC-SubSim is set using $P_0 = 0.5$ for the rest of the algorithms (see Table 7.3). This was done because the recommended near-optimal value of $P_0 = 0.2$ (see Section 7.3.2) for ABC-SubSim produced a sequence of ϵ values that decreased too quickly for ABC-PMC and ABC-SMC to work properly. It should be noted that this non-optimal choice of P_0 for ABC-SubSim and the use of its ϵ-sequence

provide considerable help for the competing algorithms. The proposal PDFs are assumed to be Gaussian for all of the algorithms.

The results shown in Figure 7.5 are evaluated over the intermediate posterior samples for each simulation level and were obtained considering the mean of 100 independent runs of the algorithms, a large enough number of runs to ensure the convergence of the mean. In this example, the focus is on the number of model evaluations together with the quality of the posterior. The left side of Figure 7.5 shows the accumulated amount of model evaluations employed by each of the competing algorithms. Note that each algorithm requires the evaluation of auxiliary calculations, like those for the evaluation of particle weights, transition kernel steps, etc. However, this cost is negligible because the vast proportion of computational time in ABC is spent on simulating the model repeatedly. The number of model evaluations for ABC-PMC and ABC-PT is variable for each algorithm run, so in both cases the mean (labelled dotted lines) and a 95% band (dashed lines) is presented. In contrast, ABC-SubSim and also ABC-SMC make a fixed number of model evaluations at each simulation level. Observe that the computational saving is markedly high when comparing with ABC-PMC.

Model	ϵ_1	ϵ_2	ϵ_3	ϵ_4	ϵ_5	ϵ_6	ϵ_7	ϵ_8	ϵ_9	ϵ_{10}
MA(2) $(\times 10^4)$	122	50.2	21.7	9.61	4.57	2.29	1.12	0.56	0.28	0.14
Oscillator $(\times 10^{-3})$	11.7	9.9	8.2	5.4	4.0	3.0	2.4	2.0	1.8	1.6

Table 7.3: *Set of tolerance values used for comparing the sequential ABC algorithms established using ABC-SubSim with* $P_0 = 0.5$

Regarding the quality of the posterior, two metrics are considered: a) the sample mean of the quadratic error between $\bar{\theta}$ and θ_{true}, i.e., $\|\bar{\theta}_j - \theta_{true}\|_2^2$, as an accuracy measure; and b) the differential entropy[3] of the final posterior, by calculating $1/2 \ln |(2\pi e)^d \det \left[cov(\theta_j)\right]|$, as a measure quantifying the posterior uncertainty of the model parameters. The results are shown on the right side of Figure 7.5. Only the last 4 simulation levels are presented for simplicity and clearness.

This comparison shows that ABC-SubSim gives the same, or better, quality than the rest of the ABC algorithms to draw ABC posterior samples when ϵ is small enough, even though it used a smaller number of model evaluations.

[3]This expression for the differential entropy is actually an upper-bound approximation to the actual differential entropy, where the exactness is achieved when the posterior PDF is Gaussian.

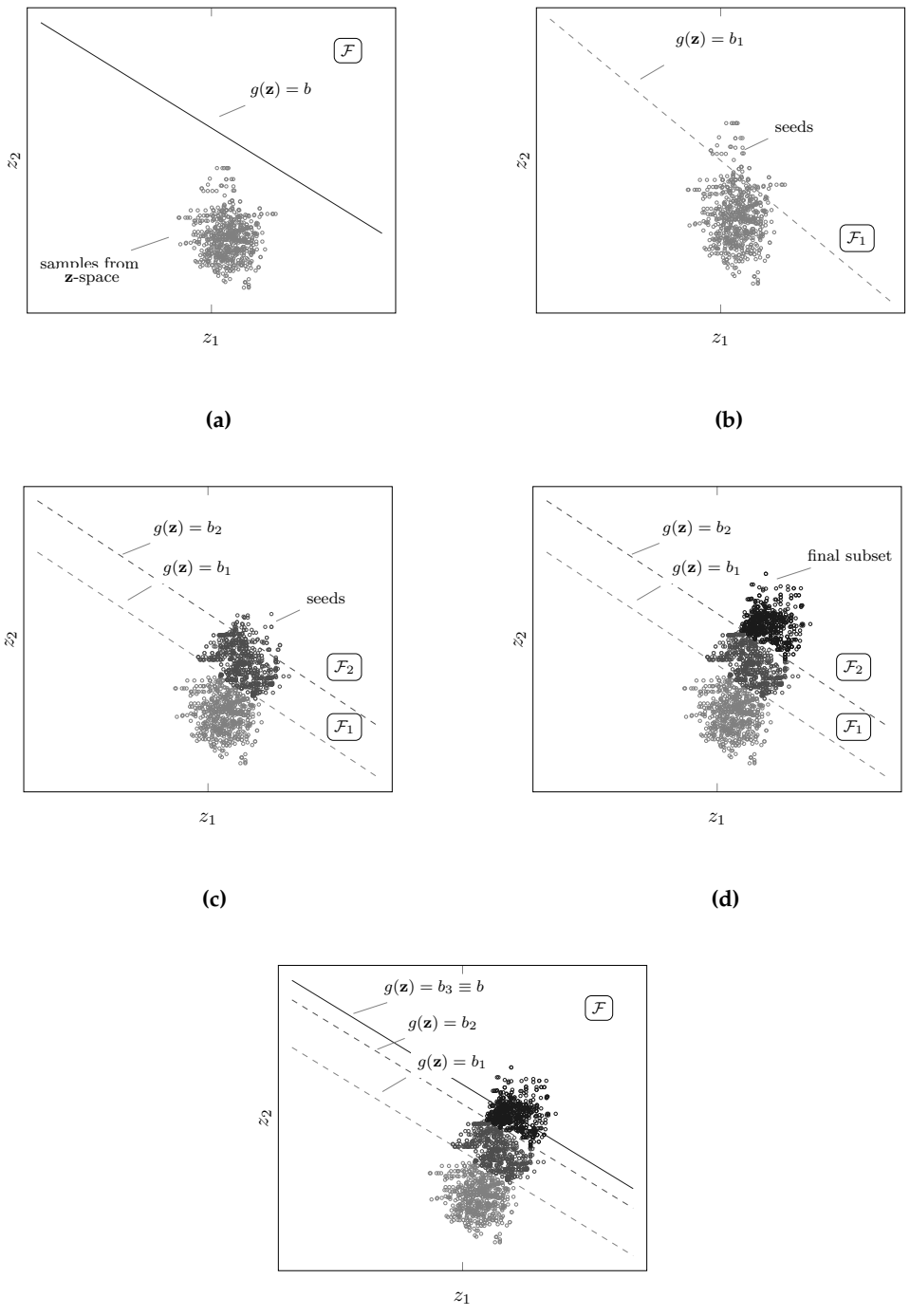

Figure 7.1: *Conceptual example of Subset Simulation. Panels (a)& (b) represent the initial set of samples of dimension two simulated according to any specified model, and the selection of seeds whereby $\mathcal{F}_1$ is defined, respectively. In (c), new samples simulated according to $p(\mathbf{z}|\mathcal{F}_1)$ are represented along with the seeds for defining the subsequent intermediate failure region, which is represented using samples in panel (d). Panel (e) represents the final step where the whole set of samples arranged through subsets is showed along with the sequence of intermediate threshold levels until the final one (solid line) is reached.*

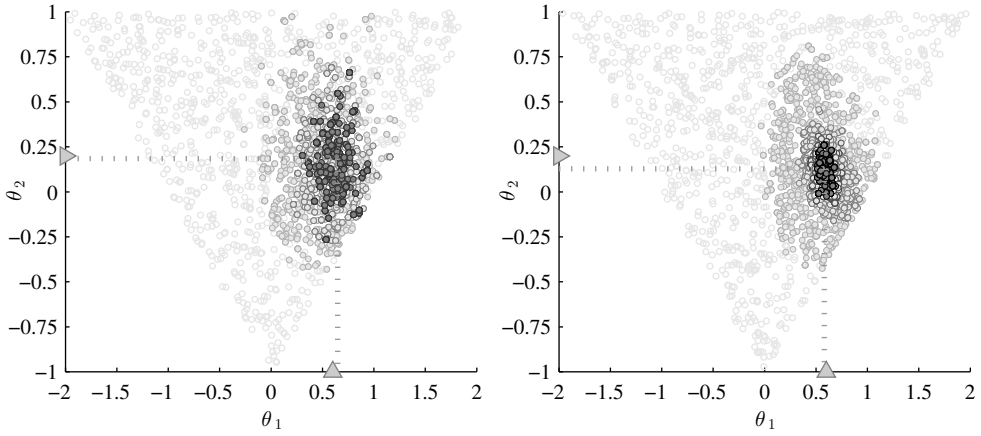

(a) $\ell = 100$ **(b)** $\ell = 1000$

Figure 7.2: *ABC-SubSim output for the MA(2) model with (a)* $\ell = 100$ *and (b)* $\ell = 1000$*. Each subplot presents samples (circles) in the model parameter space* $\boldsymbol{\Theta}$*, where the latest final posterior samples are marked using darker color. The coordinates of the mean estimate of the latest posterior are represented in dotted line. The triangles are the coordinates of* $\boldsymbol{\theta}_{true}$*. To reveal the uncertainty reduction, the intermediate posterior samples are superimposed in increasing gray tones. Gray rings correspond to prior samples.*

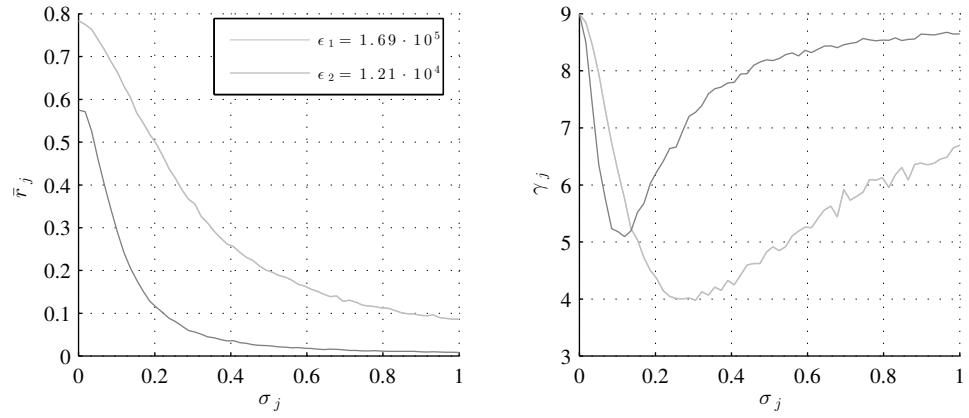

(a) $P_0 = 0.1$

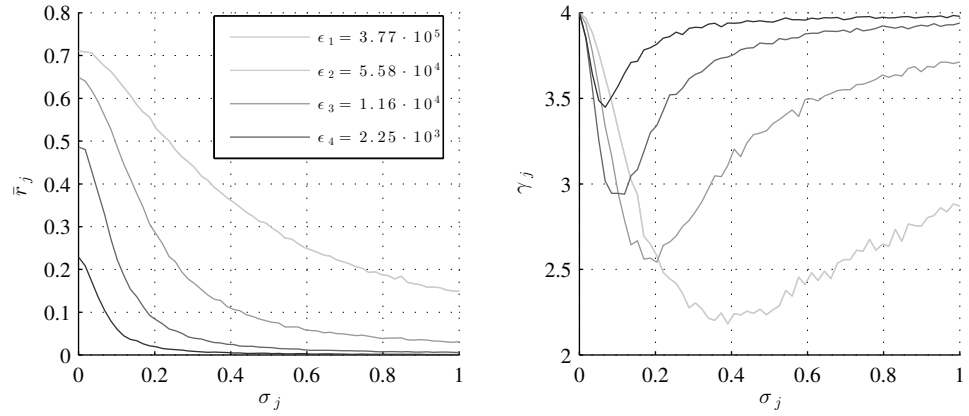

(b) $P_0 = 0.2$

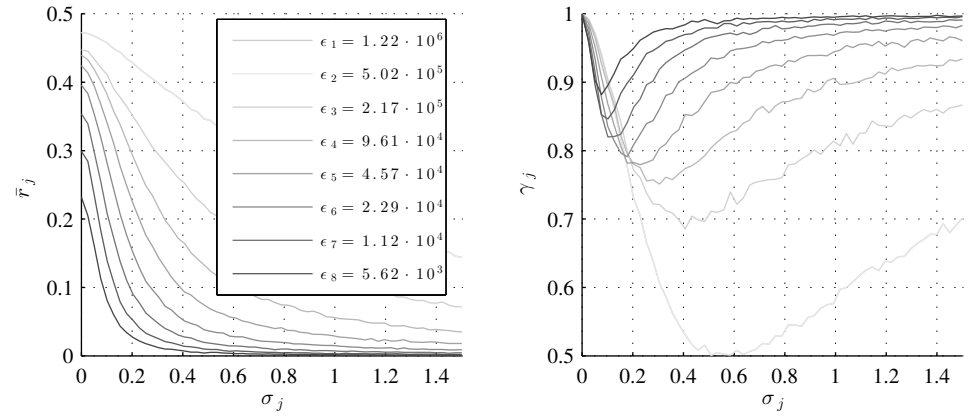

(c) $P_0 = 0.5$

Figure 7.3: *Sensitivity study of the acceptance rate $\bar{r}_j$ and autocorrelation factor γ_j in relation to different values of the standard deviation σ_j for the MA (2) model with $\ell = 1000$ and for different values of $P_0 = 0.1(a), 0.2(b),$ and $0.5(c)$. $K = 1000$ samples are employed per simulation level. Darker curves correspond to higher simulation levels. The tolerance values are indicated. The numerical values of each plot are obtained considering the mean of 50 independent runs of the algorithm.*

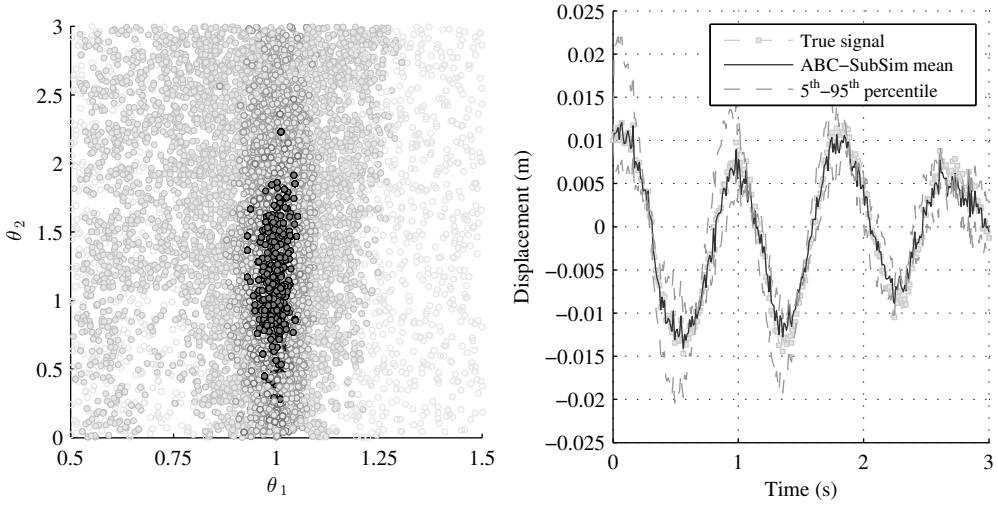

Figure 7.4: *Results of the inference for the oscillator model for a duration of $t = 3$ seconds. Left: scatter plot of posterior samples of $\boldsymbol{\theta}$ for intermediate levels and the final level (darker color). The horizontal and vertical scale are normalized by a factor of 4π and 0.4π, respectively. Right: synthetic signal response of the oscillator, together with the mean estimate of the ABC-SubSim approximation and two percentiles.*

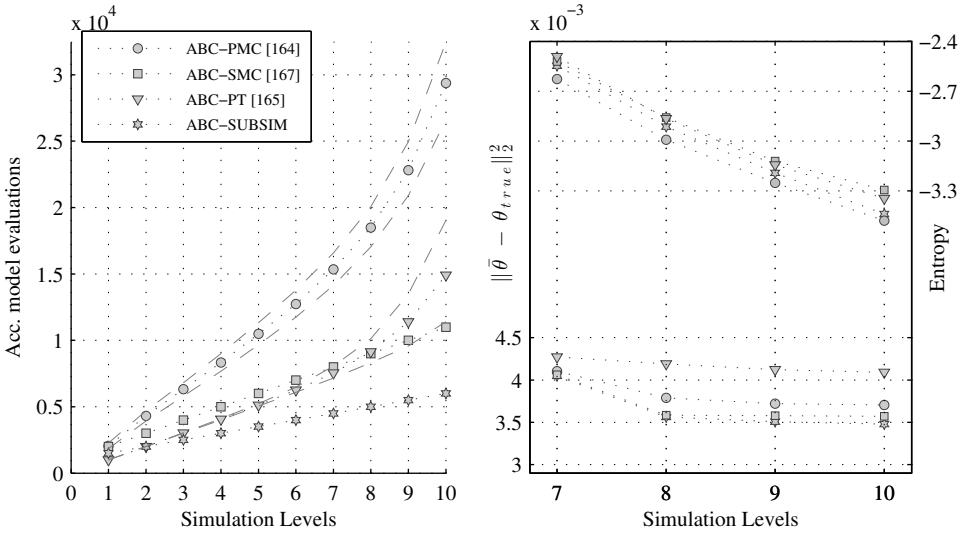

(a) MA(2)

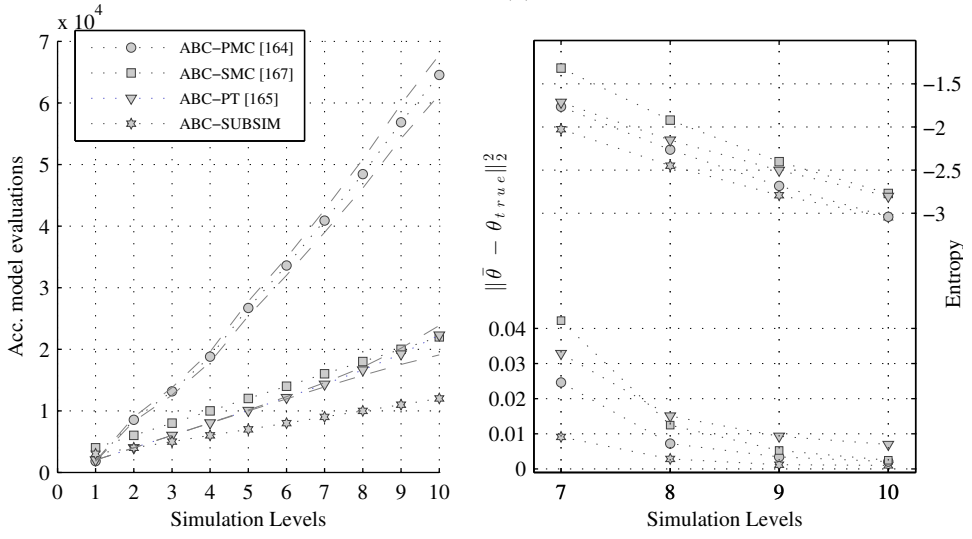

(b) Oscillator

Figure 7.5: *Left: Accumulated model evaluations per simulation level for (a) MA(2), (b) Oscillator. Right: differential entropy (right-side of the y-label) of the intermediate posterior samples and mean quadratic error between $\bar{\theta}$ and θ_{true} (left-side of the y-label). Both measures are evaluated for the last four intermediate simulation levels: ϵ_j, $j = 7, 8, 9, 10$. To be equivalent to ABC-SubSim, we consider for the implementation of the ABC-SMC algorithm a percentage of alive particles of* 50% *and only one algorithm repetition (see the implementation details in [165]).*

Part III

CASE STUDIES

8

Damage data used for validation

In this part, the theoretical contributions and research objectives proposed in this thesis are validated using two SHM datasets. This chapter summarized both datasets. The first set corresponds to several sequences of relative stiffness reduction data for GRPF laminates. This dataset is taken from the work of Wei *et al.* [11]. To avoid literature repetition, the fundamental details about this test are presented in Section 8.1. The second dataset corresponds to micro-cracks density and relative effective stiffness data. This set is taken from the NASA Ames Prognostics Data Repository [1], distributed by the Prognostics Center of Excellence (PCoE) of NASA Ames Research Center as an open-access dataset. The relevant details of this dataset for this thesis are summarized in Section 8.2.

8.1 Dataset 1: GFRP laminates

This dataset corresponds to sixteen sequences of damage for quasi-isotropic glass fiber notched laminates with lay-up $[-45/0/45/90]_S$, subjected to identical and independent fatigue tests. This set of damage data is taken from the aforementioned work of Wei *et al.* [11] (see Table 3 in [11]). In their experiment, tension-tension fatigue tests were conducted under a load-controlled loop of cyclical loadings with a frequency of $f = 5$ [Hz], a maximum applied tension of 161 [MPa] (50% of their ultimate stress), and a stress ratio $R = 0.1$ (relation between the minimum and maximum stress for each cycle). More details regarding the experimental set-up and measurement procedure are reported in [11]. For this dataset, the observed damage state y_n is computed as a relative reduction of the longitudinal Young's

modulus of the laminate, as follows:

$$y_n = \begin{cases} \dfrac{E_{x,0} - E^*_{x,n}}{0.4\, E_{x,0}} & \text{if} \quad E^*_{x,n} \geqslant 0.6\, E_{x,0} \\ 1 & \text{if} \quad E^*_{x,n} < 0.6\, E_{x,0} \end{cases} \tag{8.1}$$

where $E^*_{x,n}$ is the effective longitudinal (x-direction) Young's modulus of the laminate at fatigue cycle n, and $E_{x,0}$ is the initial (undamaged) longitudinal Young's modulus of the laminate. In view of Equation 8.1, the *absorbing* state is defined as the damage state for which the longitudinal Young's modulus is reduced to 60% of its initial value. For the sake of clarity, the damage sequences for this dataset are provided in Table 8.1, and illustrated in Figure 8.1.

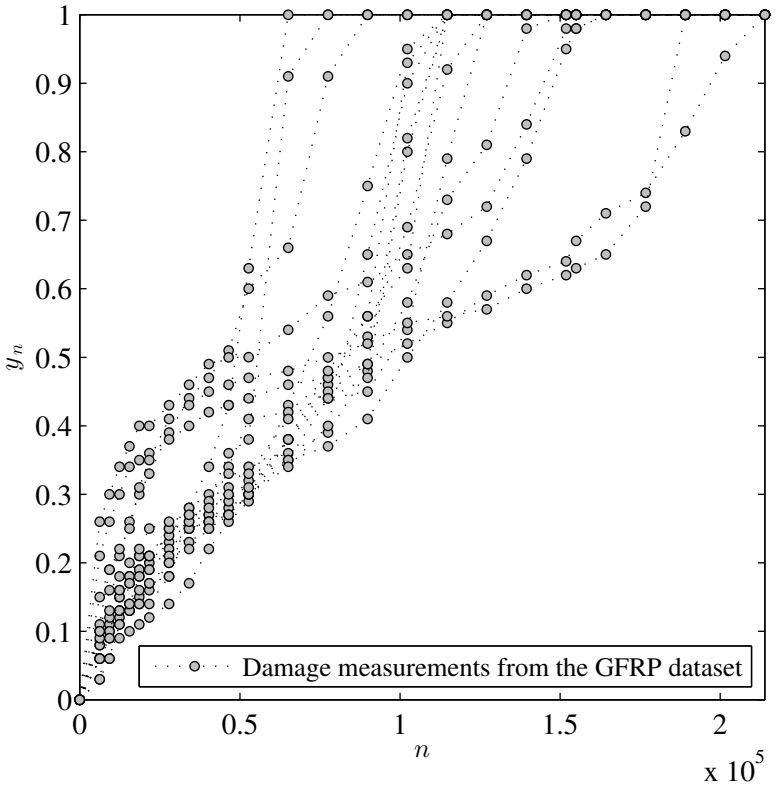

Figure 8.1: *Experimental sequences of damage for quasi-isotropic S2-Glass/E733FR laminates taken from [11].*

8.2 Dataset 2: CFRP laminates

The dataset presented in this section corresponds to run-to-failure tension-tension fatigue experiments for CFRP laminates carried out by the Stanford Structures and Composites Laboratory (SACL) and the Prognostic Center of Excellence (PCoE) of NASA Ames Research Center [1]. Both, effective stiffness data and SHM measurements of internal damage, such as micro-crack density and delamination area, were periodically measured during the fatigue

Cycle	$Y^{(1)}$	$Y^{(2)}$	$Y^{(3)}$	$Y^{(4)}$	$Y^{(5)}$	$Y^{(6)}$	$Y^{(7)}$	$Y^{(8)}$	$Y^{(9)}$	$Y^{(10)}$	$Y^{(11)}$	$Y^{(12)}$	$Y^{(13)}$	$Y^{(14)}$	$Y^{(15)}$	$Y^{(16)}$
0	0	0	0	0	0	0	0	0	0	0	0	0	0	0	0	0
6200	0.11	0.03	0.03	0.21	0.08	0.1	0.08	0.26	0.09	0.1	0.06	0.06	0.06	0.06	0.1	0.15
9300	0.19	0.11	0.06	0.26	0.09	0.11	0.11	0.3	0.1	0.12	0.1	0.06	0.13	0.09	0.16	0.19
12400	0.21	0.16	0.12	0.3	0.09	0.13	0.13	0.34	0.15	0.13	0.15	0.11	0.16	0.11	0.18	0.22
15500	0.26	0.18	0.13	0.34	0.1	0.14	0.13	0.37	0.18	0.13	0.17	0.14	0.18	0.17	0.2	0.25
18600	0.3	0.19	0.15	0.35	0.11	0.18	0.14	0.4	0.19	0.14	0.21	0.16	0.21	0.18	0.22	0.31
21700	0.33	0.2	0.16	0.36	0.12	0.19	0.14	0.4	0.21	0.17	0.21	0.17	0.21	0.19	0.25	0.35
27900	0.39	0.23	0.2	0.38	0.14	0.22	0.18	0.43	0.24	0.18	0.21	0.2	0.25	0.25	0.26	0.41
34100	0.44	0.26	0.23	0.4	0.17	0.25	0.28	0.46	0.27	0.25	0.25	0.22	0.28	0.26	0.27	0.43
40300	0.47	0.27	0.25	0.42	0.22	0.26	0.34	0.49	0.27	0.26	0.26	0.25	0.3	0.29	0.28	0.45
46500	0.51	0.31	0.27	0.43	0.26	0.28	0.43	0.5	0.34	0.27	0.29	0.27	0.33	0.36	0.3	0.46
52700	0.6	0.34	0.3	0.44	0.29	0.3	0.63	0.5	0.41	0.3	0.32	0.3	0.33	0.38	0.31	0.47
65100	0.66	0.36	0.43	0.46	0.38	0.35	1.04	0.54	0.42	0.38	0.35	0.34	0.41	0.91	0.38	0.48
77500	0.91	0.39	0.56	0.47	0.46	0.37		0.59	0.47	0.48	0.44	0.4	0.45	1.5	0.44	0.5
89900	1.16	0.48	0.75	0.49	0.56	0.41		0.61	0.53	0.56	0.47	0.65	0.49		0.45	0.52
102300		0.58	0.95	0.52	0.93	0.5		0.65	0.69	0.63	0.8	0.9	0.82		0.54	0.55
114700		0.73	1.14	0.55	1.33	0.58		0.68	0.92	1.07	1.23	1.1	1.1		0.79	0.56
127100		0.81		0.59		0.67		0.72	1.25						1.09	0.57
139500		0.98		0.62		0.79		0.84								0.6
151900		1.01		0.64		0.95		0.98								0.62
154986				0.67		0.98		0.98								0.63
164300				0.71		1.1		1.09								0.65
176700				0.74												0.72
189100				0.83												1
201500				0.94												
213900				1.15												

Table 8.1: *Dataset for $[-45/0/45/90]_S$ S2-Glass/E733FR laminates taken from [11]. Note that some measurements were taken outside of the $[0, 1]$ interval because of experimental error in measuring stiffness. Hence, to ensure the existence of an absorbent state it is redefined as the state corresponding to the first measurement that fulfills $y_n \geqslant 1$. As stated in Chapter 9, this definition only affects a small portion of measurements near the absorbent state where transition probabilities are close to value of 1 and hence the likelihood function $p(\mathcal{D}|\boldsymbol{\theta}, \mathcal{M})$ is barely affected.*

test [173–175]. The tests were performed over several laminates for three different symmetric layup configurations: *Layup 1*) $[0_2/90_4]_S$, *Layup 2*) $[0/90_2/45/-45/90]_S$, and *Layup 3*) $[90_2/45/-45]_S$.

For all the configurations, Torayca T700G unidirectional prepreg material was used for 15.24 [cm] $\times$ 25.4 [cm] coupons with dogbone geometry and a lateral notch with dimensions 5.08 [mm] $\times$ 19.3 [mm], thereby introducing additional sources of uncertainty and then demonstrating the proposed framework under more realistic conditions. The ply properties of these laminates are provided in Table 8.2. Fatigue tests were conducted under load-controlled tension-tension cyclic loading, with a maximum applied load of 31.13 [KN], a frequency $f = 5$ [Hz], and a stress ratio $R = 0.14$. Damage data were collected from a network of 12 piezoelectric (PZT) sensors using Lamb wave signals and three triaxial strain-gages. The fatigue cycling tests were stopped at periodical cycles to collect the PZT sensor data at different interrogation frequencies as well as strain-gauges data. Additionally, X-rays images were taken to visualize and characterize subsurface damage features, in particular, the micro-crack density.

The collected SHM information was then used to develop a method for on-line detecting, sizing and quantifying damage features in composites [176]. These SHM methods were mainly contributed by Larrosa [176], and Peng *et al.* [177]. In [176], a relation between PZT raw signals and micro-cracks density was proposed. In addition, a novel method was investigated to obtain an approximation of the effective stiffness of the laminate due to the micro-cracks density estimated by Lamb wave signals. In [177], a Bayesian method for locating and sizing delamination was proposed using Lamb waves.

In this thesis, the data from Layup 1 (laminate L1S19 in [1]) is taken to illustrate the proposed methodology. A summary of such dataset is presented in Table 8.3 while a graphical representation is provided in Figure 8.3. The experimental set-up is shown in Figure 8.2. More details about these tests are reported in [1, 178].

Young's Modulus (longitudinal) E_1 [GPa]	Young's Modulus (transverse) E_2 [GPa]	Poisson ratio (in plane) ν_{12}	Poisson ratio (out-of-plane) ν_{23}	Shear modulus G_{12} [GPa]	Shear modulus (out-of-plane) G_{23} [GPa]	Thickness t [mm]
127.55	8.41	0.309	0.49	6.2	2.82	0.152

Table 8.2: *Ply properties for CFRP laminates used in the calculations*

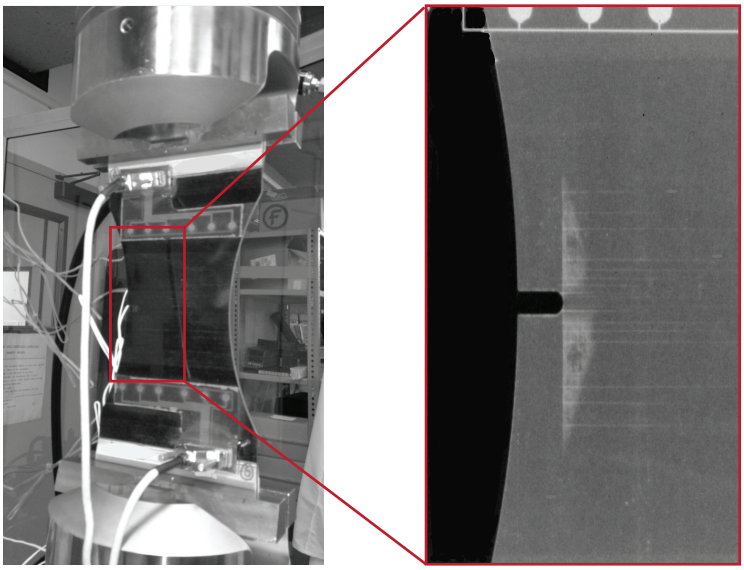

Figure 8.2: *Fatigue experiment for a T700G CFRP $[0_2/90_4]_s$ laminate. Shown in the left is the in situ set-up of the specimen on the testing machine. Observe the SHM system based on PZT sensors (SMART Layer® from Acellent Technologies Inc), which are placed on top and bottom of the specimen. The right panel shows a X-ray image of the specimen after 100 fatigue cycles. The bright white areas denote delaminated interfaces whereas the horizontal white lines are matrix cracks.*

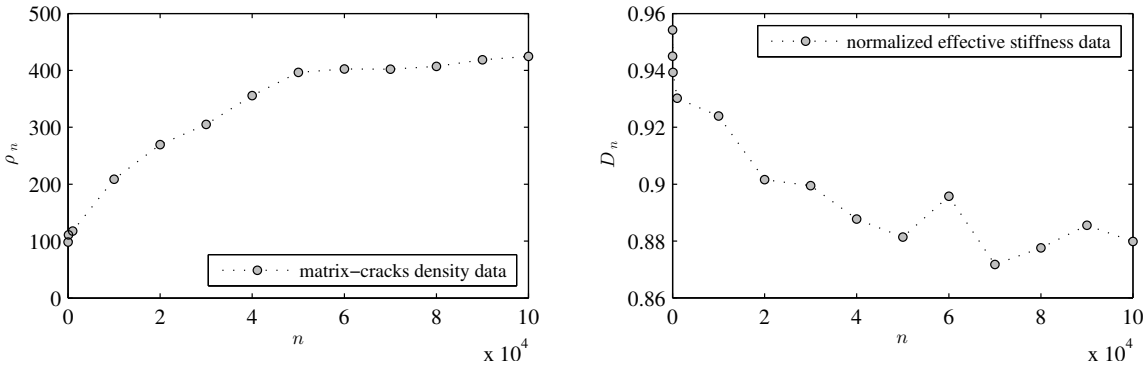

(a) Micro-cracks density **(b)** Normalized effective stiffness

Figure 8.3: *Experimental sequence of damage for cross-ply CFRP laminate (L1S19 in [1])*

Cycles, n_k	10	100	1,000	10,000	20,000	30,000	40,000	50,000	60,000	70,000	80,000	90,000	100,000
ρ_{n_k} $\left[\#\,\text{cracks}/m\right]$	98.2	111.0	117.4	208.5	269.6	305.0	355.5	396.4	402.3	402.1	407.0	418.5	424.5
D_{n_k}	0.954	0.939	0.930	0.924	0.902	0.899	0.888	0.881	0.896	0.872	0.877	0.885	0.880

Table 8.3: *Experimental sequence of damage for cross-ply $[0_2/90_4]_s$ Torayca T700 CFRP laminate taken from the Composite dataset, NASA Ames Prognostics Data Repository [1], corresponding to specimen L1S19 in the dataset. The data are presented for micro-cracks density (ρ_{n_k}) and normalized effective stiffness (D_{n_k}). Note the difference between the concept for normalized effective stiffness used in this table and relative stiffness reduction defined in Equation 8.1.*

9

Model class assessment for Markov chain model

This chapter investigates the performance of the Markov chain damage model proposed in Chapter 5 in application to the two nominally different sets of data presented in Chapter 8. To this end, the Bayesian approach proposed in Chapter 4 is applied here to assess the degree of plausibility of several candidate model classes based on Markov chains. The general problem settings are provided in Section 9.1. Section 9.2 focuses on the assessment of such models classes in application to damage data for GFRP quasi-isotropic laminates. As a side objective, the minimum required set of data is investigated using a novel information-theoretic approach. In Section 9.3, the assessment is specialized for damage data for micro-cracks density and stiffness loss from a CFRP cross-ply laminate. The results of the assessment are discussed in Section 9.4.

9.1 Methodology

To assess the performance of the Markov chain model proposed in Chapter 5, a set of four model classes $\mathbf{M} = \{\mathcal{M}_1, \ldots, \mathcal{M}_4\}$ is defined based on the methodology presented in Section 5.2.3; i.e., the j-th model class in the set $\mathbf{M}$ is represented by a Markov chain parameterized by $\boldsymbol{\theta} = \{\theta_1, \theta_1', \ldots, \theta_j, \theta_j', p\}$, along with the corresponding prior PDF of model parameters $p(\boldsymbol{\theta}|\mathcal{M}_j)$. This implies that a maximum of 9 parameters are employed for the modeling: from 3 parameters for $\mathcal{M}_1$ to 9 for $\mathcal{M}_4$ (see Table 5.1). For each model class, the prior PDF of model parameters is chosen as the product of independent uniform distributions[1] for each model parameter, i.e., $p(\boldsymbol{\theta}|\mathcal{M}_j) = \prod_{i=1}^{d} p(\theta_i|\mathcal{M}_j)$, where $p(\theta_i|\mathcal{M}_j) =$

[1] A rational way to define a probability model for the prior PDF is to select it such that it produces the largest uncertainty (largest Shannon entropy) [19, 52]. The maximum entropy PDF for a bounded variable is the uniform distribution.

$\mathcal{U}(0,1),\ i = 1,\ldots,d$ and $\boldsymbol{\theta} \in \mathbb{R}^d$. Therefore the posterior PDF of model parameters is given by Bayes' Theorem as

$$p(\boldsymbol{\theta}|\mathcal{D},\mathcal{M}_j) = c^{-1}p(\mathcal{D}|\boldsymbol{\theta},\mathcal{M}_j) \tag{9.1}$$

over the unit hypercube of dimension d, where the likelihood function $p(\mathcal{D}|\boldsymbol{\theta},\mathcal{M}_j)$ is obtained following the methodology proposed in Section 5.3 (recall Equation 5.15).

To numerically solve the Bayesian inference defined in Equation 9.1, the Metropolis-Hasting algorithm explained in Section 4.1.2 is applied here using a multivariate Gaussian proposal PDF with identical standard deviation in each dimension, which corresponds to the *Random Walk* version of the algorithm [54]. The algorithm configuration is provided in Table 9.1 for both case studies.

	Dataset 1				Dataset 2			
	$\mathcal{M}_1$	$\mathcal{M}_2$	$\mathcal{M}_3$	$\mathcal{M}_4$	$\mathcal{M}_1$	$\mathcal{M}_2$	$\mathcal{M}_3$	$\mathcal{M}_4$
σ_q	0.007	0.005	0.005	0.0035	0.01	0.01	0.006	0.006
N_s	10^4	10^4	10^4	10^4	10^5	10^5	10^5	10^5
Burn-in	400	400	500	700	10^4	10^4	10^4	10^4
Acc-rate	23%	34%	37%	40%	28%	35%	31%	38%

Table 9.1: *Metropolis Hastings algorithm configuration for Bayesian model updating using Dataset 1 (left) and Dataset 2 (right)*

Note from Table 9.1 that the more parameters that are included in the model class definition, the smaller the value of σ_q that is required to achieve an acceptance rate within the recommended interval of $[20\% - 40\%]$ for a given number of simulations, which agrees with [62, 63].

As a general comment for algorithm configuration, it is noted that choosing the first sample of the θ_i and $\theta_i^{'}$ parameters with values close to the diagonal in the unit time transformation space (recall Figure 5.1), reduces significantly the burn-in period and so the time to convergence. Mathematically: $(\theta_1 \approx \theta_1^{'}) < (\theta_2 \approx \theta_2^{'}) \ldots < (\theta_{N_M} \approx \theta_{N_M}^{'})$.

Finally, to estimate the plausibility of each model class in the set $\mathbf{M}$, the methodology for model class assessment explained in Section 4.2 is used here. Bayes' Theorem is applied at the model class level to obtain the plausibility of the j-th model class as:

$$p(\mathcal{M}_j|\mathcal{D},\mathbf{M}) = \frac{p(\mathcal{D}|\mathcal{M}_j)p(\mathcal{M}_j|\mathbf{M})}{\sum_{i=1}^{N_M} p(\mathcal{D}|\mathcal{M}_i)p(\mathcal{M}_i|\mathbf{M})} \tag{9.2}$$

where $p(\mathcal{M}_j|\mathbf{M})$ is the prior plausibility of the model class $\mathcal{M}_j$ in the set $\mathbf{M}$, that in this study is chosen as $\mathcal{M}_j = 1/4$ (i.e., all model classes in $\mathbf{M}$ are equally plausibly a priori); and $p(\mathcal{D}|\mathcal{M}_j)$ is the *evidence* for model class $\mathcal{M}_j$ (recall Equation 4.9), that expresses how likely the observed damage response is reproduced if model class $\mathcal{M}_j$ is adopted. The method proposed by Cheung and Beck [66] (summarized in Algorithm 3) is adopted here to numerically compute the evidence of each model class using posterior samples from the M-H algorithm.

9.2 Assessment for GFRP fatigue damage data

In this section, the assessment of the proposed Markov chain models is investigated in application to the set of data for GFRP quasi-isotropic laminates (Dataset 1, Section 8.1). In view of the data, some measurements were taken outside of the $[0, 1]$ interval because of experimental error in measuring stiffness. Hence, to ensure the existence of an absorbent state for the Markov chain model, it is redefined as the state corresponding to the first measurement that fulfills $y_n \geqslant 1$. This definition only affects a small portion of measurements near the absorbent state where transition probabilities are close to value of 1 and hence the likelihood function $p(\mathcal{D}|\boldsymbol{\theta}, \mathcal{M})$ is barely affected.

As a first step, the posterior PDF of model parameters is computed for models $\mathcal{M}_1$ to $\mathcal{M}_4$. The posterior results are summarized in Table 9.2.

		θ_1	θ_1'	θ_2	θ_2'	θ_3	θ_3'	θ_4	θ_4'	p
$\mathcal{M}_1$	mean	0.1083	0.1080	–	–	–	–	–	–	0.89
	std	0.0514	0.0569	–	–	–	–	–	–	0.0068
$\mathcal{M}_2$	mean	0.0593	0.0618	0.2042	0.4207	–	–	–	–	0.8516
	std	0.0167	0.0213	0.0194	0.0223	–	–	–	–	0.0110
$\mathcal{M}_3$	mean	0.1573	0.1898	0.2051	0.3212	0.4587	0.5454	–	–	0.89
	std	0.0219	0.0264	0.0202	0.0161	0.0428	0.0174	–	–	0.0087
$\mathcal{M}_4$	mean	0.1254	0.1719	0.1652	0.3715	0.4131	0.5941	0.7137	0.9353	0.8762
	std	0.0312	0.0449	0.0188	0.0173	0.0308	0.0348	0.0721	0.0152	0.0180

Table 9.2: *Posterior results for model parameters using Dataset 1*

In addition, the two-dimensional projections of the posterior samples for model classes $\mathcal{M}_1$ to $\mathcal{M}_3$ are plotted in Figures 9.1 to 9.3, respectively. The plot for model class $\mathcal{M}_4$ is avoided because the required space for printing purposes is high.

In order to choose which model class or set of model classes are more plausible based on Dataset 1, the posterior results of model parameters shown in Table 9.2 are not enough. In accordance with the theory in Section 4.2, the best choice among candidates should be based on posterior probabilities of the model classes. In Table 9.3, the results of the model class assessment are presented for $\mathcal{M}_j,\ j = 1, \ldots, 4$ using a uniform prior $p(\mathcal{M}_j|\mathbf{M}) = 1/4$.

Class	Log evidence	AGF	EIG	Post. Probability
$\mathcal{M}_1$	-183.43	-180.31	3.11	$3.5 \cdot 10^{-18}$
$\mathcal{M}_2$	-166.13	-161.61	4.52	**0.826**
$\mathcal{M}_3$	-166.73	-157.05	9.68	0.174
$\mathcal{M}_4$	-170.73	-156.25	14.47	$1.74 \cdot 10^{-5}$

Table 9.3: *Results of model class assessment for Dataset 1. The information-theoretic terms AGF and EIG are also provided for each model class (recall Equation 4.10). The 2nd column is the difference of the next two columns. The 5-th column is the posterior probability of each model class within the set of candidates* $\mathbf{M}$.

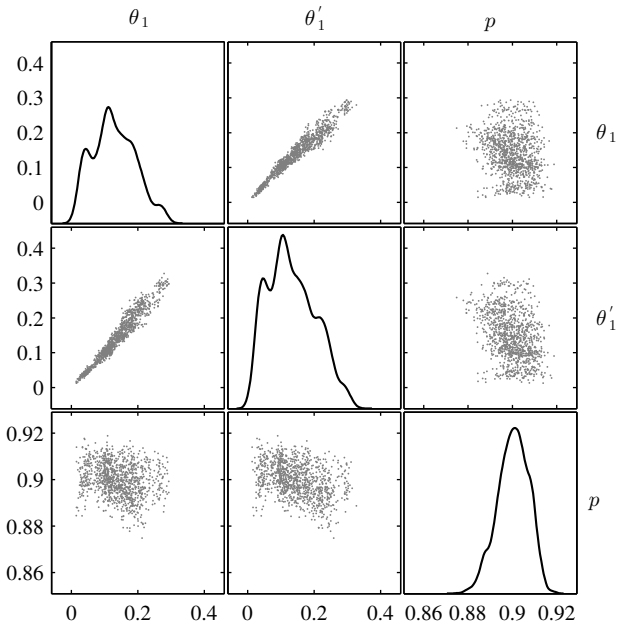

Figure 9.1: *Plots of posterior samples in the $\boldsymbol{\theta}$ space when updating model class $\mathcal{M}_1$ using Dataset 1. On the diagonal, kernel density estimates are shown for the marginal posterior PDFs of the respective parameters.*

9.2.1 Hyper-robust predictive model

As explained in Section 4.2.3, a hyper-robust predictive model can be obtained based on the complete set of models $\mathbf{M}$ through the posterior information related to both, model parameters and model classes, as follows:

$$p(x_n|\mathcal{D},\mathbf{M}) = \sum_{j=1}^{N_M} p(x_n|\mathcal{D},\mathcal{M}_j)p(\mathcal{M}_j|\mathcal{D},\mathbf{M}) \tag{9.3}$$

where $p(x_n|\mathcal{D},\mathcal{M}_j)$ is the posterior robust prediction of damage including the parameter uncertainty for model class $\mathcal{M}_j$. It is estimated by the Monte Carlo method as

$$p(x_n|\mathcal{D},\mathcal{M}_j) = \frac{1}{N_s}\sum_{k=1}^{N_s} p(x_n|\boldsymbol{\theta}^{(k)},\mathcal{M}_j) \tag{9.4}$$

where $\boldsymbol{\theta}^{(k)}$ are samples from the posterior PDFs $p(\boldsymbol{\theta}|\mathcal{D},\mathcal{M}_j)$.

If the posterior probabilities $p(\mathcal{M}_j|\mathcal{D},\mathbf{M})$ given in Table 9.3 are substituted into Equation 9.3, it is clear that the contributions of models $\mathcal{M}_1$ and $\mathcal{M}_4$ to the hyper-robust predictive model in Equation 9.3 are negligible, and so, it can be approximated by:

$$p(x_n|\mathcal{D},\mathbf{M}) \cong 0.826p(x_n|\mathcal{D},\mathcal{M}_2) + 0.174p(x_n|\mathcal{D},\mathcal{M}_3) \tag{9.5}$$

The cumulative distribution function (CDF) $F(x_n|\mathcal{D},\mathcal{M})$ based on Equation 9.5 is plotted in Figure 9.5 where it is compared with the empirical CDF based on the Dataset 1, showing

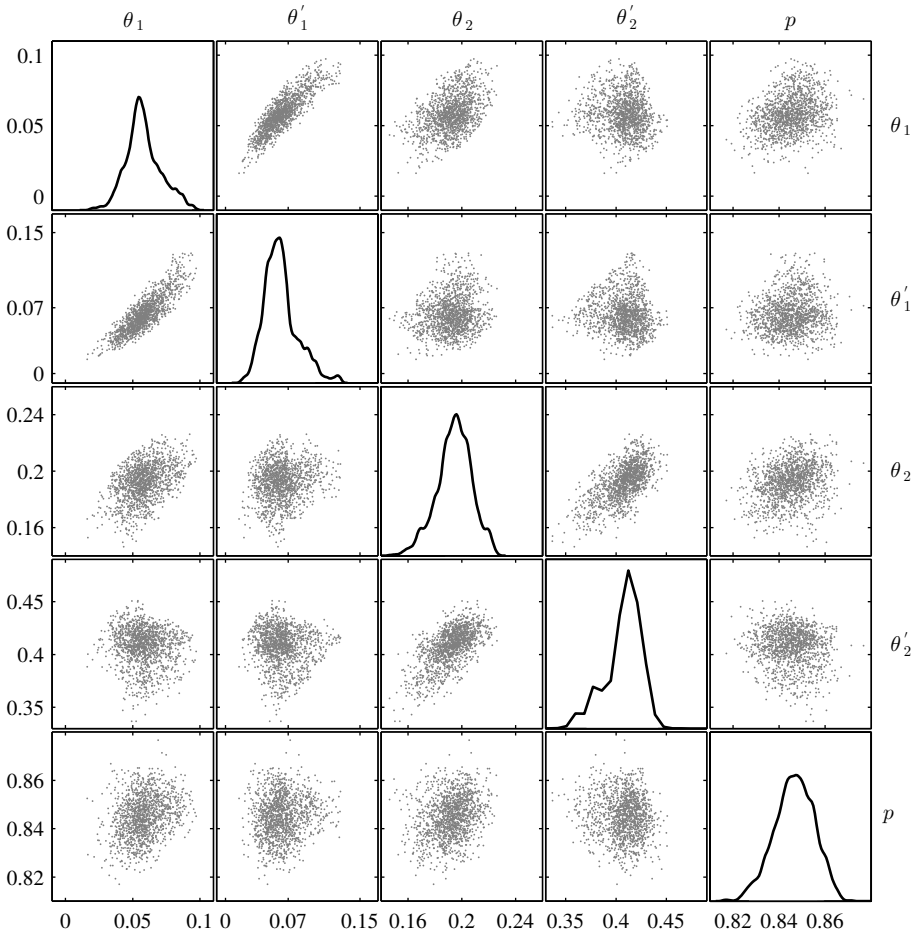

Figure 9.2: *Plots of posterior samples in the $\boldsymbol{\theta}$ space when updating model class $\mathcal{M}_2$ with fatigue data $\mathcal{D}$. On the diagonal, kernel density estimates are shown for the marginal posterior PDFs of the respective parameters.*

good agreement between these data and the posterior predictions based on models $\mathcal{M}_2$ and $\mathcal{M}_3$.

9.2.2 Minimum required set of data

One of the relevant issues when making inference with a dataset based on repeated testing of specimens is to assess the minimum required amount of test specimens to update the model classes and their predictions. From an information point of view, this is equivalent to determining the size of the dataset by which the information gain from new test data becomes relative small. This can be done by computing the relative entropy [67] between the posterior from adding the k-th partition of the dataset and its prior, which corresponds to the posterior based on the previous $(k-1)$ partitions. To this end, let us consider the model class $\mathcal{M}_j$ with model parameters $\boldsymbol{\theta}$, which are updated with data $\mathcal{D}_k$ consisting of k experimental sequences of fatigue-damage: $\left\{\hat{Y}^{(1)}, \ldots, \hat{Y}^{(k)}\right\}$, $k = 1, \ldots, K$, such that $\mathcal{D}_{k-1} \subset \mathcal{D}_k$ and $\mathcal{D}_K \equiv \mathcal{D}$. The relative entropy (also called *cross-entropy* and *Kullback-Liebler distance*)

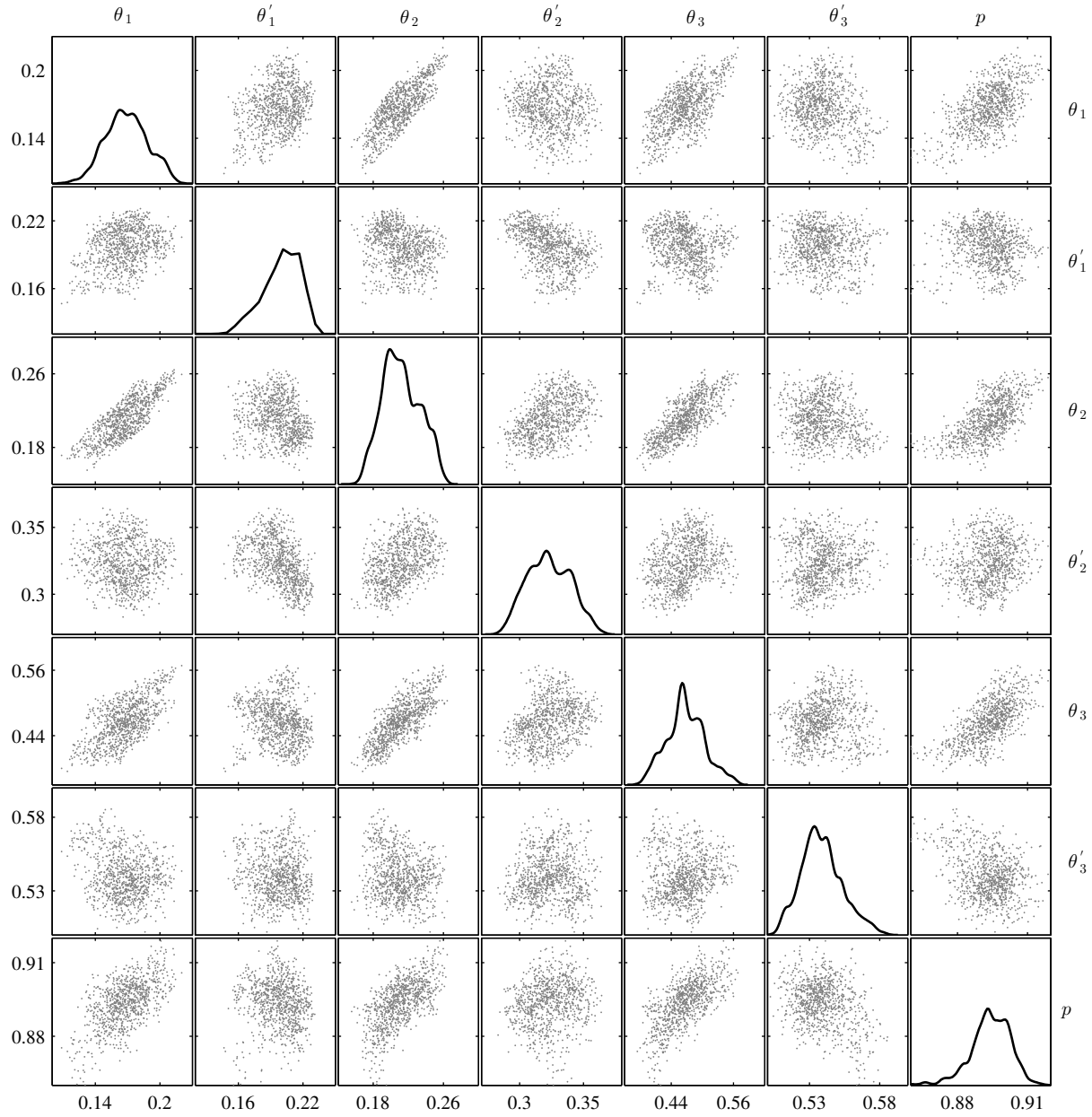

Figure 9.3: *Plots of posterior samples in the $\boldsymbol{\theta}$ space when updating model class $\mathcal{M}_3$ with fatigue data $\mathcal{D}$. On the diagonal, kernel density estimates are shown for the marginal posterior PDFs of the respective parameters.*

between the posterior PDFs $p(\boldsymbol{\theta}|\mathcal{D}_k, \mathcal{M}_j)$ and $p(\boldsymbol{\theta}|\mathcal{D}_{k-1}, \mathcal{M}_j)$ is defined as:

$$\int_{\Theta} p(\boldsymbol{\theta}|\mathcal{D}_k, \mathcal{M}_j) \log_2 \left[\frac{p(\boldsymbol{\theta}|\mathcal{D}_k, \mathcal{M}_j)}{p(\boldsymbol{\theta}|\mathcal{D}_{k-1}, \mathcal{M}_j)} \right] d\boldsymbol{\theta} \tag{9.6}$$

Observe that the relative entropy is the expected information gain (in bits) about $\boldsymbol{\theta}$ from $\mathcal{D}_k$ relative to $\mathcal{D}_{k-1}$, so hereinafter we refer to it as the relative information gain (RIG). By the fact that in our framework the posterior PDF $p(\boldsymbol{\theta}|\mathcal{D}_k, \mathcal{M}_j)$ is presented by the set of posterior

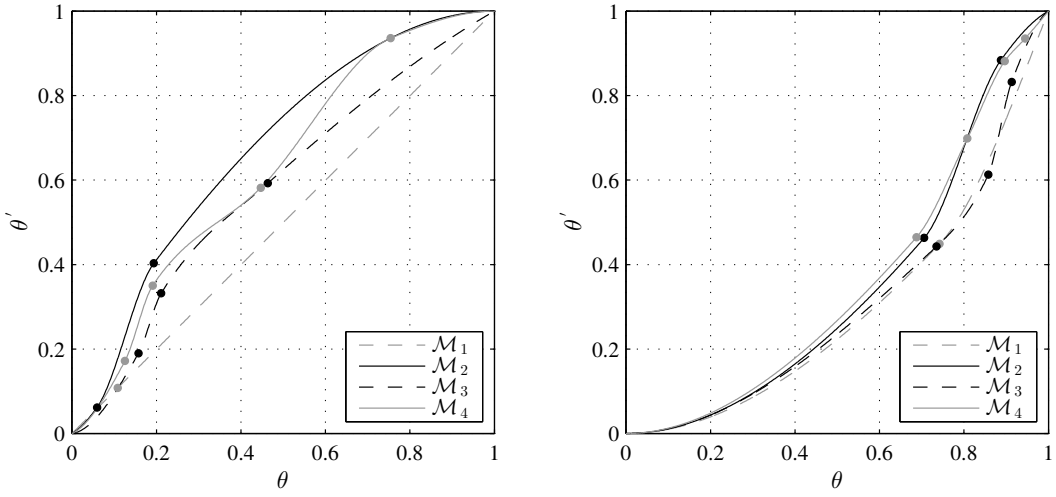

(a) Dataset 1 **(b)** Dataset 2

Figure 9.4: *Plots of interpolation curves of unit-time transformation for model classes $\mathcal{M}_1$ to $\mathcal{M}_4$ using Datasets 1 (left) and 2 (right). The interpolation points are the mean values of (θ_i, θ_i').*

samples $\{\theta_k^{(t)}\}_{t=1}^{N_s}$, then the relative information gain of this set can be approximated by [2]:

$$\text{RIG} \approx \sum_{t=1}^{N_s} \frac{p(\mathcal{D}_k|\theta_k^{(t)}, \mathcal{M}_j)\, p(\theta_k^{(t)}|\mathcal{M}_j)}{p(\mathcal{D}_k|\mathcal{M}_j)} \log_2 \left[\frac{p(\mathcal{D}_k|\theta_k^{(t)}, \mathcal{M}_j)\, p(\theta_k^{(t)}|\mathcal{M}_j)\, p(\mathcal{D}_{k-1}|\mathcal{M}_j)}{p(\mathcal{D}_{k-1}|\theta_{k-1}^{(t)}, \mathcal{M}_j)\, p(\theta_{k-1}^{(t)}|\mathcal{M}_j)\, p(\mathcal{D}_k|\mathcal{M}_j)} \right] \tag{9.7}$$

Notice that in the last equation, the posterior PDFs $p(\boldsymbol{\theta}|\mathcal{D}_k, \mathcal{M}_j)$ and $p(\boldsymbol{\theta}|\mathcal{D}_{k-1}, \mathcal{M}_j)$ are expanded by making substitutions according to Bayes' Theorem.

Figure 9.6 shows the plots of the cumulative sum of values of RIG from the sequence of specimen fatigue tests for model classes $\mathcal{M}_1$ to $\mathcal{M}_4$. The numbering of the specimen tests is the actual order in which the experiments appear in Table 8.1. These plots clearly show that there exist a specific size of the dataset, expressed as a number of test specimens, after which the inference does not gain significant information. Based on these results, we may choose the value of 11 as the minimum required number of test specimens for adequate inference in our problem, although this value actually depends on each of model classes. In fact, observe that the more complex the model is (in the sense of the more number of model parameters), the bigger the size of the required dataset, resulting in an optimal number of specimens from 8 to 11 for model classes $\mathcal{M}_1$ to $\mathcal{M}_4$, respectively. Notice also that more complex models acquire more information from each test. Both of these experimental observations make sense with the results obtained for the complexity of model classes shown in Table 9.3.

9.3 Assessment for CFRP fatigue damage data

In this section, the dataset for cross-ply CFRP laminates (Dataset 2, Section 8.2) is used to assess the performance of the proposed Markov chain models. Since the dataset is compounded by two different-scale sequences of damage (micro-cracks density and stiffness

[2] The burn-in period must be discarded from the sample approximation of the posteriors.

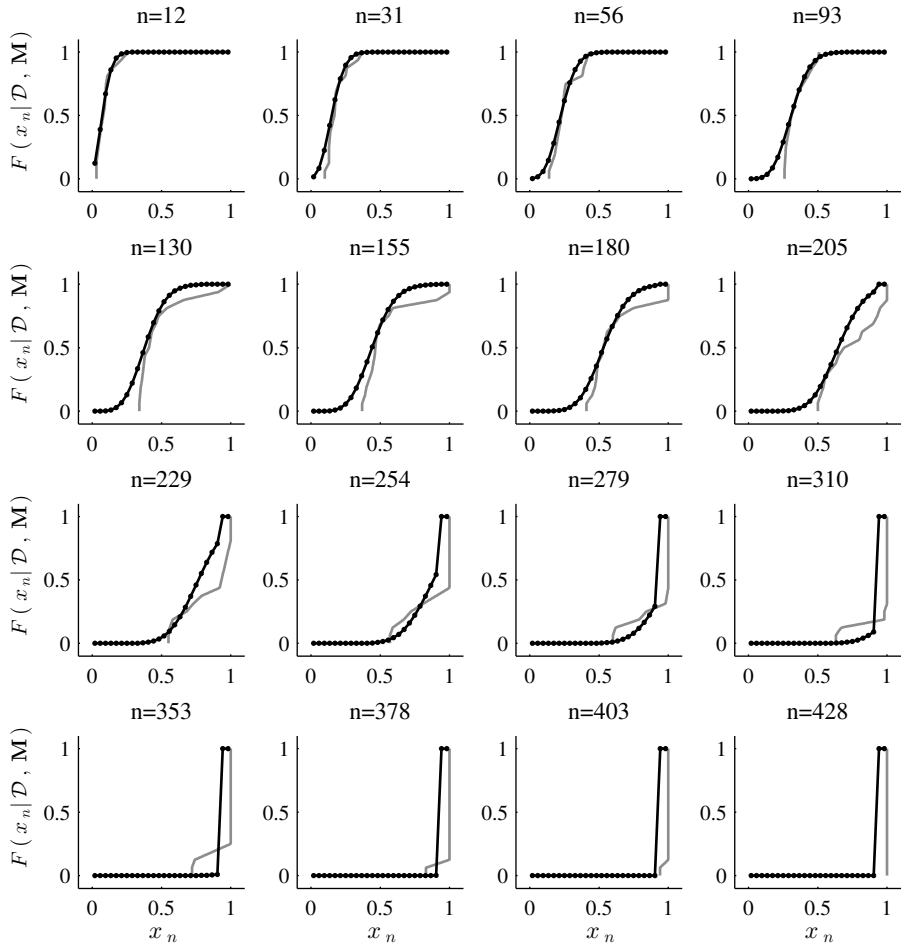

Figure 9.5: *Plots of CDF of the posterior hyper-robust predictive damage model for 16 duty cycles covering the full fatigue time (dark dotted curves). The empirical CDF of damage based on Dataset 1 are given as the grey solid curves.*

loss), the overall system is idealized as a latent damage process modeled as a parameterized Markov chain, for which the matrix micro-cracks and the stiffness reduction are external manifestations. See Figure 9.7 for illustration. For this example, any measurement error when assigning the i-th damage state based on the observed value $y_n = (\rho_n, D_n) \in \mathcal{X}_i$ is assumed to be subsumed by the uncertainty in the damage states described by the Markov chain model, and so it is not explicitly modeled. In other words, the observation equation for the Hidden Markov model described in Figure 9.7 is modeled as an identity function.

As a first step, the posterior PDF of model parameters is obtained for model classes $\mathcal{M}_1$ to $\mathcal{M}_4$ by means of Bayes' Theorem using the M-H algorithm (see algorithm configuration in Table 9.1). To this end, the likelihood function in Equation 5.13 is computed as the probability to simultaneously observe both sequences of data, the micro-cracks density data and the stiffness loss data. The posterior results for model parameter updating are summarized in

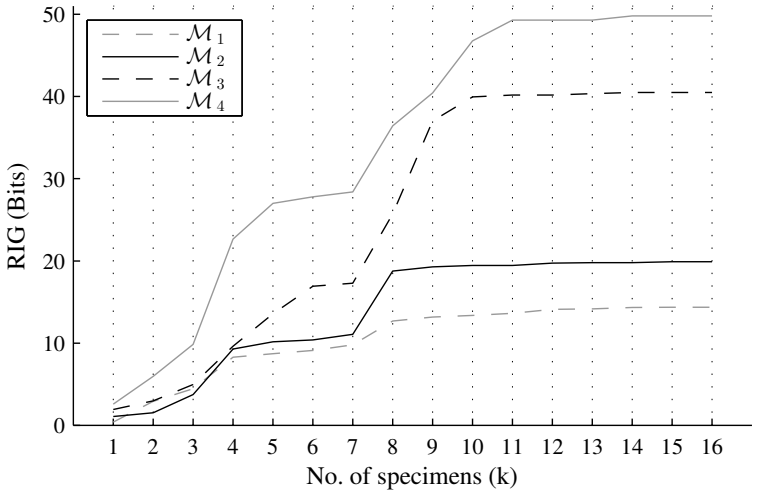

Figure 9.6: *Plots of the cumulative sum of RIG between consecutive posteriors $p(\boldsymbol{\theta}|\mathcal{D}_k, \mathcal{M}_j)$, $k = 1, \ldots, K$, for models classes $\mathcal{M}_1$ to $\mathcal{M}_4$. When $k = 1$, the RIG about $\boldsymbol{\theta}$ is computed from $\mathcal{D}_1$ relative to the prior PDF.*

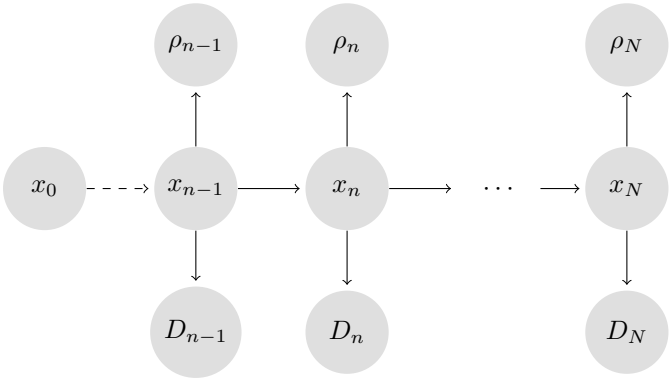

Figure 9.7: *Scheme for idealization of system response for Dataset 2 using Markov chains. The latent damage sequence $\{x_0, \ldots, x_{n-1}, x_n, \ldots, x_N\}$ is modeled as a Markov chain parameterized by $\boldsymbol{\theta}$ in the model class $\mathcal{M}_j$*

Table 9.4. In addition, a graphical representation of the two-dimensional projections of the posterior samples is provided in Figure 9.8 for the most plausible model class $\mathcal{M}_1$, as shown below.

Regarding the problem of model class assessment, the Bayesian approach proposed in Section 4.2 is used here in application to Dataset 2 with a uniform prior $p(\mathcal{M}_j|\mathbf{M}) = 1/4$ for each model class. The results of the assessment are shown in Table 9.5.

As a final outcome, a hyper-robust model of damage is obtained using the posterior information contained in the complete set of model classes, following the formulation previously explained in Section 9.2.1. The hyper-robust simulation is shown in Figure 9.9 in comparison with the experimental data from Dataset 2.

		θ_1	θ_1'	θ_2	θ_2'	θ_3	θ_3'	θ_4	θ_4'	p
$\mathcal{M}_1$	mean	0.7422	0.4489	–	–	–	–	–	–	0.9538
	std	0.1319	0.1100	–	–	–	–	–	–	0.0054
$\mathcal{M}_2$	mean	0.7058	0.4630	0.6173	0.7839	–	–	–	–	0.9485
	std	0.1125	0.0652	0.2747	0.1749	–	–	–	–	0.0114
$\mathcal{M}_3$	mean	0.7349	0.4427	0.4626	0.3053	0.3892	0.5669	–	–	0.9514
	std	0.1146	0.0897	0.2240	0.1856	0.2156	0.2137	–	–	0.0109
$\mathcal{M}_4$	mean	0.6877	0.4648	0.3854	0.4369	0.4617	0.6076	0.4655	0.4521	0.9472
	std	0.1319	0.1032	0.1672	0.2486	0.2752	0.2361	0.2363	0.2347	0.0130

Table 9.4: *Posterior results for model parameters using Dataset 2*

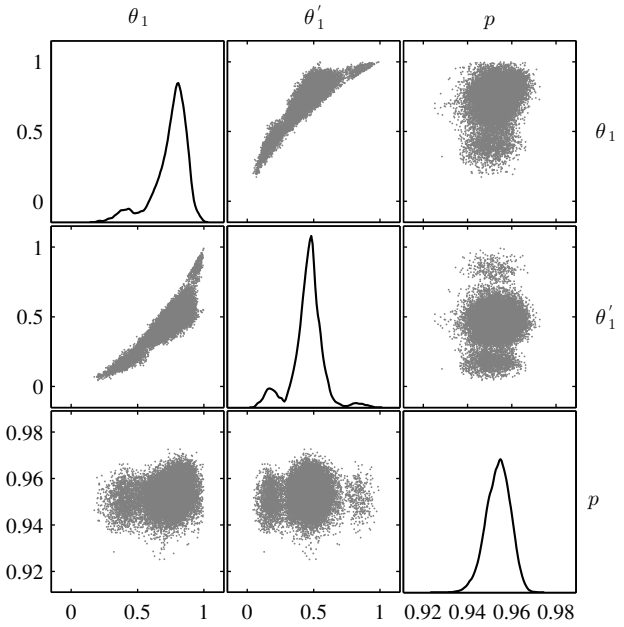

Figure 9.8: *Posterior samples in the $\boldsymbol{\theta}$ space when updating model class $\mathcal{M}_1$ using Dataset 2. On the diagonal, kernel density estimates are shown for the marginal posterior PDFs of the respective parameters.*

9.4 Discussion

The proposed model class selection framework was used to quantify the uncertainty and also to select the optimum model parameterization for cumulative damage models based on Markov chains. Several competing model classes based on Markov chains were defined to represent the fatigue behavior for two nominally different sets of data. As apparent from the results, the simpler model classes that accounts for the non-stationarity are the most plausible in representing the observed damage response for both sets of data. These results are consistent with Hypothesis 3 in Chapter 2, by which *simpler models for fatigue damage evolution in composites that agree reasonably well with the data are expected to overperform more sophisticated competing candidates*. It is an example of the Principle of Model Parsimony in the context of fatigue damage modeling in composites, that comes into play through the Bayesian approach adopted in thesis.

Class	Log evidence	AGF	EIG	Post. Probability
$\mathcal{M}_1$	-21.58	-18.84	2.74	0.983
$\mathcal{M}_2$	-23.35	-17.41	5.94	0.016
$\mathcal{M}_3$	-26.11	-17.15	8.96	$2.90 \cdot 10^{-5}$
$\mathcal{M}_4$	-28.51	-17.05	11.46	$1.15 \cdot 10^{-7}$

Table 9.5: *Results of model class assessment for Dataset 2. The information-theoretic terms AGF and EIG are also provided for each model class (recall Equation 4.10). The 2nd column is the difference of the next two columns. The 5th column is the posterior probability of each model class within the set of candidates* **M**.

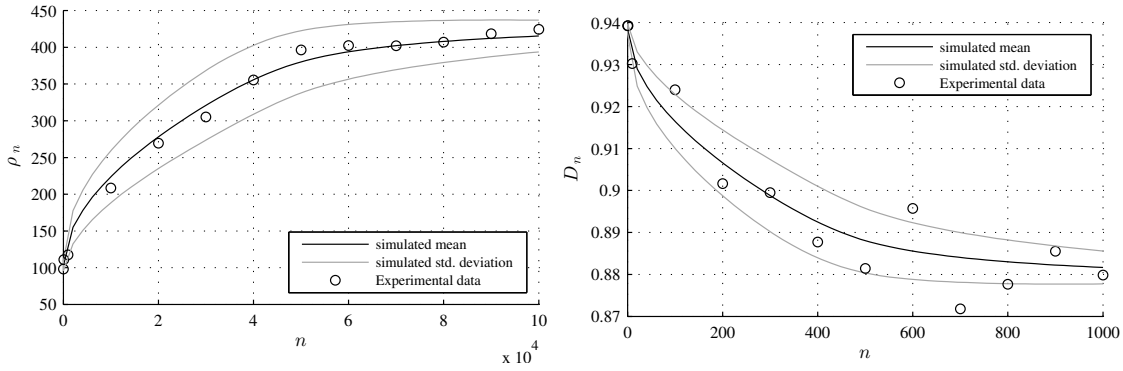

(a) Micro-cracks density **(b)** Normalized effective stiffness

Figure 9.9: *Hyper-robust damage response using the posterior information of models $\mathcal{M}_1$ to $\mathcal{M}_4$ for Dataset 2*

In view of results from Table 9.3, the assessment for Dataset 1 shows that accounting for the non-stationarity greatly increases the relative plausibility of the proposed stochastic models, since the posterior results in Figure 9.1 show that model $\mathcal{M}_1$ is similar to a stationary model with only p as model parameter (observe from Figure 9.1 that the posterior samples from θ_1 and $\theta_1^{'}$ are highly correlated along the straight line from $(0,0)$ to $(1,1)$, but they are practically uncorrelated with p). In addition, the results in Table 9.3 show that models $\mathcal{M}_2$ to $\mathcal{M}_4$ have increasingly higher values of the data fit (AGF) in comparison with model $\mathcal{M}_1$. A possible reason for this can be inferred by observing Figure 9.4a, in which the interpolation curves of unit time transformation are displayed using the mean parameter values for the interpolation points. For models $\mathcal{M}_2$ to $\mathcal{M}_4$, the first two interpolation points are dedicated to capturing a significant source of non-stationarity observed in data within the first stage of fatigue (refers to Figure 8.1), leading to a marked improvement in the data fit compared with $\mathcal{M}_1$. Models $\mathcal{M}_3$ and $\mathcal{M}_4$ include additional interpolation points that capture the transformation of unit time in the middle-end of the fatigue process, where the modulus reduction data are appreciably dispersed, as shown in Figure 8.1. This markedly improves the data fit of models $\mathcal{M}_3$ and $\mathcal{M}_4$. Model $\mathcal{M}_4$, which has the most parameters, fits the data the best but also implies less robustness, in the sense of a small variation of model parameters may confer a significant change in the model prediction. This fact is reflected in the increasing value of the EIG. Table 9.3 also shows that $\mathcal{M}_1$ and $\mathcal{M}_4$ have negligible posterior probability with the other model classes $\mathcal{M}_2$ and $\mathcal{M}_3$, showing the best trade-off

between the data and model complexity, leading to posterior probabilities of 0.83 and 0.17, respectively.

Regarding the assessment using Dataset 2, Table 9.5 shows that the simplest model class $\mathcal{M}_1$ is the most plausible in explaining the damage behavior observed in such dataset. It is consistent with the above discussion for which simpler model classes that account for the non-stationarity are the most plausible in explaining the observed damage response, given that $\mathcal{M}_1$ for Dataset 2 results to be the simplest non-stationary model class in the set. In fact, observe in Figure 9.8 that the posterior samples for θ_1 and $\theta_1^{'}$ are correlated along the diagonal but without being excessively so, in comparison with that of $\mathcal{M}_1$ using Dataset 1 (Figure 9.1). It is also supported by Figure 9.4b, in which the interpolation curve for unit time transformation using $\mathcal{M}_1$ clearly separates from the diagonal, what means that for this dataset, model class $\mathcal{M}_1$ accounts for the non-stationarity turning out to be the most plausible in the set $\mathbf{M}$. In addition, it can be observed that models $\mathcal{M}_2$ to $\mathcal{M}_4$ have increasingly higher values of the data fit (AGF) in comparison with model $\mathcal{M}_1$, but it is at the cost of an increasing amount of information gain from data, resulting in lower evidences. This result is also in agreement with the interpolation curves for the unit time transformation in Figure 9.4b. Models $\mathcal{M}_2$ to $\mathcal{M}_4$ include additional interpolation points that capture the transformation of unit time near the end of the fatigue process, where the Markov chain is reaching the absorbing state, what slightly improves the datafit of such models. However it implies an unnecessary information gain from data and in consequence, the evidences of such model classes are penalized.

In summary, the following conclusions are extracted from the case study presented in this chapter: (a) Accounting for the non-stationarity of the fatigue-damage evolution significantly improves the model datafit; (b) simpler models that are consistent with data are more plausible than more complex competing candidates; (c) a measure of the information gain from a specimen test can be used to select a minimum set of specimens for damage characterization and prediction; (d) several damage phenomena like matrix-crack density, stiffness loss, etc., that imply cumulative damage processes, can benefit by applying a similar Bayesian approach for Markov chain models.

10

Model class assessment for physics-based models

In this chapter, the Bayesian model class selection methodology presented in this thesis is applied to investigate the performance of the damage mechanics model classes proposed in Chapter 6. An overview of the methodology and the main problem settings are provided in Section 10.1. In Section 10.2, the results of the assessment are presented in application to damage data for micro-cracks density and stiffness loss, corresponding to Dataset 2 in Section 8.2. In Section 10.3, the assessment is exemplified using the ABC-SubSim algorithm proposed in Chapter 7. Finally, a thorough discussion of results is provided in Section 10.4.

10.1 Methodology

To assess the performance of the physics-based modeling approach proposed in Chapter 6, a set of five model classes $\mathbf{M} = \{\mathcal{M}_1, \mathcal{M}_2, \ldots, \mathcal{M}_5\}$ are considered for the inference. Three of them are based on the shearlag analysis ($\mathcal{M}_1$: classical [132, 141], $\mathcal{M}_2$: bi-dimensional [142, 143], $\mathcal{M}_3$: interlaminar [9]), and the rest are based on the variational [133] and COD [134] approaches, $\mathcal{M}_4$ and $\mathcal{M}_5$ respectively[1]. Details about model class definition using the aforementioned damage mechanics approaches are provided in Section 6.3, so they are not repeated here.

Multi-scale damage data for cross-ply CFRP laminates are used to perform the model class assessment, corresponding to Dataset 2 in Section 8.2; i.e., $\mathcal{D} = \{\mathbf{y}_{n_1}, \ldots, \mathbf{y}_{n_k}, \ldots, \mathbf{y}_{n_N}\}$,

[1] Note that model classes $\mathcal{M}_1$ to $\mathcal{M}_5$ have an increasing level of analysis complexity: from the 1-dimensional (1-D) analysis for shear-lag models and the 2-D analysis for variational models, up to the 3-D analysis for COD-based models.

where $\mathbf{y}_{n_k} = (\rho_{n_k}, D_{n_k})$, $n_k \in \mathbb{N}$. For the sake of clarity, a summary of Dataset 2 is provided here in Table 10.1.

Fatigue cycles, n_k	10^1	10^2	10^3	10^4	$2{\cdot}10^4$	$3{\cdot}10^4$	$4{\cdot}10^4$	$5{\cdot}10^4$	$6{\cdot}10^4$	$7{\cdot}10^4$	$8{\cdot}10^4$	$9{\cdot}10^4$	10^5
ρ_{n_k} [# cracks/m]	98.2	111.0	117.4	208.5	269.6	305.0	355.5	396.4	402.3	402.1	407.0	418.5	424.5
D_{n_k}	0.954	0.939	0.930	0.924	0.902	0.899	0.888	0.881	0.896	0.872	0.877	0.885	0.880

Table 10.1: *Summary of damage data (micro-cracks density, ρ_{n_k}, and normalized effective stiffness, D_{n_k}) for Dataset 2, corresponding to a cross-ply $[0_2/90_4]_s$ CFRP laminate.*

As a first step, the posterior PDF of model parameters for the j-th model class is obtained by means of the Bayes' Theorem,

$$p(\boldsymbol{\theta}|\mathcal{D}, \mathcal{M}_j) = c^{-1} p(\mathcal{D}|\boldsymbol{\theta}, \mathcal{M}_j) p(\boldsymbol{\theta}|\mathcal{M}_j) \tag{10.1}$$

where the likelihood function $p(\mathcal{D}|\boldsymbol{\theta}, \mathcal{M}_j)$ is computed as (recall Section 6.4) the probability to simultaneously observe the sequences of damage data in Table 10.1, micro-cracks density data and stiffness loss, by the stochastic forward model defined in Equation 6.10. To find the optimal set of model parameters $\boldsymbol{\theta}$ to be updated by Bayes' Theorem, each model class is previously parameterized by Global Sensitivity Analysis (GSA) following the methodology presented in Section 6.5. Results and more insight about GSA parameterization in the context of this case study are provided in Section 10.1.1. The definition of the prior PDF of model parameters $p(\boldsymbol{\theta}|\mathcal{M}_j)$ to be updated by Bayes' Theorem (Equation 10.1) is specified in detail in Section 10.1.2, further below.

Finally, to perform the model class assessment, the Bayesian approach presented in Section 4.2 is applied here using a uniform prior $p(\mathcal{M}_j|\mathbf{M}) = 1/5$ for each model class (i.e. all model classes are considered equally plausible a priori). The choice for the most plausible model class among the set of candidates $\mathbf{M}$ is based on higher posterior probabilities $p(\mathcal{M}_j|\mathcal{D}, \mathbf{M})$, given by Bayes' Theorem as

$$p(\mathcal{M}_j|\mathcal{D}, \mathbf{M}) = \frac{p(\mathcal{D}|\mathcal{M}_j) p(\mathcal{M}_j|\mathbf{M})}{\sum_{i=1}^{N_M} p(\mathcal{D}|\mathcal{M}_i) p(\mathcal{M}_i|\mathbf{M})} \tag{10.2}$$

where $p(\mathcal{D}|\mathcal{M}_j)$ is the *evidence* for model class $\mathcal{M}_j$ (recall Equation 4.9), that expresses how likely the observed damage response is reproduced if model class $\mathcal{M}_j$ is adopted. The method by Cheung and Beck [66] (summarized in Algorithm 3) is adopted here to numerically solve the evidence of each model class using samples form the posterior PDF of model parameters. Results for the overall assessment are provided in Section 10.2.

10.1.1 Model parameterization by GSA

As explained in Section 6.5, GSA aims at selecting the subset $\mathbf{m}$ of influential model parameters among the mechanical and fitting parameters listed in Table 10.2 below, which are further updated using Bayes' Theorem. To compute the total effect index S_i^T of each candidate parameter (recall Equation 6.17), a double-loop Monte Carlo algorithm is implemented

using 10^3 and 10^4 samples for the inner and outer loops, respectively. Results from GSA are shown in Figure 10.1 for model classes $\mathcal{M}_1$ to $\mathcal{M}_3$, and in Figure 10.2 for model classes $\mathcal{M}_4$ and $\mathcal{M}_5$.

To obtain the set of parameters to be updated by Bayes' Theorem, namely $\boldsymbol{\theta}$, the subset of error parameters $\mathbf{v} = \{\mu_{e_1}, \sigma_{e_1}, \mu_{e_2}, \sigma_{e_2}\}$ is added to $\mathbf{m}$, the subset of "sensitive" parameters identified by GSA. To serve as an example, the model parameter vector for the shear-lag model class $\mathcal{M}_1$ would be $\boldsymbol{\theta} = \{\alpha, E_1, E_2, t, \mu_{e_1}, \sigma_{e_1}, \mu_{e_2}, \sigma_{e_2}\}$. The rest of parameters would define the set of constant parameters $\mathbf{u}$, i.e., $\mathbf{u} = \{A, G_{12}, G_{23}, \nu_{12}\}$, which may be represented by their nominal values (specified in Table 10.2) without any associated uncertainty. The set $\boldsymbol{\theta}$ of model parameters for each model class is found in Table 10.4.

It is important to remark here that, for all model classes, the influence of the modified Paris' law fitting parameter A is found to be insignificant as compared to the sensitivity of most mechanical parameters (see Figures 10.1 and 10.2). This is especially convenient given that mechanical parameters are usually benefited from less uncertain prior information. In other words, mechanical parameters are likely to capture much less information from data as compared to fitting parameters, which (recall Equation 4.10) leads to model parameterizations with lower associated EIG terms. As discussed further below, this results in more robust model classes, i.e., with a lower dependence on the details of data.

Finally, in view of Figures 10.1 and Figures 10.2, a possible question that arises in regards to GSA is that what would be the choice if any of the candidate parameters ψ_i becomes influential but only for a certain stage of the process (e.g., the initial or the final stage). In this case, the recommendation is to consider ψ_i as influential for all the process since the unnecessary increase of model output uncertainty incurred when considering ψ_i as influential (when it is actually non-influential) is by definition null or at least negligible [49]. As stated before, a non-influential parameter can be fixed anywhere in their range of variation without effect in the model output uncertainty.

10.1.2 Prior information of model parameters

Table 10.2 lists the prior information (namely, the prior PDF) of candidate model parameters for all model classes, including the fitting parameters in the modified Paris' law and the error parameters. As explained before, the set of parameters that compound each model class is determined using Global Sensitivity Analysis. Since mechanical and fitting parameters are non-negative, their associated prior information can be modeled as a lognormal distribution, i.e., $p(\theta_i|\mathcal{M}) = \mathcal{LN}(\mu_{\theta_i}, \sigma_{\theta_i})$, $i = 1, \ldots, N_m$, with $\mu_{\theta_i} = \ln \bar{\theta}_i$, being $\bar{\theta}_i$ the nominal value of $\theta_i \in \boldsymbol{\theta}$ (e.g., the mean), and σ_{θ_i} the shape parameter of the lognormal distribution. Both, the nominal values and shape parameters are listed in Table 10.2. For the error parameters $\mathbf{v} = \{\mu_{e_1}, \sigma_{e_1}, \mu_{e_2}, \sigma_{e_2}\} \subset \boldsymbol{\theta}$, a uniform distribution defined over a sufficiently-large predefined interval (conservatively chosen after some initial test runs) is selected as the prior PDF. This choice is preferred instead of the common choice of using "non-informative" priors [19] (e.g., a uniform distribution over a very large interval), which would better represent our prior state of information about these parameters. While such a choice may not

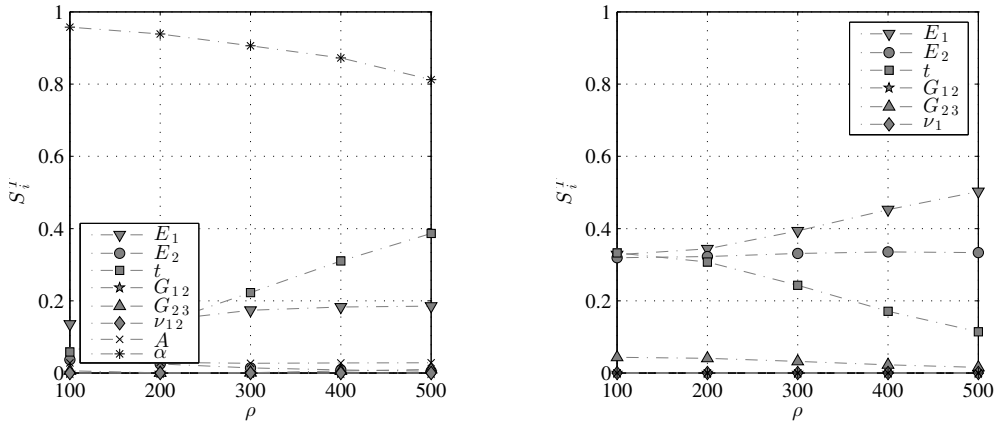

(a) Paris' law ($\mathcal{M}_1$)

(b) Stiffness model ($\mathcal{M}_1$)

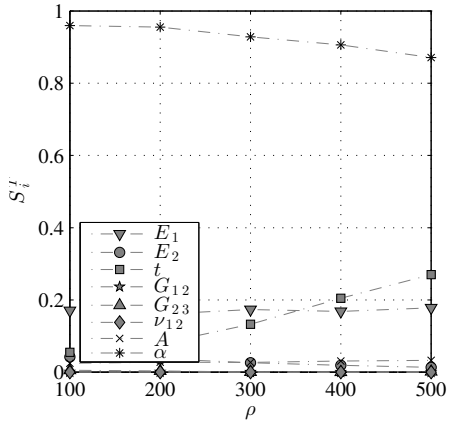

(c) Paris' law ($\mathcal{M}_2$)

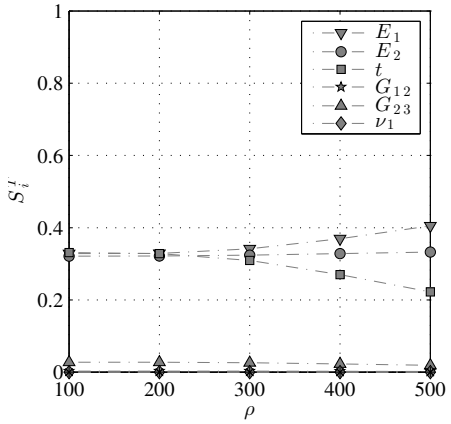

(d) Stiffness model ($\mathcal{M}_2$)

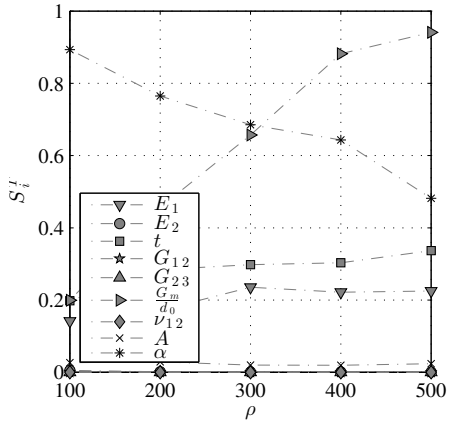

(e) Paris' law ($\mathcal{M}_3$)

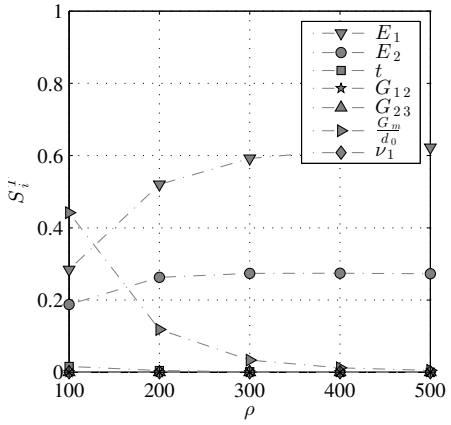

(f) Stiffness model ($\mathcal{M}_3$)

Figure 10.1: *Total effects index S_i^T of candidate parameters for both, matrix-cracks evolution model (Paris' law) and effective stiffness model, using the approaches: (a) & (b) classical shearlag, (c) & (d) bi-dimensional shearlag, (e) & (f) interlaminar shearlag. Observe that the ply properties E_1, E_2 and t are revealed as influential parameters in all model classes.*

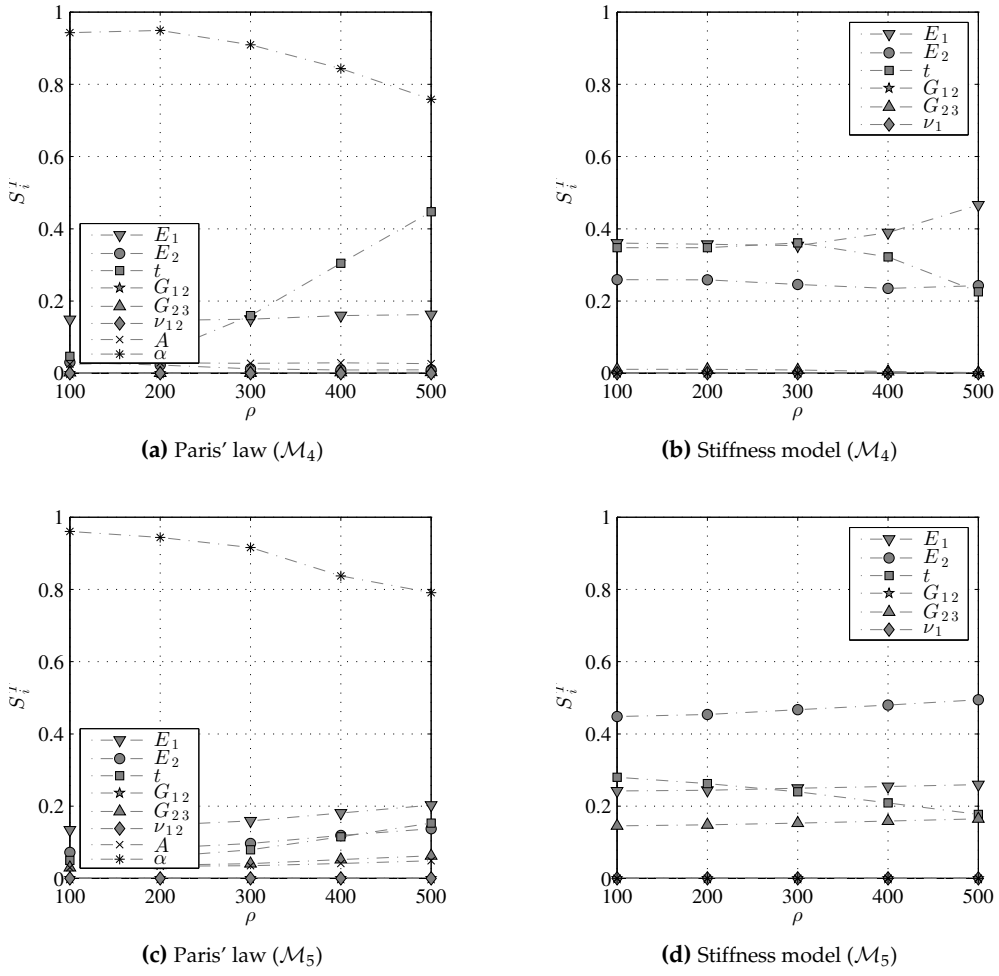

(a) Paris' law ($\mathcal{M}_4$)

(b) Stiffness model ($\mathcal{M}_4$)

(c) Paris' law ($\mathcal{M}_5$)

(d) Stiffness model ($\mathcal{M}_5$)

Figure 10.2: *Total effects index S_i^T of candidate parameters for both, matrix-cracks evolution model (Paris' law) and effective stiffness model, using the approaches: (a) & (b) variational, (c) & (d) COD. Observe that the ply properties E_1, E_2 and t are revealed as influential parameters in all model classes.*

significantly influence the posterior PDF of parameters, the use of excessively diffuse priors may lead to a markedly high information gain from data, which would induce a bias in the model-class selection problem [22]. Note also that our assumptions about the prior PDFs given in Table 10.2 can be conveniently updated if more information is available, for example from expert judgement.

10.2 Model class assessment for CFRP fatigue damage data

As stated before, multi-scale damage data for micro-cracks density and stiffness loss is used to perform the model class assessment (see Table 10.1). To this end, the likelihood function in Equation 6.13 is computed as the probability to simultaneously observe both experimental sequences. For each model class, the posterior PDF of model parameters is obtained from the prior PDF of parameters (specified in Section 10.1.2) using Bayes' Theorem given by Equation 10.1. The M-H algorithm is applied to numerically solve Equation 10.1 with a multivariate Gaussian for the proposal PDF, i.e. $q(\boldsymbol{\theta}'|\boldsymbol{\theta}^{(\zeta)}) = \mathcal{N}(\boldsymbol{\theta}^{(\zeta)}, \boldsymbol{\Sigma}_q)$, where

Type	Parameter	Nominal value	Units	Prior PDF
Mechanical	E_1	$127.55 \cdot 10^9$	Pa	$\mathcal{LN}(\ln(127.55 \cdot 10^9), 0.1)$
	E_2	$8.41 \cdot 10^9$	Pa	$\mathcal{LN}(\ln(8.41 \cdot 10^9), 0.1)$
	G_{12}	$6.20 \cdot 10^9$	Pa	$\mathcal{LN}(\ln(6.20 \cdot 10^9), 0.1)$
	$\frac{G_m}{d_0}$	$1 \cdot 10^{14}$	Pa/m	$\mathcal{LN}(\ln(1 \cdot 10^{14}), 0.5)$
	ν_{12}	0.31	–	$\mathcal{LN}(\ln(0.31), 0.1)$
	G_{23}	$2.82 \cdot 10^9$	Pa	$\mathcal{LN}(\ln(2.82 \cdot 10^9), 0.1)$
	t	$1.5 \cdot 10^{-4}$	m	$\mathcal{LN}(\ln(1.5 \cdot 10^{-4}), 0.1)$
Fitting	α	1.80	–	$\mathcal{LN}(\ln(1.80), 0.2)$
	A	$1 \cdot 10^{-4}$	–	$\mathcal{LN}(\ln(1 \cdot 10^{-4}), 0.2)$
Errors	μ_{e_1}	Not applicable	$\frac{\#\text{ cracks}}{m \cdot \text{cycle}}$	$\mathcal{U}(-2, 2)$
	σ_{e_1}	Not applicable	$\frac{\#\text{ cracks}}{m \cdot \text{cycle}}$	$\mathcal{U}(0.5, 8)$
	μ_{e_2}	Not applicable	–	$\mathcal{U}(-0.08, 0)$
	σ_{e_2}	Not applicable	–	$\mathcal{U}(0.001, 0.02)$

Table 10.2: *Prior information of parameters used in calculations. The rest of parameters in damage mechanics models (Eq. 6.1 to 6.4) are obtained using the classical laminate plate theory [145] and the relations given in Appendix A. The nominal values for fitting parameters have been defined through initial fitting tests.*

$\boldsymbol{\Sigma}_q \in \mathbb{R}^{d \times d}$ is the covariance matrix of the random walk. Given that model parameters are assumed to be stochastically independent a priori (recall Section 6.3), $\boldsymbol{\Sigma}_q$ is a diagonal matrix, i.e., $\boldsymbol{\Sigma}_q = diag(\sigma^2_{q,1}, \cdots, \sigma^2_{q,d})$, and each individual parameter in $\boldsymbol{\theta}$ performs an independent random walk. The diagonal elements of $\boldsymbol{\Sigma}_q$ are appropriately selected through initial test runs such that the monitored acceptance rate (ratio between accepted M-H samples over total amount of samples) is within the suggested range $\bar{r} \in [0.2, 0.4]$ for M-H algorithm [63]. See algorithm configuration in Table 10.3.

	$\mathcal{M}_1$	$\mathcal{M}_2$	$\mathcal{M}_3$	$\mathcal{M}_4$	$\mathcal{M}_5$
$\sigma_{q,i}$ (Prop. std. dev.)	4%	4%	2%	3.5%	1.5%
N_s (M-H samples)	$5 \cdot 10^5$	$5 \cdot 10^5$	10^6	$5 \cdot 10^5$	10^6
T (in Eq. 6.15)	10^4	10^4	10^4	10^4	10^4

Table 10.3: *Metropolis Hastings algorithm configuration for models classes $\mathcal{M}_1$ to $\mathcal{M}_5$. The diagonal elements $\sigma_{q,i}$ of covariance matrix $\boldsymbol{\Sigma}_q$ are defined as the specified percent (1st row) of the 5-th-95-th inter-percentile range of the prior PDFs for each of the i-th component of the parameter vector, $i = 1, \ldots, d$*

For illustration purposes, the prior and updated PDFs of model parameters are presented in Figure 10.3 for the most plausible model class $\mathcal{M}_1$, as shown further below. The mean and standard deviation of the updated parameters for model classes $\mathcal{M}_1$ to $\mathcal{M}_5$ are further summarized in Table 10.4. As a comment, observe in Table 10.4 that the estimated posterior mean of the bias parameter for the effective stiffness model μ_{e_2} takes non-zero values for all model classes. The corresponding posterior mean values for the bias parameter μ_{e_1} are also non-zero although they take relative lower values. It is interpreted as a systematic discrepancy the between model output and the data, which may be attributed to missing damage modes like delamination (see Figure 8.2), among other causes. Thus, if a

delamination model would have been considered within the equation of system response, it would probably have captured a part of such bias, leading to better inferences.

		Fitting param.	Mechanical parameters					Error param.			
		α	E_1 ($\times 10^9$)	E_2 ($\times 10^9$)	t ($\times 10^{-4}$)	$\frac{G_m}{d_0}$ ($\times 10^{14}$)	G_{23} ($\times 10^9$)	μ_{e_1} ($\times 10^{-1}$)	σ_{e_1}	μ_{e_2} ($\times 10^{-2}$)	σ_{e_2} ($\times 10^{-3}$)
$\mathcal{M}_1$	mean	1.86	123.16	8.72	1.52	–	–	0.05	4.25	-2.92	8.1
	std	0.13	10.3	0.73	0.14	–	–	2.02	0.99	0.64	1.9
$\mathcal{M}_2$	mean	1.96	116.21	9.28	1.61	–	–	-2.35	4.27	-3.95	8.7
	std	0.15	10.2	0.81	0.14	–	–	3.22	1.00	0.64	2.2
$\mathcal{M}_3$	mean	2.03	134.43	9.98	1.59	0.25	–	-6.37	4.41	-4.9	10.4
	std	0.21	10.9	0.96	0.15	0.13	–	6.89	1.03	1.01	3.1
$\mathcal{M}_4$	mean	1.89	124.54	8.59	1.54	–	–	-1.52	3.95	-3.55	8.4
	std	0.12	10.4	0.75	0.14	–	–	2.86	0.68	0.58	2.1
$\mathcal{M}_5$	mean	1.99	133.21	7.60	1.46	–	2.99	-13.6	4.30	-3.08	8.3
	std	0.15	12.3	0.52	0.14	–	0.28	7.93	0.98	0.62	1.9

Table 10.4: *Mean and standard deviation of the updated model parameters for models classes $\mathcal{M}_1$ to $\mathcal{M}_5$, estimated from samples of the marginal posterior PDFs. Units are specified in Table 10.2. In this table, the set of parameters that compound each model class is also found, e.g., for $\mathcal{M}_5$, $\boldsymbol{\theta} = \{\alpha, E_1, E_2, t, G_{23}, \mu_{e_1}, \sigma_{e_1}, \mu_{e_2}, \sigma_{e_2}\}$*

Results for model class assessment are shown in Table 10.5. Model class $\mathcal{M}_1$ (classical shear-lag) is revealed as the most evident to explain the observed damage data, hence the one that shows the best trade-off between datafit and model complexity, thus resulting in the highest posterior probability. In contrast, models classes $\mathcal{M}_3$ (interlaminar shear-lag) and $\mathcal{M}_5$ (COD), that involve more model parameters and more complex analysis, show negligible posterior probabilities through relatively low evidence values. It can be observed that $\mathcal{M}_5$ provides a negligible posterior probability even though it reaches the best average goodness of fit. In addition, it is noted that model class $\mathcal{M}_4$ provides a good average goodness of fit (similar than that for $\mathcal{M}_1$), but it is penalized for a relatively high information gain. These results are further discussed in Section 10.4.

As a final outcome, a forward model simulation using the most probable model $\mathcal{M}_1$ is shown in Figure 10.4 in comparison with the experimental damage data.

Model class	Log evidence	EIG	AGF	Post. Probability
$\mathcal{M}_1$ (classical SL)	-9.99	3.73	-6.26	**0.745**
$\mathcal{M}_2$ (2D-SL)	-10.80	4.22	-6.58	0.115
$\mathcal{M}_3$ (interlaminar SL)	-16.62	**8.88**	-7.74	$1.75 \cdot 10^{-7}$
$\mathcal{M}_4$ (variational)	-10.72	4.47	-6.25	0.139
$\mathcal{M}_5$ (COD)	-14.16	7.95	**-6.21**	$5.02 \cdot 10^{-5}$

Table 10.5: *Results of Bayesian model class assessment. The 2nd column (Log evidence) is the difference of the next two columns (EIG= Expected Information Gain, AGF= Average Goodness of Fit). The 5th column is the estimated posterior probability of each model class, i.e., $p(\mathcal{M}_j|\mathcal{D}, \mathbf{M})$, using a uniform prior $p(\mathcal{M}_j|\mathbf{M}) = 1/5$.*

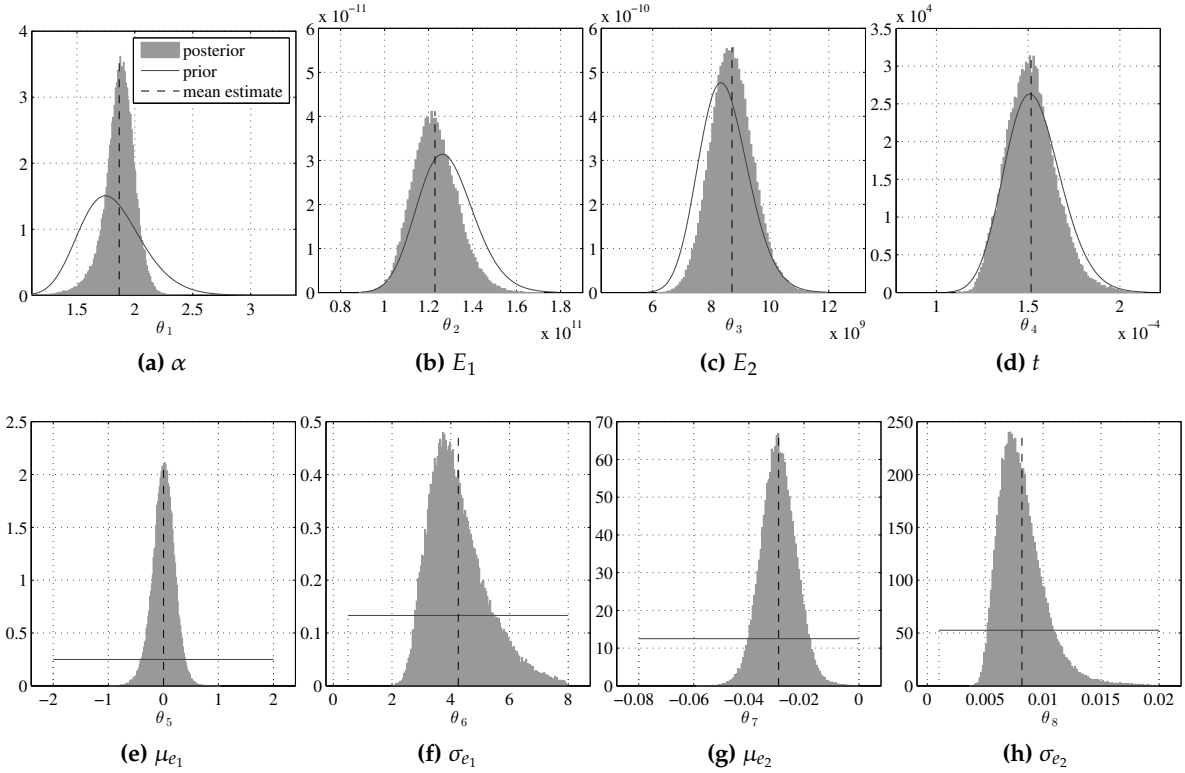

(a) α **(b)** E_1 **(c)** E_2 **(d)** t

(e) μ_{e_1} **(f)** σ_{e_1} **(g)** μ_{e_2} **(h)** σ_{e_2}

Figure 10.3: *Normalized histograms for the marginalized posterior PDFs $p(\theta_i|\mathcal{D}, \mathcal{M}_1), i = 1 \ldots 8$, after updating model class $\mathcal{M}_1$ (classical shear-lag). The posterior mean estimate for each parameter is represented by the vertical-dashed line. Note that the "difference" between the prior and the posterior PDF is larger for fitting parameter α than for mechanical parameters E_1, E_2, t.*

10.3 Assessment using ABC-SubSim algorithm

As explained in Section 6.4.1, each MCMC step requires the evaluation of the overall likelihood function $p(\mathcal{D}|\boldsymbol{\theta}, \mathcal{M}_j)$, which involves the evaluation of multi-dimensional integrals such as those defined in Equation 6.14. The Monte Carlo method can be applied to numerically solve those integrals, as shown in Equation 6.15, however it requires the simulation of T (large enough) damage growth sequences from the model, which implies $T \times N$ model evaluations for each MCMC step. It leads to a total amount of $N_s \times T \times N$ model evaluations, where N_s is the length of the Markov chain and N the number of simulated fatigue cycles. To serve as an example, a total amount of $5 \cdot 10^5 \times 10^4 \times 10^5 = 5 \cdot 10^{14}$ model evaluations were required to obtain the posterior PDF of model parameters for $\mathcal{M}_1$ shown in Figure 10.3. It motivates the use of a GPU to accelerate the Metropolis-Hasting algorithm. See Section 6.4.1 for details about M-H implementation using a GPU.

In this section, the ABC-SubSim algorithm proposed in Chapter 7 is used instead of the M-H algorithm to efficiently obtain the posterior PDF of model parameters for model class $\mathcal{M}_1$, which is enough to demonstrate the computational savings that can be achieved. The algorithm is implemented following the pseudocode given in Section 7.3. The Euclidean

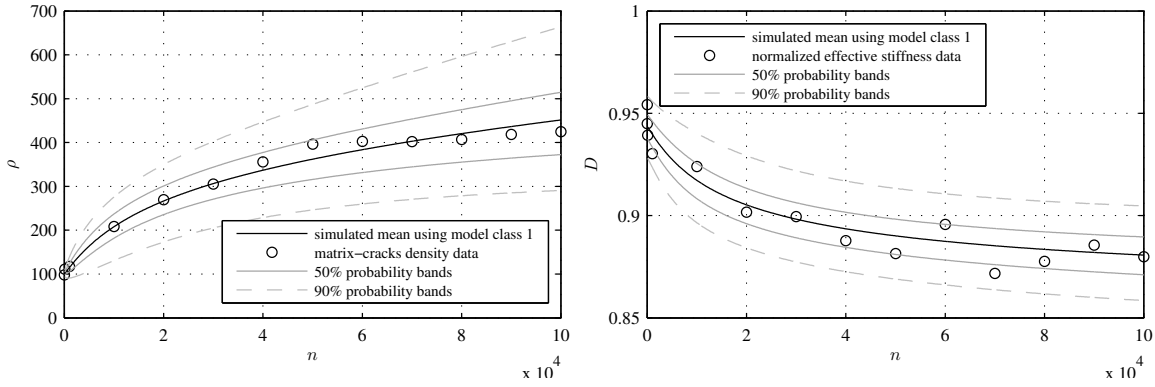

(a) Micro-cracks density **(b)** Normalized effective stiffness

Figure 10.4: *Simulated damage response using the posterior PDF of parameters for model class $\mathcal{M}_1$ (classical shear-lag). Observe that bounds cover well the experimental realizations.*

distance between $X_N = \{x_1, \ldots, x_n, \ldots, x_N\}$ and $\mathcal{D} = \{y_1, \ldots, y_n, \ldots, y_N\}$ is adopted as metric, as follows:

$$\rho_{xy} = \left[\sum_{n=1}^{N} (x_n - y_n)^2 \right]^{1/2} \tag{10.3}$$

where X_N is a sequence of damage of length N simulated from the stochastic forward model defined in Equation 6.10. The scaling parameters for the ABC-SubSim algorithm used for this example are given in Table 10.6.

sample size	cond. probability	proposal std. deviation						sim. levels
(K)	(P_0)	$(\sigma_{q,i}^{(1)})$	$(\sigma_{q,i}^{(2)})$	$(\sigma_{q,i}^{(3)})$	$(\sigma_{q,i}^{(4)})$	$(\sigma_{q,i}^{(5)})$	$(\sigma_{q,i}^{(6)})$	(m)
10,000	0.2	10%	2%	1%	0.5%	0.1%	0.01%	6

Table 10.6: *Parameter configuration of ABC-SubSim algorithm for $\mathcal{M}_1$. The values for $\sigma_{q,i}^{(j)}$ are defined for the j-th simulation level as the specified percent of the 5-th-95-th inter-percentile range of the prior PDFs for the i-th component of the parameter vector, $i = 1, \ldots, d$.*

Figure 10.5 shows the posterior samples of model parameters calculated by ABC-SubSim algorithm with $m = 6$ simulation levels and $K = 10^4$ samples per simulation level. It implies that $N \times K \times (1 + m(1 - P_0)) = 5.8 \cdot 10^9$ model evaluations are used, which implies a significant computational saving when compared to the $5 \cdot 10^{14}$ model evaluations required by MCMC, as shown before.

The posterior information on model parameters obtained from ABC-SubSim algorithm is further used to obtain simulated sequences of damage which are represented in Figure 10.6. Note that the results are satisfactory in the sense that, in average, ABC-SubSim algorithm can reconstruct the observed damage response with precision with only a moderate computational cost. Note also that, the distributional tails are not being well covered using ABC-SubSim algorithm, as can be observed when Figure 10.6 is compared with the results from MCMC method shown in Figure 10.4. The lack of correspondence is expected

even if a larger amount of samples were used, since a non-null approximation error for the inference is implicit to the use ABC methods due to the circumvention of the likelihood function by means of simulations, as stated in Section 7.2.

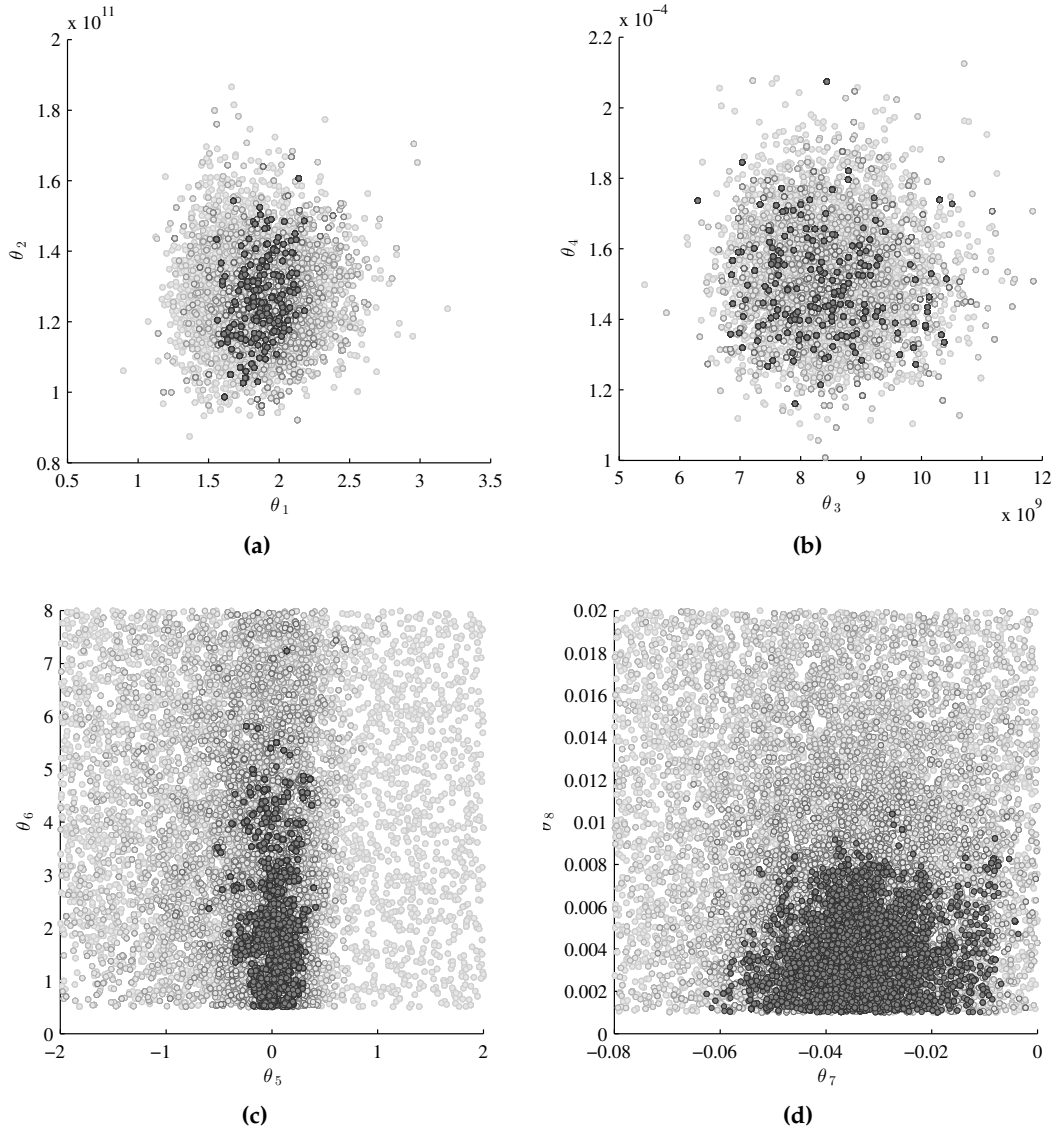

Figure 10.5: *Posterior samples from the marginalized posterior PDFs $p(\theta_i|\mathcal{D}, \mathcal{M}_1), i = 1 \dots 8$, after updating model class $\mathcal{M}_1$ (classical shear-lag) using ABC-SubSim algorithm. To reveal the uncertainty reduction, the intermediate posterior samples are superimposed in increasing gray tones. Gray rings correspond to prior samples.*

To provide further discussion about this matter, the quality of the inference using ABC-SubSim algorithm is examined. Two metrics are considered: a) the sample mean of the quadratic error between $\bar{\boldsymbol{\theta}}$ and $\bar{\boldsymbol{\theta}}_{MCMC}$, i.e., $\|\bar{\boldsymbol{\theta}} - \bar{\boldsymbol{\theta}}_{MCMC}\|_2^2$, being $\bar{\boldsymbol{\theta}}_{MCMC}$ the mean value of posterior model parameters obtained with MCMC and $\bar{\boldsymbol{\theta}}$ the mean of posterior model parameters at the last simulation level of ABC-SubSim algorithm; and b) the differential entropy of the final posterior by calculating $1/2 \ln |(2\pi e)^d \det [cov(\boldsymbol{\theta})]|$, where d is the dimension of the parameter space. The results are shown in Figure 10.7. Notice from panel (a)

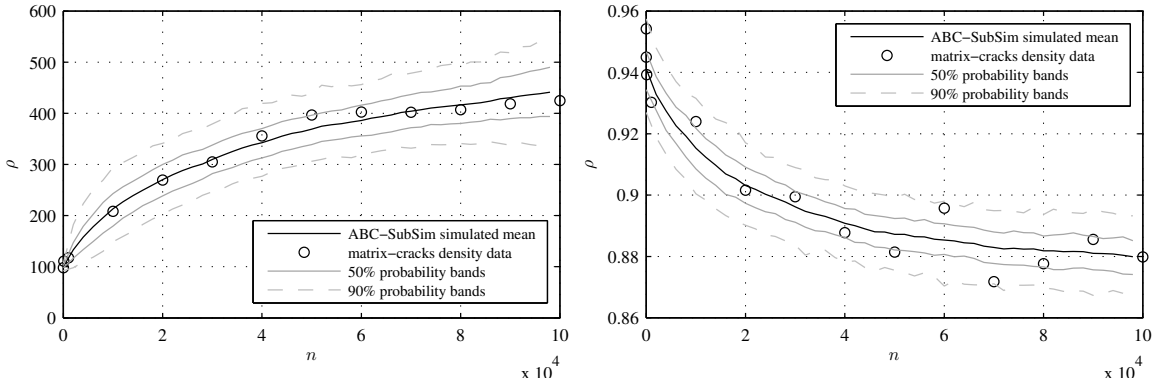

(a) Micro-cracks density **(b)** Normalized effective stiffness

Figure 10.6: *Simulated damage response using posterior parameters estimated from ABC-SubSim for model class $\mathcal{M}_1$ (classical shear-lag).*

that only five simulation levels are required to achieve a measure of uncertainty in posterior model parameters equal or similar than the uncertainty achieved when MCMC is used for the inference. Note also that $\|\bar{\boldsymbol{\theta}} - \bar{\boldsymbol{\theta}}_{MCMC}\|_2^2$ stabilizes for simulation level 5, which indicates that $m = 5$ can be considered as the final simulation level for the inference. The adoption of $m = 6$ as in Figure 10.5 is, thus, a safe choice.

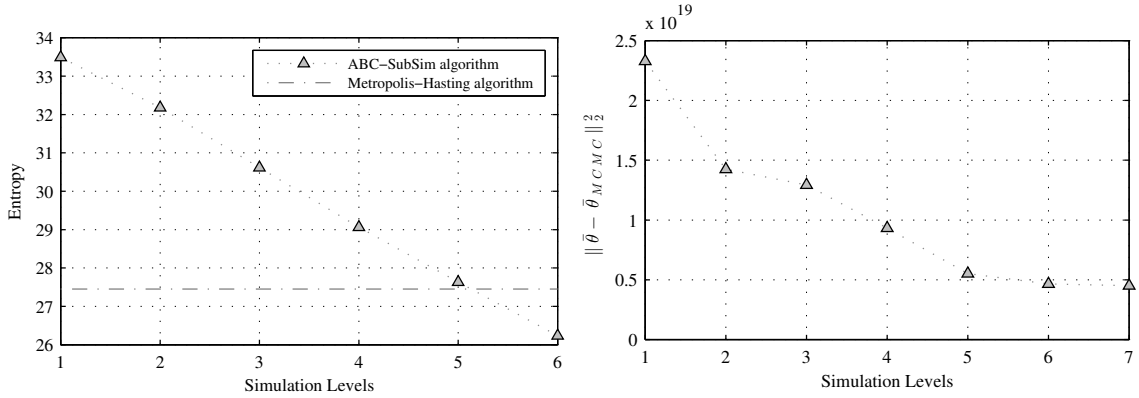

(a) Differential entropy **(b)** Mean quadratic error

Figure 10.7: *Differential entropy (left side) of the intermediate posterior samples using ABC-SubSim and mean quadratic error (right side) between $\bar{\boldsymbol{\theta}}$ and $\bar{\boldsymbol{\theta}}_{MCMC}$. Observe that ABC-SubSim algorithm gets posteriors with a differential entropy close to that obtained using MCMC algorithm from the 5-th simulation level. In addition, the accuracy of simulation gets an asymptotic behavior from the 5-th simulation level, so $m = 6$ is a safe choice.*

10.4 Discussion

The proposed Bayesian approach for model class selection is exemplified using several competing damage mechanics models, which represent physically different models with different degrees of non-linearity and dimensionality. As apparent from the results, the model classes that involve more complex analysis (i.e., variational and COD analysis, $\mathcal{M}_4$ and $\mathcal{M}_5$ respectively) do not necessarily provide higher probabilities in explaining the observed

damage response. This result contradicts the general conception that more complex analysis may be necessary to capture the various fatigue damage mechanisms and thus, to obtain better predictive performance. It is an example of the Principle of Model Parsimony in the context of fatigue damage modeling in composites, that comes into play through the information-theoretic interpretation of the evidence presented in Section 4.2.1. However, these results are based on data for one particular laminate configuration, so further investigations are needed to validate the results on other layups for a broader generalization.

More specifically, it can be observed in Table 10.5 that the evidence reaches the lowest values for either models classes that involve more complex damage-mechanics analysis, like $\mathcal{M}_5$, or models classes that involve parameters which are difficult to establish priors for, like $\mathcal{M}_3$. These low values for the evidence can be explained based on the likelihood function, that is actually evaluated using prior samples from a region of the parameters space far from the region of high likelihood (recall Equation 4.9). It is a consequence of (1) using high-sensitivity parameters as model parameters within the model class, which favors a narrower concentration of the high-likelihood region over the parameter space, and (2) having diffuse prior information for some of those parameters (such as the normalized shear modulus $\frac{G}{d_0}$ in $\mathcal{M}_3$). This, in turn, enforces a larger distance between the prior and the posterior PDFs that leads to a larger EIG term, thereby penalizing the evidence by Equation 4.10.

Notwithstanding, it should be noted that the use of high-sensitivity parameters does not automatically force the model class to extract more information from the data. It will ultimately depend on the "distance" between the likelihood function $p(\mathcal{D}|\boldsymbol{\theta}, \mathcal{M}_j)$ and the prior information $p(\boldsymbol{\theta}|\mathcal{M}_j)$ PDFs. In other words, the data make a difference only when they tell us something about the model parameters that the prior information does not [19]. This is typically the case for "fitting" parameters, that tend to capture much more information from the data than, for example, mechanical parameters, as shown in Figure 10.3. In this sense, the choice of widely dispersed priors for high-sensitivity parameters, such as non-informative priors, should be avoided since it leads to a huge information gain from the data. Thus, the contribution of the data-fit term (AGF) to the overall evidence of the model class may become negligible in relation to the high contribution of the EIG term, creating a bias in the model-class assessment problem [22]. Therefore, if such model class is utilized for future prediction, as arises in prognostics, the results are expected to significantly depend on the details of the data.

As a drawback of the method, it is remarked the high computational cost of the Bayesian inference problem, that would make difficult the extension to more sophisticated model classes for damage growth (e.g., FEM models). The use of a GPU accelerated MCMC algorithm is shown to drastically reduce the computational complexity of the problem, but the implementation is not trivial. However, the use of likelihood-free methods such as the one proposed in this thesis (ABC-SubSim algorithm) is shown to provide satisfactory results with a moderate computational cost.

In summary, the results have highlighted the relevance of the information-theoretic approach for model class assessment in the context of fatigue damage modeling in composites. The amount of information that the model class needs to extract from the data to update its prior information emerges as a key variable for model class assessment, which is in accordance with that obtained in Chapter 9 for Markov chain model classes. It actually determines the "information-theoretic complexity" of the model class, rather than the use of a more complex damage-mechanics approach or a larger number of parameters. Then, the evidence of the model class accounts for such information gain as a penalty term and implicitly enforces a quantitative Ockham's razor, such that simpler models that are consistent with data are favored through a healthy balance between the information gained from data and the average goodness of fit.

11

Bayesian model set assessment for damage models

This chapter aims at investigating the Hypothesis 2 of this thesis, by which *physics-based models are expected to better represent the fatigue behavior of composites as compared to data-driven approaches*. To this end, the performance of two different sets of models classes (e.g., Markov chain models (data-driven) and damage mechanics models (physics-based)) is compared and ranked based on probabilities that measure the relative plausibility/suitability of each individual set of classes in representing the observed damage response. The assessment is based on an extension of the Bayesian model class assessment methodology to the level of the set of models classes. In Section 11.1, the new methodology for Bayesian model set assessment is presented. The results of the assessment are presented in Section 11.2 and discussed in Section 11.3.

11.1 Methodology for Bayesian model set assessment

The most commonly encountered problem in the Bayesian literature is the model updating problem, i.e., find the set of most plausible/suitable values for model parameters in representing the system behavior, given data from the system response. To this end, Bayes' Theorem is applied to obtain the posterior PDF for the values of model parameters over a predefined set of possible values, as explained in Section 4.1. An extension of such problem, that has not been so well explored in the literature, is to find the most plausible/suitable model class representing an observed system output. This problem is referred to as Bayesian model class assessment and has been extensively discussed along this thesis, so it is not repeated here. The fundamentals about Bayesian model class assessment are provided in

Section 4.2. Here, an extension of the Bayesian model class assessment problem is proposed, i.e., find the most plausible/suitable set of classes that better represent an observed system output among a superset of candidates.

Let us consider N_S sets of models classes $\mathbf{M}_1, \mathbf{M}_2 \ldots, \mathbf{M}_{N_S}$ defining a superset of (mutually exclusive) candidates $\mathfrak{M}$=$\{\mathrm{M}_1, \mathbf{M}_2 \ldots, \mathbf{M}_{N_S}\}$, such that $p(\mathfrak{M}) = \sum_{i=1}^{N_S} p(\mathbf{M}_i) = 1$. Each set $\mathbf{M}_i \subset \mathfrak{M}$ is compounded by $N_M^{(i)}$ model classes, i.e., $\mathbf{M}_i = \{\mathcal{M}_1^{(i)}, \mathcal{M}_2^{(i)} \ldots, \mathcal{M}_{N_M^{(i)}}^{(i)}\}$. Thus, the goal is to use data $\mathcal{D}$ from the system response to assess the posterior probability of a particular set $\mathbf{M}_i$ for representing the system. This is accomplished by applying Bayes' Theorem at the level of the set of classes, as follows:

$$p(\mathbf{M}_i|\mathcal{D}, \mathfrak{M}) = \frac{p(\mathcal{D}|\mathbf{M}_i, \mathfrak{M})p(\mathbf{M}_i|\mathfrak{M})}{\sum_{j=1}^{N_S} p(\mathcal{D}|\mathbf{M}_j, \mathfrak{M})p(\mathbf{M}_j|\mathfrak{M})} \tag{11.1}$$

where $p(\mathbf{M}_i|\mathfrak{M})$ is the prior plausibility of the set $\mathbf{M}_i \subset \mathfrak{M}$, and $p(\mathcal{D}|\mathbf{M}_i, \mathfrak{M})$ is the evidence of $\mathbf{M}_i \subset \mathfrak{M}$ for the data $\mathcal{D}$, which expresses how likely the system response is reproduced if the complete set of classes $\mathbf{M}_i$ is adopted.

The evidence of the set can be obtained as a generalization of the evidence of the model class using Total Probability Theorem, as

$$p(\mathcal{D}|\mathbf{M}_i, \mathfrak{M}) = \sum_{j=1}^{N_M^{(i)}} p(\mathcal{D}|\mathcal{M}_j^{(i)}\mathbf{M}_i, \mathfrak{M})p(\mathcal{M}_j^{(i)}|\mathbf{M}_i, \mathfrak{M}) \tag{11.2}$$

where $p(\mathcal{D}|\mathcal{M}_j^{(i)}\mathbf{M}_i, \mathfrak{M})$ is the "regular" evidence of model class $\mathcal{M}_j^{(i)}$ in the set $\mathbf{M}_i$, (as defined in Section 4.2), and $p(\mathcal{M}_j^{(i)}|\mathbf{M}_i, \mathfrak{M})$ the "regular" prior plausibility of $\mathcal{M}_j^{(i)}$ in $\mathbf{M}_i$. In the next section, the method presented here is applied for the two sets of damage models proposed in this thesis.

11.2 Results for Bayesian model set assessment

In this section, the performance of both set of classes, Markov chain models and damage-mechanics models, is compared based on posterior probabilities using the methodology presented in Section 11.1. The data used for the assessment corresponds to Dataset 2 (presented in Section 8.2), given that the model class assessment of each individual model class is available for both set of classes using this dataset (e.g., Markov chain models in Chapter 9, and damage mechanics models in Chapter 10). For the sake of clarity, this dataset is summarized in Table 11.1 below.

Fatigue cycles, n_k	10^1	10^2	10^3	10^4	$2{\cdot}10^4$	$3{\cdot}10^4$	$4{\cdot}10^4$	$5{\cdot}10^4$	$6{\cdot}10^4$	$7{\cdot}10^4$	$8{\cdot}10^4$	$9{\cdot}10^4$	10^5
ρ_{n_k} [# cracks/m]	98.2	111.0	117.4	208.5	269.6	305.0	355.5	396.4	402.3	402.1	407.0	418.5	424.5
D_{n_k}	0.954	0.939	0.930	0.924	0.902	0.899	0.888	0.881	0.896	0.872	0.877	0.885	0.880

Table 11.1: *Summary of damage data for Dataset 2, corresponding to a cross-ply* $[0_2/90_4]_s$ *CFRP laminate; i.e.,* $\mathcal{D} = \{\mathbf{y}_{n_1}, \ldots, \mathbf{y}_{n_k}, \ldots, \mathbf{y}_{n_N}\}$, *where* $\mathbf{y}_{n_k} = (\rho_{n_k}, D_{n_k})$, $n_k \in \mathbb{N}$.

Let us consider $\mathbf{M}_1 = \{\mathcal{M}_1^{(1)}, \mathcal{M}_2^{(1)}, \mathcal{M}_3^{(1)}, \mathcal{M}_4^{(1)}\}$, the set of Markov chain models classes defined in Chapter 9, and $\mathbf{M}_2 = \{\mathcal{M}_1^{(2)}, \mathcal{M}_2^{(2)}, \mathcal{M}_3^{(2)}, \mathcal{M}_4^{(2)}, \mathcal{M}_5^{(2)}\}$ the set of damage mechanics models classes defined in Chapter 10. To differentiate both sets of model classes the superscripts (1) and (2) are used for the set of Markov chain models and the set of damage mechanics models, respectively. These sets of classes define the superset $\mathfrak{M} = \{\mathbf{M}_1, \mathbf{M}_2\}$, such that $p(\mathbf{M}_1) + p(\mathbf{M}_2) = 1$ and $p(\mathbf{M}_i|\mathfrak{M}) = 0.5,\ i = 1, 2$, i.e., both sets are considered equally plausible a priori. Therefore, the posterior probability of the set $\mathbf{M}_i \subset \mathfrak{M},\ i = 1, 2$, can be readily obtained from Equation 11.1, as

$$p(\mathbf{M}_i|\mathcal{D}, \mathfrak{M}) = \frac{p(\mathcal{D}|\mathbf{M}_i, \mathfrak{M})}{p(\mathcal{D}|\mathbf{M}_1, \mathfrak{M}) + p(\mathcal{D}|\mathbf{M}_2, \mathfrak{M})} \tag{11.3}$$

where $p(\mathcal{D}|\mathbf{M}_i, \mathfrak{M})$ is the evidence of the set $\mathbf{M}_i$ in the superset $\mathfrak{M}$ of model classes. As explained in Chapters 9 and 10, the prior probability of each model class was chosen as $p(\mathcal{M}_j^{(i)}|\mathfrak{M}) = 1/N_M^{(i)}$, being $N_M^{(1)} = 4$ and $N_M^{(2)} = 5$; therefore, from Equation 11.2, the evidence of the set of model classes $\mathbf{M}_i$ can be calculated as the averaged mean of the evidences of the individual model classes that compound the set, as follows:

$$p(\mathcal{D}|\mathbf{M}_i, \mathfrak{M}) = \frac{1}{N_M^{(i)}} \sum_{j=1}^{N_M^{(i)}} p(\mathcal{D}|\mathcal{M}_j^{(i)}\mathbf{M}_i, \mathfrak{M}) \tag{11.4}$$

where $p(\mathcal{D}|\mathcal{M}_j^{(i)}\mathbf{M}_i, \mathfrak{M})$ is the evidence of model class $\mathcal{M}_j^{(i)}$ in the set $\mathbf{M}_i$. By substituting the values for the evidences of each model class (provided in Tables 9.5 and 10.5, for Markov chain models and damage mechanics models, respectively) into Equation 11.4, the evidence of the overall set is obtained. Finally, the posterior probability of the set of classes is given by Equation 11.3, using the values of the evidence for the set previously obtained. The results are shown in Table 11.2.

	model set $\mathbf{M}_1$				model set $\mathbf{M}_2$				
	$\mathcal{M}_1^{(1)}$	$\mathcal{M}_2^{(1)}$	$\mathcal{M}_3^{(1)}$	$\mathcal{M}_4^{(1)}$	$\mathcal{M}_1^{(2)}$	$\mathcal{M}_2^{(2)}$	$\mathcal{M}_3^{(2)}$	$\mathcal{M}_4^{(2)}$	$\mathcal{M}_5^{(2)}$
$\log p(\mathcal{D}\|\mathcal{M}_j^{(i)}\mathbf{M}_i, \mathfrak{M})$	-21.58	-23.35	-26.11	-28.51	-9.99	-10.80	-16.62	-10.72	-14.16
$p(\mathcal{M}_j^{(i)}\|\mathfrak{M})$	0.25	0.25	0.25	0.25	0.2	0.2	0.2	0.2	0.2
$p(\mathcal{D}\|\mathbf{M}_i, \mathfrak{M})$	$6.65 \cdot 10^{-23}$				$2.75 \cdot 10^{-11}$				
$p(\mathbf{M}_i\|\mathfrak{M})$	0.5				0.5				
$p(\mathbf{M}_i\|\mathcal{D}, \mathfrak{M})$	$2.42 \cdot 10^{-12} \approx 0$				$0.9999 \approx 1$				

Table 11.2: *Results of Bayesian model set assessment for two sets of model classes ($\mathbf{M}_1$: Markov chain models, $\mathbf{M}_2$: damage mechanics models) using data from Dataset 2. The values for the log-evidences of each model class $\log p(\mathcal{D}|\mathcal{M}_j^{(i)}\mathbf{M}_i, \mathfrak{M})$ are taken from Tables 9.5 and 10.5 for $\mathbf{M}_1$ and $\mathbf{M}_2$ respectively.*

11.3 Discussion

A novel procedure for Bayesian model set assessment is proposed in this chapter in response to the Hypothesis 2 of this thesis (see Chapter 2). The Bayesian model set assessment

approach is exemplified for two sets of model classes which represent physically different models with different hypothesis about damage growth, using damage data from Dataset 2 (Section 8.2). As apparent from the results, the set of damage mechanics model classes $\mathbf{M}_2$ turns out to be the most plausible in explaining the system response conditional on the data, as compared to the set of Markov chain model classes, $\mathbf{M}_1$, whose relative plausibility is almost zero. A first indication of such extreme result can be found in the evidence of the sets of classes $p(\mathcal{D}|\mathbf{M}_i, \mathfrak{M}),\ i = 1, 2$, where in view of the results in Section 11.2, the evidence of the set $\mathbf{M}_2$ is several orders of magnitude larger than that for $\mathbf{M}_1$. It means that models classes in $\mathbf{M}_2$ concentrate much more prior probability density in the region of high-likelihood of the parameter space than that of the set of Markov chain model classes. In other words, model classes in $\mathbf{M}_2$ extracts, in average, less information from data to update their associated prior information, which according to the information-theoretic interpretation of the evidence (recall Section 4.2.1), leads to higher evidences. In contrast, Markov chain models need the support from data to get the information about model parameters that the prior PDF of parameters does not provide, thus penalizing drastically their evidences.

However, these results should not be taken as an authoritative assertion that Markov chain models are not valid to predict damage growth. Or even more, that the hypothesis made about damage accumulation for $\mathbf{M}_1$ are *false* while the hypothesis for $\mathbf{M}_2$ are *true*[1]. A suitable judgment about these results is that the set of Markov chain model classes turns out to be extremely improbable as compared to the set of damage mechanics model classes, conditional on the data at hand (Dataset 2) and provided a specified prior information for model parameters, model classes, and set of classes. If any of the given conditions change, a different problem would be considered instead of the one just discussed, so a different outcome would be expected. In such case, Bayes' Theorem enables us to update the previous *state of knowledge* about the system being assessed, leading to new posterior probabilities for $\mathbf{M}_1$ and $\mathbf{M}_2$. Therefore, a broad generalization could lead to wrong conclusions about the accuracy and range of validity of such results.

In summary, the results have highlighted the relevance of the Bayesian model set approach proposed in this chapter in the context of fatigue damage modeling. The evidence of the set of model classes emerges as a key variable for the assessment of the overall set of classes, as it accounts for the averaged amount of information that the set of models needs to extract from data to make accurate predictions. Then, Bayes' Theorem converts such evidences into posterior probabilities that rigorously allows us for model set comparison.

[1] which would be an instance of the Mind Projection Fallacy [19], confusing reality with a state of knowledge about reality.

Part IV

CONCLUSIONS AND FUTURE WORKS

I used to be indecisive, but now
I'm not so sure

Boscoe Pertwee (s. XVIII)

12

Conclusions and future works

Modeling the progression of fatigue damage in composite materials is a challenge mainly due to the lack of knowledge about the multi-scale physics of the fatigue damage process. As a result, there is uncertainty related to the choice of a particular model class among a set of possible candidates for predicting damage behavior. In this doctoral thesis, a full Bayesian framework was presented to give a rigorous way to incorporate the modeling uncertainties for the inference about damage progression in composites. Several model classes were defined and ranked based on estimated probabilities that measure the relative degree of plausibility of each model class within the set of candidates for representing the system (fatigue damage degradation) based on data from the system response. The overall procedure was demonstrated by several case studies using damage data from CFRP and GFRP laminates subjected to tension-tension fatigue loads. The results showed that the most probable model classes among the competing candidates result to be the simplest models that provided reasonable goodness of fit with data. Thus, the principle of Ockham's razor, that in this context can be stated as *simpler models that are consistent with data are to be preferred over unnecessarily complicated ones*, seems to hold true for the fatigue modeling framework investigated in this thesis. This conclusion should not be interpreted as an imposed condition but a natural outcome when dealing with models informed by data within a Bayesian framework, since the application of Bayes' Theorem has been shown to automatically enforce a quantitative Ockham's razor.

In addition, the following general conclusions are also extracted from each of the hypothesis investigated in this thesis, outlined in Chapter 2. Further works and limitations are also highlighted:

Hypothesis 1: *Damage progression in composites can be idealized as a Markovian-type stochastic process.*

A new modeling scheme based on Markov chains was developed in Chapter 5 to deal with the well-known variability that is observed in the fatigue damage accumulation process in composite materials. The key contribution was a new model parameterization to efficiently account for the non-stationarity of the damage process based on a generalization of the time transformation-condensation method by Bogdanoff and Kozin [47]. The model was validated in Chapter 9 for two datasets through the definition of several model parameterizations, showing efficiency and accuracy in the predictions. As a general comment, it was observed that accounting for the non-stationarity significantly improves the model datafit but also implies less robustness, in the sense of a small variation of model parameters may confer a significant change in the model prediction. Then, the Bayesian model class assessment framework adopted in this thesis enables us to rigorously select the "optimal" model class among the set of candidates through a balance between the information gained from data and the average goodness of fit. In addition, the Bayesian approach proposed for fatigue modeling has allowed us to obtain a measure of the information gain from each test repetition that can be used to select a minimum set of specimens for the dataset, with the ultimate benefit being the avoidance of unnecessary costs in fatigue experimental programs.
A typical criticism of Markov chain models is their lack of a physical basis, given that they are purely based on statistical concepts and monitoring data. However, we find clear advantages with respect to other models due to their ability to deal with complex processes with no further computational effort. Hence, a future work in this direction would be the extension of the proposed Markov chain models in application to problems of damage accumulation in the context of a full-scale composite component or structure. In addition, as further works, it would be desirable to obtain plausible relations between the predominance of certain fatigue damage mechanisms (e.g., microcracks, delamination, etc.) and the parameters of the Markov chain. Furthermore, a continuous-time version of the Markov chain model would be beneficial, given that it would eliminate the dependence of the estimated value of the model parameters on the selected duty cycle.

Hypothesis 2: *Physics-based models are expected to better represent the fatigue behavior of composites as compared to data-driven approaches.*

In Chapter 11, the set of damage mechanics model classes defined in Chapter 6 was compared to the set of Markov chain model classes defined in Chapter 5. The comparison was carried out using multi-scale damage data from CFRP laminates (Dataset 2) by means of an extension of the Bayesian model class selection methodology to

the level of the set of models classes. As apparent from the results, the set of damage mechanics model classes resulted in the most plausible set (with almost total probability) to represent the observed damage response in relation to the set of Markov chain model classes. As with model class assessment, the amount of information that the overall set of model classes needs to extract from the data emerged as a key measure for the model set assessment. The evidence of the set of classes accounts for such information gain and Bayes' Theorem at the level of the set of model classes converts such evidences to posterior probabilities, which rigorously allowed us for the model set comparison.

As discussed in Chapter 11, these results may not serve to conclude that Markov chain models are not valid to predict damage growth, or even more, that the hypothesis made about damage accumulation for Markov chain models are *false* while the hypothesis for damage mechanics models are *true*. From a pragmatic point of view, all we can say is that, conditional on the data and the available prior information, the set of Markov chain model classes is not plausible in relation to the set of damage mechanics model classes. If any of the given conditions change, Bayes' Theorem enables us to update the previous state of knowledge about these sets of model classes, leading to new posterior probabilities for the set.

Given that the proposed methodology for model set assessment is general in nature, it can be extended to a wide range of modeling problems in which not one but several families of model classes can be formulated and hypothesized to represent the system.

Hypothesis 3: *Simpler models for fatigue damage evolution in composites that agree reasonably well with the data are expected to overperform more sophisticated competing candidates.*

The Bayesian model class selection approach pursued in thesis was applied to two sets of model classes for damage growth (Markov chain models and damage mechanics models) to assess the relative degree of plausibility of each model class within the set of candidates. This plausibility was computed by means of Bayes' Theorem using the evidence for the model class given by the data and the choice of the prior probability for each model class. In view of the results, the simpler model classes that provided reasonable goodness of fit turned out to be the most probable candidates when selected by striking a balance between average goodness of fit and amount of information extracted from data. This conclusion holds true for the two sets of model classes investigated in this thesis, namely, the Markov chain models and the damage mechanics models. The amount of information that each model class gains from the data emerged as a key variable for the Bayesian assessment since it actually determines the "information-theoretic complexity" of the model class, rather than the use of more complex formulations for the damage models. The evidence of the model class

accounts for such information gain as a penalty term and implicitly enforces a quantitative Ockham's razor, such that simpler models that are consistent with data are preferred.

As a limitation of the method, it is highlighted the high computational cost of the Bayesian inference problem using the Metropolis-Hasting (M-H) algorithm. The use of a GPU accelerated M-H algorithm was shown to drastically reduce the computational complexity of the problem, however the implementation in the GPU is not a trivial task. Then, the use of the ABC-SubSim algorithm proposed in Chapter 7 was revealed as a promising solution since it provided satisfactory results for the inference with a moderate computational cost. In addition, this algorithm has raised to an original contribution in the specialized literature for Approximate Bayesian Computation due to its higher efficiency in relation to most recent ABC algorithms. A future work in this context would be the use of ABC-SubSim algorithm to efficiently estimate the evidence of a model class for Bayesian model class assessment, as well as the extension of ABC-SubSim algorithm for real-time filtering problems for prognostics applications.

Finally, as further works, more research effort would be needed to incorporate the effects of other manifestations of fatigue damage such as delamination in the proposed Bayesian framework, and in general, to extend this approach to other engineering materials with uncertain damage or evolutive behavior, such as biomaterials.

Solía estar indeciso, pero ahora
no estoy tan seguro

Boscoe Pertwee (s. XVIII)

13

Conclusiones y trabajos futuros

La modelización del proceso de daño por fatiga en materiales compuestos es un reto de investigación debido principalmente a la falta de conocimiento sobre la física del proceso subyacente de daño. En consecuencia, existe incertidumbre en relación con la selección de una determinada clase de modelos de entre un conjunto de posibles candidatos para la predicción de la evolución del daño por fatiga. En esta tesis doctoral se ha propuesto un marco Bayesiano que permite incorporar de forma rigurosa la incertidumbre procedente de la selección de un modelo particular en la inferencia del daño en materiales compuestos. Varias clases de modelos han sido definidas y clasificadas en base a valores de probabilidad que miden el grado de plausibilidad relativo de cada clase para representar un sistema según la información procedente de la respuesta del sistema. Este procedimiento ha sido demostrado mediante varios casos de estudio que usan datos reales de daño en laminados de fibra de carbono y vidrio expuestos a cargas de fatiga tipo tensión-tensión. Los resultados mostraron que las clases más probables entre las posibles candidatas resultaron ser aquellas que, siendo las más simples, proporcionaron un ajuste razonable con los datos. Se observa por tanto el principio del "cuchillo de Ockham" para los modelos de fatiga investigados en esta tesis, que en este contexto puede enunciarse como *los modelos más simples que sean consistentes con los datos son preferibles sobre aquellos innecesariamente más complejos*. Esta conclusión no debe interpretarse como una condición impuesta, sino como un resultado natural cuando se trata de modelos informados por datos dentro de un marco Bayesiano, ya que se ha demostrado que la aplicación del Teorema de Bayes automáticamente implica una expresión cuantitativa del principio del cuchillo de Ockham.

A continuación se exponen una serie de conclusiones generales que son extraídas de cada una de las hipótesis iniciales investigadas en esta tesis, descritas en el Capítulo 2. Así mismo se exponen las limitaciones de esta investigación así como futuras líneas de trabajo.

Hipótesis 1: *La evolución del daño en materiales compuestos puede ser idealizada como un proceso estocástico de tipo Markoviano*

Un nuevo modelo escotástico basado en cadenas de Markov se ha presentado en el Capítulo 5 con objeto de idealizar el proceso de acumulación de daño en materiales compuestos teniendo en cuenta la manifiesta variabilidad del proceso. Un punto clave fue la propuesta de una nueva parametrización del modelo estocástico basado en una generalización del método de condensación del tiempo propuesta por Bogdanoff y Kozin [47], con objeto poder considerar de forma eficiente la no estacionariedad del proceso de daño. El modelo estocástico fue validado en el Capítulo 9 usando dos conjuntos distintos de datos de daño, demostrando eficacia y precisión en la predicción. Como comentario general, se ha observado que la consideración de la no estacionariedad mejora significativamente el ajuste a los datos pero a su vez implica una menor robustez, en el sentido de que una pequeña variación en el valor de los parámetros del modelo puede ocasionar un cambio significativo en la predicción del modelo. En este contexto, el marco Bayesiano de evaluación de clases de modelos propuesto en esta tesis ha permitido seleccionar rigurosamente el modelo "óptimo" de entre un conjunto de posibles candidatos considerando para ello un balance entre la bondad de ajuste de cada modelo y la información extraída de los datos. Además el enfoque Bayesiano propuesto ha permitido obtener una medida de la ganancia de información procedente de la incorporación de una nueva repetición al conjunto de datos, que puede ser usado para seleccionar el número mínimo de muestras a ensayar, con el beneficio final de evitar costes innecesarios en los programas experimentales de fatiga.

Una crítica típica de los modelos de daño basados en cadenas de Markov es la falta de significado físico, en el sentido de que están basados netamente en conceptos estadísticos y en datos de monitorización. Sin embargo, estos modelos ofrecen claras ventajas con respecto a otro tipo de modelos debido a su eficacia para hacer frente a procesos complejos de daño sin necesidad de altos requerimientos computacionales. Por lo tanto, una línea futura trabajo en este sentido sería la extensión de los modelos basados en cadenas de Markov en aplicación a problemas de acumulación de daño en el contexto de un componente o estructura de material compuesto a escala real. Sería así mismo deseable obtener relaciones plausibles entre el predominio de ciertos mecanismos físicos de daño por fatiga (microgrietas, delaminación, etc.) y los parámetros del modelo de Markov. Además, una versión en tiempo continuo del

modelo de cadenas de Markov sería beneficiosa puesto que eliminaría la dependencia del valor de los parámetros en la elección de la discretización del tiempo de ensayo.

Hipótesis 2: *Se espera que los modelos basados en física representen mejor el comportamiento a fatiga en materiales compuestos en comparación a otros modelos basados en datos*

En el Capítulo 11, el conjunto de modelos basados en mecánica del daño (definidos en el Capítulo 6) fue comparado con el conjunto de modelos basados en cadenas de Markov, presentados en el Capítulo 5. La comparación se llevó a cabo mediante una extensión de la metodología Bayesiana de selección de modelos al nivel del conjunto de modelos, utilizando para ello datos multi-escala de daño por fatiga en laminados de fibra de carbono (presentado como "Dataset 2" en esta tesis). Los resultados evidenciaron que el conjunto de modelos basados en mecánica del daño resultó ser el más plausible (con una probabilidad casi total) para representar la respuesta observada por los datos en relación al conjunto de modelos basados en cadenas de Markov. Al igual que fue observado con la evaluación Bayesiana para un modelo, la cantidad de información que el conjunto de modelos necesita extraer de los datos emergió como una medida clave para la evaluación de la plausibilidad del conjunto de modelos. La evidencia del conjunto modelos tiene en cuenta dicha medida de la ganancia de información y posteriormente el Teorema de Bayes convierte dicha evidencia en valores de probabilidad a posteriori, posibilitando una comparación rigurosa entre conjuntos de modelos.

Como fue discutido en el Capítulo 11, estos resultados no deben servir para concluir que los modelos basados en cadenas de Markov no son válidos para predecir la evolución del daño por fatiga, o incluso, que las hipótesis adoptadas sobre evolución de daño para los modelos de Markov son *falsas*, mientras que las hipótesis de los modelos basados en mecánica de daño son las *verdaderas*. Desde un punto de vista pragmático, lo único que se puede afirmar es que, según los datos y teniendo en cuenta la información a priori disponible, el conjunto de modelos basados en cadenas de Markov no es plausible en relación al conjunto de modelos basados en mecánica del daño. Si se diese algún cambio en alguna de las condiciones iniciales dadas, el Teorema de Bayes permitiría actualizar la información a priori disponible, dando lugar a nuevas probabilidades a posteriori.

Dado que la metodología propuesta para la evaluación de un conjunto de modelos es general, esta puede ser extendida a una amplia gama de problemas de modelización en los que existan varias familias posibles de modelos para representar un mismo sistema.

Hipótesis 3: *Se espera que los modelos más simples para la evolución de daño por fatiga en materiales compuestos, que ajusten razonablemente bien a los datos, se comporten mejor que*

otros modelos más sofisticados

El marco de selección Bayesiana de modelos propuesto en esta tesis fue aplicado a dos conjuntos de modelos para evolución de daño por fatiga (los basados en cadenas de Markov y aquellos basados en mecánica del daño) para evaluar el grado relativo de plausibilidad de los modelos pertenecientes a cada conjunto de candidatos. La plausibilidad fue calculada mediante el Teorema de Bayes utilizando la evidencia de cada clase según la información procedente de los datos y la información a priori. En vista de los resultados obtenidos, las clases más simples que proporcionaron un ajuste razonable con los datos resultaron ser las más probables mediante un equilibrio entre la bondad media de ajuste y la cantidad de información extraída de los datos. Esta conclusión es válida para los dos conjuntos de modelos investigados en esta tesis. La cantidad de información que los modelos obtienen de los datos emergió como una medida clave para la evaluación Bayesiana, puesto que realmente determina la complejidad de los modelos desde el punto de vista de la teoría de la información, en lugar de la utilización de expresiones de mayor complejidad para los modelos de daño. La evidencia de cada modelo tiene en cuenta la ganancia de información como un término de penalización, de forma que hace cumplir de manera cuantitativa el principio del cuchillo de Ockham, mediante el cual los modelos más simples que sean consistentes con los datos resultan ser los más evidentes.

Como limitación del método se destaca el alto coste computacional del algoritmo Metropolis-Hasting (M-H) usado para la inferencia Bayesiana de los modelos. La aceleración del algoritmo mediante su implementación en GPU ha demostrado reducir drásticamente el tiempo de computación, aunque es de destacar que la implementación en GPU no es trivial. Una solución prometedora a este problema se obtuvo mediante el uso del algoritmo ABC-SubSim propuesto en el Capítulo 7, puesto que proporciona soluciones satisfactorias para la inferencia con un coste computacional moderado. Además, este algoritmo ha propiciado una contribución original en la literatura especializada de Computación Bayesiana Aproximada (en inglés, ABC) debido a su mayor eficiencia en relación con la mayoría de los algoritmos propuestos recientemente para ABC. Un trabajo futuro en este contexto sería el uso del algoritmo ABC-SubSim para estimar de manera eficiente la evidencia de una clase de modelos, así como su extensión a problemas de filtrado de información en tiempo real en aplicaciones de pronóstico.

Por último, como trabajos futuros se proponen la incorporación de los efectos de otras manifestaciones de daño por fatiga, como delaminación, etc., en el marco Bayesiano propuesto, y en general, ampliar el marco Bayesiano en aplicación a otros materiales de ingeniería cuya evolución temporal o comportamiento frente daño sea incierto, como ocurre por ejemplo con ciertos biomateriales.

A

Basics relations

This appendix provides the expressions of some of the terms and relations used in the formulation of the damage mechanics models defined in Chapter 6.

The function a in Equation 6.1 for the effective longitudinal Young's modulus is defined as:

$$a = \frac{E_2 t_{90}}{E_1 t_\phi} \left(1 - \nu_{xy}^{(\phi)} \frac{\frac{\nu_{xy}^{(\phi)} t_{90}}{E_y^{(\phi)}} + \frac{\nu_{12} t_\phi}{E_2}}{\frac{t_{90}}{E_y^{(\phi)}} + \frac{t_\phi}{E_1}} \right) \frac{1 - \nu_{12} \nu_{xy}^{(\phi)}}{1 - \nu_{12}^2 \frac{E_2}{E_1}} \tag{A.1}$$

In the last and subsequent equations, the subscripts $\{1, 2, 3\}$ refer to ply properties defined in local axis while subscripts $\{x, y, z\}$ refer to sub-laminate or laminate properties defined in global axis, that corresponds to the laminate coordinate system. Note that the first local direction "1" coincides with fibers direction in a given ply or lamina, and directions "2-3" are the in-plane and out-of-plane transverse directions. For global axes, "x" refers to the fatigue loading direction, while "y" and "z" refer to the in-plane and out-of-plane transverse directions, respectively. In addition, superscript (ϕ) denotes "property referred to the $\left[\phi_{\frac{n_\phi}{2}}\right]$-sublaminate".

The ply and laminate properties appearing in Equation A.1 and rest of equations in this appendix are defined in the List of Symbols of this thesis, however for the sake of clarity they are reproduced here in Table A.1 below.

The constants α_1, α_2 involved in the average stress perturbation function of Equation 6.2b are defined as $\alpha_1 = \frac{1}{2}\sqrt{2\sqrt{q} - p}$, and $\alpha_2 = \frac{1}{2}\sqrt{2\sqrt{q} + p}$ respectively, where p

Laminate	$E_{x,0}$	Initial longitudinal Young's modulus		t_ϕ	$[\phi_{\frac{n_\phi}{2}}]$-sublaminate thickness
	E_x^*	Effective long. Young's modulus	Ply	t	Ply thickness
	h	Laminate half-thickness		d_0	Interlaminar layer thickness
	B	Laminate half-width		G_m	Interlaminar layer shear modulus
Sublaminate	$E_x^{(\phi)}$	Longitudinal Young's modulus		E_1	Longitudinal Young's modulus
	$E_y^{(\phi)}$	Transverse Young's modulus		E_2	Transverse Young's modulus
	$\nu_{xy}^{(\phi)}$	In-plane Poisson ratio		ν_{12}	In-plane Poisson ratio
	$G_{xy}^{(\phi)}$	In-plane shear modulus		ν_{23}	Out-of-plane Poisson ratio
	$G_{xz}^{(\phi)}$	Out-of-plane shear modulus		G_{12}	In-plane shear modulus
	t_{90}	$[90_{n_{90}}]$-sublaminate half-thickness		G_{23}	Out-of-plane shear modulus

Table A.1: *Nomenclature table. Nominal values of main ply and geometry parameters are provided in Table 10.2*

and q are known functions of the ply properties defined as $p = \frac{C_2 - C_4}{C_3}$, $q = \frac{C_1}{C_3}$. The terms $C_i,\ i : \{1, \ldots, 4\}$ in last equations are calculated as follows:

$$C_1 = \frac{1}{E_2} + \frac{1}{\lambda E_x^{(\phi)}} \tag{A.2}$$

$$C_2 = \left(\lambda + \frac{2}{3}\right) \frac{\nu_{23}}{E_2} - \frac{\lambda \nu_{xz}^{(\phi)}}{3E_x^{(\phi)}} \tag{A.3}$$

$$C_3 = (1 + \lambda)\left(3\lambda^2 + 12\lambda + 8\right) \frac{1}{60E_2} \tag{A.4}$$

$$C_4 = \frac{1}{3}\left(\frac{1}{G_{23}} + \frac{\lambda}{G_{xz}^{(\phi)}}\right) \tag{A.5}$$

In Equations A.2 to A.5, $\lambda = \frac{t_\phi}{t_{90}}$ and ν_{23} and G_{23} are the out-of-plane Poisson ratio and shear modulus of the ply, respectively. Both terms are related as $G_{23} = \frac{E_2}{2(1+\mu_{23})}$. For the cross-ply laminates considered in Chapter 10, the fibers direction in the outer sub-laminate is $\phi = 0°$, and thus, the laminate and sub-laminate global axes $\{x, y, z\}$ coincide with ply local axes $\{1, 2, 3\}$. In this particular case, the following identities hold:

$$E_x^{(0)} = E_1; \quad E_y^{(0)} = E_2; \quad \nu_{xy}^{(0)} = \nu_{12}; \quad G_{xy}^{(0)} = G_{12}; \quad G_{xz}^{(0)} = G_{12}$$

The initial longitudinal Young's modulus of the laminate $E_{x,0}$ can be obtained using the classical laminate plate theory [145]; however, for the composite materials considered in Chapter 10 it can be readily approximated using a simple rule of mixtures:

$$E_{x,0} \approx \frac{t_0 E_1 + t_{90} E_2}{t_0 + t_{90}} \tag{A.6}$$

Regarding the COD-based model by [134], the matrices $\mathbf{A}^k$ are given by (k denotes that it is referred to the k-th ply):

$$\mathbf{A}^k = \mathbf{N}_I^k (\mathbf{S}^k)^{-1} \tag{A.7}$$

where $\mathbf{S}^k$ is the inplane compliance matrix of ply k, and $\mathbf{N}_I^k$ is a matrix defined by the vector normal to the surface of transverse crack, $\mathbf{n}^k$, as:

$$\mathbf{N}_I^k = \begin{pmatrix} n_1^k & 0 & n_2^k \\ 0 & n_2^k & n_1^k \\ 0 & 0 & 0 \end{pmatrix}, \mathbf{n}^k = \begin{pmatrix} n_1^k \\ n_2^k \\ 0 \end{pmatrix} \tag{A.8}$$

The matrix $\boldsymbol{\beta}^{ki}$ is related to the average crack opening displacement of matrix micro-cracks and also with the tension on the crack surface:

$$\boldsymbol{\beta}^{ki} = 0, \forall k \neq i; \quad \boldsymbol{\beta}^{kk} = \begin{pmatrix} \beta_1^k & 0 & 0 \\ 0 & \beta_2^k & 0 \\ 0 & 0 & \beta_3^k \end{pmatrix} \tag{A.9}$$

where

$$\beta_1^k = \frac{4}{\pi}\gamma_1 \frac{\ln\left(\cosh\left(\frac{\pi t^k \rho^k}{2}\right)\right)}{(t^k\rho^k)^2} \tag{A.10a}$$

$$\beta_2^k = \frac{\pi}{2}\gamma_2 \sum_{j=1}^{10} \frac{a_j}{(1+t^k\rho^k)^j} \tag{A.10b}$$

$$\beta_3^k = \frac{\pi}{2}\gamma_3 \sum_{j=1}^{9} \frac{b_j}{(1+t^k\rho^k)^{j-2}} \tag{A.10c}$$

$$\gamma_1 = \frac{1}{2G_{12}} \tag{A.10d}$$

$$\gamma_2 = \gamma_3 = \frac{1}{E_2} - \frac{\nu_{12}^2}{E_1} \tag{A.10e}$$

The constants a_j and b_j can be found in the literature (see for example Table 1 in [134] or Table 4.2 in [7]).

B

Related publications

The outcomes of the research presented in this thesis and other related contributions of the author are partially reflected in the refereed journal papers, book chapters and conference papers listed below:

B.1 Journal articles

- Juan Chiachío, Manuel Chiachío, Abhinav Saxena, Shankar Sankararaman, Guillermo Rus, Kai Goebel. Bayesian model selection and parameter estimation for fatigue damage progression models in composites. *International Journal of Fatigue (2014)* DOI:10.1016/j.ijfatigue.2014.08.003 (I.F.: 1.694, Rank: 31-126=24%)
- Manuel Chiachío, Juan Chiachío, Guillermo Rus, James L. Beck. Predicting Fatigue in Composites. A Bayesian Framework. *Structural Safety (2014), 51, 57-68.* (I.F.: 2.392, Rank: 11-124=8%, 1 cite)
- Manuel Chiachío, James L. Beck, Juan Chiachío, Guillermo Rus. Approximate Bayesian Computation by Subset Simulation. *SIAM Journal on Scientific Computing (2014), 36 (3), A1339-A1358* (I.F.: 1.940, Rank: 19-250=7%)
- Manuel Chiachío, Juan Chiachío, Guillermo Rus. Reliability in composites-A selective review and survey of current development. *Composites Part B: Engineering (2012), 43, 902-913.* (I.F.: 2.604, Rank: 7-87=8%, 22 cites)

B.2 Book chapters

- Juan Chiachío, Manuel Chiachío, Shankar Sankararaman, Abhinav Saxena, Kai Goebel. Prognostics Design for Structural Health Management, *To appear in: Emerging*

Design Solutions in Structural Health Monitoring Systems, Advances in Civil and Industrial Engineering Series (September 2014), Ed. IGI Global.

- Manuel Chiachío, Juan Chiachío, Abhinav Saxena, Kai Goebel. An Energy-based Prognostic Framework to Predict Evolution of Damage in Aerospace Structures, *To appear in: Structural Health Monitoring (SHM) in Aerospace Structures (November 2014), Ed. Woodhead Publishing Limited.*
- R. Muñoz, G. Rus, N. Bochud, D. Barnard, J. Melchor, J. Chiachío, M. Chiachío, S. Cantero, A. Callejas, L. Peralta. Nonlinear ultrasonics as an early damage signature, *To appear in: Emerging Design Solutions in Structural Health Monitoring Systems, Advances in Civil and Industrial Engineering Series (September 2014), Ed. IGI Global.*

B.3 Conference papers

- Juan Chiachío, Manuel Chiachío, Abhinav Saxena, Guillermo Rus, Kai Goebel. A model-based prognostics framework to predict fatigue damage evolution and reliability in composites. *In Proceedings of the European Conference of the Prognostics and Health Management Society, 2014, ISBN-978-1-936263-16-5 pp. 732-742.* (BEST-PAPER AWARD)
- Manuel Chiachío, Juan Chiachío, Abhinav Saxena, Guillermo Rus, Kai Goebel. An efficient simulation framework for prognostics of asymptotic processes-a case study in composite materials. *In Proceedings of the European Conference of the Prognostics and Health Management Society, 2014, ISBN-978-1-936263-16-5, pp. 202-214.* (NOMINATED TO BEST-PAPER AWARD)
- Juan Chiachío, Juan Chiachío, Abhinav Saxena, Shankar Sankaraman, Kai Goebel. A robust modeling approach for fatigue damage in composites based on Bayesian model class selection. *In Proceedings of the American Society for Composites 29th Technical Conference, 16th US-Japan Conference on Composites Materials, and ASTM D30 meeting, 2014, pp. 1-18, (pending ISBN assignment).*
- Manuel Chiachío, Juan Chiachío, Abhinav Saxena, Shankar Sankaraman, Kai Goebel. Predicting remaining useful life in CRFP laminates under fatigue loads: A new efficient algorithm. *In Proceedings of the American Society for Composites 29th Technical Conference, 16th US-Japan Conference on Composites Materials, and ASTM D30 meeting, 2014, pp. 1-20, (pending ISBN assignment).*
- Manuel Chiachío, Juan Chiachío, Abhinav Saxena, Guillermo Rus, Kai Goebel. An efficient algorithm to predict the expected end-of-life in composites. *In Proceedings of the 16th European Conference on Composite Materials, 2014, pp.1-8, (pending ISBN assignment).*
- Juan Chiachío, Manuel Chiachío, Abhinav Saxena, Guillermo Rus, Kai Goebel. An Energy- Based Prognostic Framework to Predict Fatigue Damage Evolution in Composites. *In Proceedings of the Annual Conference of the Prognostics and Health Management Society, 2013, ISBN-978-1-936263-06-6 pp. 363-371.*
- Manuel Chiachío, Juan Chiachío, Abhinav Saxena, Guillermo Rus, Kai Goebel. Fatigue damage prognosis in FRP composites by combining multi-scale degradation fault

modes in an uncertainty Bayesian framework. *In Proceedings of the Structural Health Monitoring, 2013, ISBN: 978-1-60595-115-7, pp.1368-1376,*

- Juan Chiachío, Manuel Chiachío, Guillermo Rus. Fatigue diagnosis in composites-A Robust Bayesian approach. *In Proceedings of the 15th European Conference on Composite Materials, 2012, pp.1-8, ISBN: 978-88-88785-33-2.*
- Juan Chiachío, Manuel Chiachío, Guillermo Rus, Nicolas Bochud, Laura Maria Peralta, Juan M. Melchor. A stochastic model for tissue consistence evolution based on the inverse problem. *In Proceedings of the ESB2012, Journal of Biomechanics, 45, Supplement 1, July 2012, pp. S652.*
- Juan Chiachío, Manuel Chiachío, Guillermo Rus. An Inverse-Problem Based Stochastic Approach to Model the Cumulative Damage Evolution of Composites. *Procedia Engineering, Volume 14, 2011, pp. 1557-1563*.

B.4 International conferences

- Juan Chiachío, Manuel Chiachío, Abhinav Saxena, Guillermo Rus, Kai Goebel. A model-based prognostics framework to predict fatigue damage evolution and reliability in composites. 2nd European Conference of the Prognostics and Health Management Society, Nantes, France, July 7-10, 2014.
- Juan Chiachío, Juan Chiachío, Abhinav Saxena, Shankar Sankaraman, Kai Goebel. A robust modeling approach for fatigue damage in composites based on Bayesian model class selection. 29th Technical Conference of the American Society for Composites, 16th US-Japan Conference on Composites Materials, and ASTM D30 meeting. San Diego (USA), September 2014
- Juan Chiachío, Juan Chiachío, Abhinav Saxena, Shankar Sankaraman, Kai Goebel. Predicting remaining useful life in CRFP laminates under fatigue loads: A new efficient algorithm. 29th Technical Conference of the American Society for Composites, 16th US-Japan Conference on Composites Materials, and ASTM D30 meeting. San Diego (USA), September 2014
- Juan Chiachío, Manuel Chiachío, Guillermo Rus. Tissue consistence evolution: A statistical approach. Work Conference on Bioinformatics and Biomedical Engineering (IWBBIO 2014), EU Annual Meeting, Granada (Spain), June 7-10, 2014.
- Juan Chiachío, Manuel Chiachío, Abhinav Saxena, Kai Goebel. An Energy-Based Prognostic Framework to Predict Fatigue Damage Evolution in Composites. Conference of the Prognostics and Health Management Society (PHM'13), New Orleans-(USA) October 14-17, 2013.
- Juan Chiachío, Manuel Chiachío, Abhinav Saxena, Guillermo Rus, Kai Goebel. Robust fatigue damage prognostics in composites. International Congress on Numerical Methods in Engineering 2013, Bilbao (Spain), June 25-28, 2013.

- Juan Chiachío, Manuel Chiachío, Guillermo Rus. Fatigue Diagnosis in Composites. A Robust Bayesian Approach. 15th European Conference on Composite Materials, Venice (Italy), 24-28 June, 2012.
- Juan Chiachío, Manuel Chiachío,Guillermo Rus. Bayesian state estimation for on line assessment and prognosis of fatigue damage in composite materials. 6th European Congress on Computational Methods in Applied Sciences, Vienna (Austria), 6-14 September, 2012.
- Juan Chiachío, Manuel Chiachío, Guillermo Rus. Tissue Consistence Evolution: A Statistical Approach. Tissue Engineering and Regenerative Medicine International Society (TERMIS), 31th Annual Meeting, Granada (Spain), June 7-10, 2011.
- Juan Chiachío, Manuel Chiachío, Guillermo Rus. Predicting the evolution of damage of composites materials-An inverse stochastic approach. Congresso de Metodos Numericos em Engenharia CEMNI Coimbra (Portugal), 20-25 June, 2011.

B.5 Patents

- Manuel Chiachio, Juan Chiachio, Guillermo Rus. Self-stressed structure for all-composite bridge (ES 2332442 B1). Spanish Bureau of Patents (OEPM).
- G. Rus, N. Bochud, J. Melchor, J. Chiachio, M. Chiachio. Petri-dish ultrasound-based monitoring device. (ES 2387770 B1). Spanish Bureau of Patents (OEPM).

References

[1] Abhinav Saxena, Kai Goebel, Cecilia Larrosa, and Fu-Kuo Chang. CFRP composites dataset, 2008. NASA Ames Prognostics Data Repository, [http://ti.arc.nasa.gov/project/prognostic-data-repository], NASA Ames, Moffett Field, CA.

[2] KL Reifsnider and A. Talug. Analysis of fatigue damage in composite laminates. *International Journal of Fatigue*, 2(1):3–11, 1980.

[3] R.D. Jamison, K. Schulte, K.L. Reifsnider, and W.W. Stinchcomb. Characterization and analysis of damage mechanisms in tension-tension fatigue of graphite/epoxy laminates. *Effects of defects in composite materials, ASTM STP*, 836:21–55, 1984.

[4] B. Harris. *Fatigue in composites*. CRC Press, 2003.

[5] Joris Degrieck and Wim Van Paepegem. Fatigue damage modeling of fibre-reinforced composite materials: Review. *Applied Mechanics Reviews*, 54(4):279, 2001.

[6] Ramesh Talreja. Damage and fatigue in composites – A personal account. *Composites Science and Technology*, 68:2585–2591, 2008.

[7] Ramesh Talreja and Chandra Veer Singh. *Damage and Failure of Composite Materials*. Cambridge University Press, 2012.

[8] H.T. Hahn and R.Y. Kim. Fatigue behavior of composite laminate. *Journal of Composite Materials*, 10(2):156, 1976.

[9] AL Highsmith and KL Reifsnider. Stiffness-reduction mechanisms in composite laminates. *Damage in composite materials, ASTM STP*, 775:103–117, 1982.

[10] J.D. Rowatt and P.D. Spanos. Markov chain models for life prediction of composite laminates. *Structural Safety*, 20:117–135, 1998.

[11] Bo-Siou Wei, Shane Johnson, and Rami Haj-Ali. A stochastic fatigue damage method for composite materials based on Markov chains and infrared thermography. *International Journal of Fatigue*, 32(2):350–360, February 2010.

[12] K Potter, C Langer, B Hodgkiss, and S Lamb. Sources of variability in uncured aerospace grade unidirectional carbon fibre epoxy preimpregnate. *Composites Part A*, 38:905–916, 2007.

[13] K Potter, B Khan, M Wisnom, T Bell, and J Stevens. Variability , fibre waviness and misalignment in the determination of the properties of composite materials and structures. *Composites Part A*, 39:1343–1354, 2008.

[14] K. Potter. 2 - manufacturing defects as a cause of failure in polymer matrix composites. In Paul Robinson, Emile Greenhalgh, and Silvestre Pinho, editors, *Failure Mechanisms in Polymer Matrix Composites*, Woodhead Publishing Series in Composites Science and Engineering, pages 26 – 52. Woodhead Publishing, 2012.

[15] S.L. Lemanski, J. Wang, M.P.F. Sutcliffe, K.D. Potter, and M.R. Wisnom. Modelling failure of composite specimens with defects under compression loading. *Composites Part A: Applied Science and Manufacturing*, 48(0):26 – 36, 2013.

[16] Manuel Chiachio, Juan Chiachio, Guillermo Rus, and James L. Beck. Predicting fatigue damage in composites: A Bayesian framework. *Structural Safety*, 51:57 – 68, 2014.

[17] Shankar Sankararaman, You Ling, Christopher Shantz, and Sankaran Mahadevan. Uncertainty quantification in fatigue crack growth prognosis. *International Journal of Prognostics and Health Management*, 2(1), 2011.

[18] R T. Cox. *The Algebra of Probable Inference*. The Johns Hopkins University Press, 1961.

[19] E.T. Jaynes. *Probability Theory: The Logic of Science*. Cambridge University Press, 2003.

[20] Karl R Popper. *The logic of scientific discovery.* Basic Books, 1959.

[21] Albert Tarantola. Popper, bayes and the inverse problem. *Nature Physics*, 2(8):492–494, 2006.

[22] James L Beck. Bayesian system identification based on probability logic. *Structural Control and Health Monitoring*, 17:825–847, 2010.

[23] E.T. Jaynes. Information theory and statistical mechanics. *The Physical Review*, 106(4):620–630, 1957.

[24] R Ganesan. A data-driven stochastic approach to model and analyze test data on fatigue response. *Computers & Structures*, 76(4):517–531, 2000.

[25] YA Dzenis. Cycle-based analysis of damage and failure in advanced composites under fatigue-2. Stochastic mesomechanics modeling. *International Journal of Fatigue*, 25(6):511–520, 2003.

[26] M Kamiski. On probabilistic fatigue models for composite materials. *International Journal of Fatigue*, 24(2-4):477–495, April 2002.

[27] Juan Chiachío, Manuel Chiachío, Abhinav Saxena, Shankar Sankararaman, Guillermo Rus, and Kai Goebel. Bayesian model class selection and parameter estimation for fatigue damage progression in composites. *International Journal of Fatigue*, 2014.

[28] Kenneth P Burnham and David R Anderson. *Model Selection and Multi-Model Inference: A Practical Information-Theoretic Approach*. Springer, 2002.

[29] James L Beck and Ka-Veng Yuen. Model selection using response measurements: Bayesian probabilistic approach. *Journal of Engineering Mechanics*, 130(2):192–203, 2004.

[30] Marc C Kennedy and Anthony O'Hagan. Bayesian calibration of computer models. *Journal of the Royal Statistical Society: Series B (Statistical Methodology)*, 63(3):425–464, 2001.

[31] Albert Tarantola. *Inverse Problem Theory and Methods for Model Parameters Estimation*. SIAM, 2005.

[32] Ruoxue Zhang and Sankaran Mahadevan. Model uncertainty and Bayesian updating in reliability-based inspection. *Structural Safety*, 22(2):145–160, 2000.

[33] R. Cross, A. Makeev, and E. Armanios. Simultaneous uncertainty quantification of fracture mechanics based life prediction model parameters. *International Journal of Fatigue*, 29(8):1510–1515, 2007.

[34] Shankar Sankararaman, You Ling, and Sankaran Mahadevan. Statistical inference of equivalent initial flaw size with complicated structural geometry and multi-axial variable amplitude loading. *International Journal of Fatigue*, 32(10):1689–1700, 2010.

[35] Xuefei Guan, Ratneshwar Jha, and Yongming Liu. Model selection, updating, and averaging for probabilistic fatigue damage prognosis. *Structural Safety*, 33(3):242–249, 2011.

[36] Shankar Sankararaman, You Ling, and Sankaran Mahadevan. Uncertainty quantification and model validation of fatigue crack growth prediction. *Engineering Fracture Mechanics*, 78(7):1487–1504, 2011.

[37] Xuefei Guan, Yongming Liu, Ratneshwar Jha, Abhinav Saxena, Jose Celaya, and Kai Geobel. Comparison of two probabilistic fatigue damage assessment approaches using prognostic performance metrics. *International Journal of Prognostics and Health Management*, 2(1), 2011.

[38] Maurizio Gobbato, John B Kosmatka, and Joel P Conte. A recursive bayesian approach for fatigue damage prognosis: an experimental validation at the reliability component level. *Mechanical Systems and Signal Processing*, 45:448–467, 2014.

[39] V.V. Bolotin. Stochastic models of cumulative damage in composite materials. *Engineering Fracture Mechanics*, 8(1):103–113, 1976.

[40] ASD Wang, PC Chou, and SC Lei. A stochastic model for the growth of matrix cracks in composite laminates. *Journal of Composite Materials*, 18(3):239–254, 1984.

[41] W. Hwang and KS Han. Fatigue of composites-fatigue modulus concept and life prediction. *Journal of Composite Materials*, 20(2):154–165, 1986.

[42] S. Abrate. Matrix cracking in laminated composites: a review. *Composites Engineering*, 1(6):337–353, 1991.

[43] ASD Wang. Strength, failure, and fatigue analysis of laminates. *ASM International, Engineered Materials Handbook.*, 1:236–251, 1987.

[44] Srinivas Sriramula and Marios K Chryssanthopoulos. Composites : Part A Quantification of uncertainty modelling in stochastic analysis of FRP composites. *Composites Part A*, 40(11):1673–1684, 2009.

[45] S F Gull. Developments in maximum-entropy data analysis. *Maximum Entropy and Bayesian Methods*, pages 53–71, 1989.

[46] Yuri Suhov and Mark Kelbert. *Markov Chains: A Primer in Random Processes and their Applications*. Cambrigde University Press, 2008.

[47] J.L. Bogdanoff and F. Kozin. *Probabilistic Models of Cumulative Damage*. John Wiley & Sons, 1985.

[48] JA Nairn and S Hu. The initiation and growth of delaminations induced by matrix microcracks in laminated composites. *International Journal of Fracture*, 57(1):1–24, 1992.

[49] Andrea Saltelli, Marco Ratto, Terry Andres, Francesca Campolongo, Jessica Cariboni, Debora Gatelli, Michaela Saisana, and Stefano Tarantola. *Global Sensitivity Analysis: The Primer*. Wiley-Interscience, 2008.

[50] S.K. Au and J.L. Beck. Estimation of small failure probabilities in high dimensions by subset simulation. *Probabilistic Engineering Mechanics*, 16(4):263–277, 2001.

[51] R. T. Cox. Probability, frequency and reasonable expectation. *American Journal of Physics*, (17):1–13, 1946.

[52] E T Jaynes. *Papers on Probability, Statistics and Statistical physics*. (Ed. R.D. Rosenkrantz) Kluwer Academic Publishers, 1983.

[53] James L. Beck and Siu-Kui Au. Bayesian Updating of Structural Models and Reliability using Markov Chain Monte Carlo Simulation. *Journal of Engineering Mechanics*, 128(4):380–391, 2002.

[54] WR Gilks, S Richardson, and D J Spiegelhalter. *Markov Chain Monte Carlo in Practice*. Chapman and Hall, 1996.

[55] R.M. Neal. Probabilistic inference using Markov chain Monte Carlo methods. *Intelligence*, 62, 1993.

[56] A. F. M. Smith and G. O. Roberts. Bayesian computation via the gibbs sampler and related markov chain monte carlo methods. *Journal of the Royal Statistical Society. Series B (Methodological)*, 55(1):3–23, 1993.

[57] Dani Gamerman and Hedibert F Lopes. *Markov chain Monte Carlo: stochastic simulation for Bayesian inference*. CRC Press, 2006.

[58] M. Muto and J L Beck. Bayesian updating and model class selection for hysteretic structural models using stochastic simulation. *Journal of Vibration and Control*, 14(1-2):7–34, 2008.

[59] F. Liang, C. Liu, and J. Chuanhai. *Advanced Markov Chain Monte Carlo Methods*. Wiley Online Library, 2010.

[60] N. Metropolis, A W Rosenbluth, M N Rosenbluth, A H Teller, and E. Teller. Equation of state calculations by fast computing machines. *The Journal of Chemical Physics*, 21:1087–1092, 1953.

[61] W.K. Hastings. Monte Carlo sampling methods using Markov chains and their applications. *Biometrika*, 57(1):97–109, 1970.

[62] A. Gelman, G. Roberts, and W. Gilks. Efficient Metropolis jumping rules. *Bayesian Statistics*, 5:599–608, 1996.

[63] G.O. Roberts and J.S. Rosenthal. Optimal scaling for various Metropolis-Hastings algorithms. *Statistical Science*, 16(4):351–367, 2001.

[64] SK Au and JL Beck. Subset simulation and its application to seismic risk based on dynamic analysis. *Journal of Engineering Mechanics*, 129(8):901–917, 2003.

[65] James Litz. Beck and Ka Veng. Yuen. Model selection using response measurements: Bayesian probabilistic approach. *Journal of Engineering Mechanics*, 130:192, 2004.

[66] S H Cheung and J L Beck. Calculation of posterior probabilities for bayesian model class assessment and averaging from posterior samples based on dynamic system data. *Computer-Aided Civil and Infrastructure Engineering*, 25(5):304–321, 2010.

[67] S. Kullback and R. A. Leibler. On information and sufficiency. *The Annals of Mathematical Statistics*, 22(1):79–86, 1951.

[68] J L Beck and L S Katafygiotis. Updating models and their uncertainties. i: Bayesian statistical framework. *Journal of Engineering Mechanics*, 124(4):455–462, 1998.

[69] L S Katafygiotis and H F Lam. Tangential projection algorithm for manifold representation in unidentifiable model updating problems. *Earthquake Engineering & Structural Dynamics*, 31(4):791–812, 2002.

[70] C Papadimitriou, J L Beck, and L S Katafygiotis. Asymptotic expansions for reliability and moments of uncertain systems. *Journal of Engineering Mechanics*, 123(12):1219–1229, 1997.

[71] Bernard W Silverman. *Density estimation for statistics and data analysis*, volume 26. CRC press, 1986.

[72] M.A. Newton and A.E. Raftery. Approximate bayesian inference with the weighted likelihood bootstrap. *Journal of the Royal Statistical Society. Series B (Methodological)*, 56(1):3–48, 1994.

[73] A E Gelfand and D K Dey. Bayesian model choice: asymptotics and exact calculations. *Journal of the Royal Statistical Society. Series B (Methodological)*, 56(3):501–514, 1994.

[74] S. Chib and E. Greenberg. Understanding the metropolis-hastings algorithm. *The American Statistician*, 49(4):327–335, 1995.

[75] SK Au and James L Beck. A new adaptive importance sampling scheme for reliability calculations. *Structural Safety*, 21(2):135–158, 1999.

[76] Siddhartha Chib and Ivan Jeliazkov. Marginal likelihood from the metropolis–hastings output. *Journal of the American Statistical Association*, 96(453):270–281, 2001.

[77] J.A. Hoeting, D. Madigan, A.E. Raftery, and C.T. Volinsky. Bayesian model averaging: A tutorial. *Statistical Science*, pages 382–401, 1999.

[78] GP Sendeckyj. Life prediction for resin-matrix composite materials. *Fatigue of Composite Materials*, 4:431–483, 1990.

[79] P.J.C.L. Read and R.A. Shenoi. A review of fatigue damage modeling in the context of marine FRP laminates. *Marine Structures*, 8(3):257 – 278, 1995.

[80] N.L. Post, S.W. Case, and J.J. Lesko. Modeling the variable amplitude fatigue of composite materials: A review and evaluation of the state of the art for spectrum loading. *International Journal of Fatigue*, 30(12):2064 – 2086, 2008.

[81] X Diao. Statistical model for multiaxial fatigue behavior of unidirectional plies. *Composites Science and Technology*, 59(13):2025–2035, October 1999.

[82] Y Liu and S Mahadevan. Probabilistic fatigue life prediction of multidirectional composite laminates. *Composite Structures*, 69(1):11–19, June 2005.

[83] A Papoulis. *Probability, Random Variables, and Stochastic Processes*. McGraw Hill, 1965.

[84] Kenneth L. Reifsnider. The critical element model: A modeling philosophy. *Engineering Fracture Mechanics*, 25(5/6):739–749, 1986.

[85] E.T. Jaynes. Information theory and statistical mechanics. II. *The Physical Review*, 108(2):171–190, 1957.

[86] Y.Z. Pappas, P.D. Spanos, and V. Kostopoulos. Markov chains for damage accumulation of organic and ceramic matrix composites. *Journal of Engineering Mechanics*, 127(9):915–926, 2001.

[87] S. Johnson, B. Wei, and R. Haj-Ali. A stochastic fatigue damage model for composite single lap shear joints based on Markov chains and thermoelastic stress analysis. *Fatigue & Fracture of Engineering Materials & Structures*, 33(12):897–910, 2010.

[88] YK Lin and JN Yang. A stochastic theory of fatigue crack propagation. *AIAA journal*, 23(1):117–124, 1985.

[89] Wen-Fang Wu. On the Markov approximation of fatigue crack growth. *Probabilistic Engineering Mechanics*, 1(4):224–233, 1986.

[90] Tom Lassen. Markov modelling of the fatigue damage in welded structures under in-service inspection. *International Journal of Fatigue*, 13(5):417–422, September 1991.

[91] K. Sobczyk and B.F. Spencer. *Random Fatigue: From Data to Theory*. Academic Press, 1992.

[92] Yunping Xi and Z.P Bazant. Random growth of crack with R-curve: Markov process model. *Engineering Fracture Mechanics*, 57(6):593–608, 1997.

[93] J A Bea, M Doblaré, and L Gracia. Evaluation of the probability distribution of crack propagation life in metal fatigue by means of probabilistic finite element method and B-models. *Engineering Fracture Mechanics*, 63(6):675–711, August 1999.

[94] Y.S. Roh and Y Xi. A general formulation for transition probabilities of Markov model and the application to fracture of composite materials. *Probabilistic Engineering Mechanics*, 15:241–250, 2000.

[95] W.F. Wu and C.C. Ni. A study of stochastic fatigue crack growth modeling through experimental data. *Probabilistic Engineering Mechanics*, 18:107–118, April 2003.

[96] W.F. Wu and C.C. Ni. Probabilistic models of fatigue crack propagation and their experimental verification. *Probabilistic Engineering Mechanics*, 19(3):247–257, July 2004.

[97] J Grasa, MA Pérez, JA Bea, JM García-Aznar, and M Doblaré. A probabilistic damage model for acrylic cements. Application to the life prediction of cemented hip implants. *International Journal of Fatigue*, 27(8):891–904, 2005.

[98] W Wu and C Ni. Statistical aspects of some fatigue crack growth data. *Engineering Fracture Mechanics*, 74(18):2952–2963, December 2007.

[99] Massimiliano Giorgio, Maurizio Guida, and Gianpaolo Pulcini. An age- and state-dependent Markov model for degradation processes. *IIE Transactions*, 43:621–632, 2011.

[100] Maurizio Guida and Gianpaolo Pulcini. A continuous-state Markov model for age- and state-dependent degradation processes. *Structural Safety*, 33(6):354–366, 2011.

[101] K. Sobczyk. Stochastic models for fatigue damage of materials. *Advances in Applied Probability*, 19(3):652–673, 1987.

[102] BF Spencer Jr and J Tang. Markov process model for fatigue crack growth. *Journal of Engineering Mechanics*, 114(12):2134–2157, 1988.

[103] J. Lemaitre, J.P. Cordebois, and J. Dufailly. Sur le couplage endommagement-elasticité. *Comptes rendus de l'Académie des Sciences, Paris, B. (1979)*, 391.

[104] S.L. Ogin, P.A. Smith, and P.W.R. Beaumont. Matrix cracking and stiffness reduction during the fatigue of a (0/90)s GFRP laminate. *Composites Science and Technology*, 22(1):23 – 31, 1985.

[105] H Mao and S Mahadevan. Fatigue damage modelling of composite materials. *Composite Structures*, 58(4):405–410, December 2002.

[106] George Z Voyiadjis and Peter I Kattan. A comparative study of damage variables in continuum damage mechanics. *International Journal of Damage Mechanics*, 18(4):315–340, 2009.

[107] George Z Voyiadjis and Peter I Kattan. Mechanics of small damage in fiber-reinforced composite materials. *Composite Structures*, 92(9):2187–2193, 2010.

[108] Jean Lemaitre. How to use damage mechanics. *Nuclear Engineering and Design*, 80:233–245, 1984.

[109] J.L. Chaboche. Continuum damage mechanics: Present state and future trends. *Nuclear Engineering and Design*, 105:19–33, 1987.

[110] Jean Lemaitre and Jacques Dufailly. Damage Measurements. *Engineering Fracture Mechanics*, 28(516):643–661, 1987.

[111] L. M Kachanov. *Introduction to continuum damage mechanics*. Dordrecht: M. Nijhoff, 1986.

[112] RE Carlson and FN Fritsch. Monotone piecewise cubic interpolation. *SIAM journal on numerical analysis*, 22(2):386–400, 1985.

[113] P. Whittle. Some distribution and moment formulae for the markov chain. *Journal of the Royal Statistical Society. Series B (Methodological)*, pages 235–242, 1955.

[114] Patrick Billingsley. Statistical Methods in Markov Chains. *The Annals of Mathematical Statistics*, 32(1):12–40, 1961.

[115] H. Cramer. On the composition of elementary errors. *Skandinavisk Aktuarietidskrift*, 11(13-74):141–180, 1928.

[116] R. Von Mises. Wahrscheinlichkeitsrechnung und ihre anwendung in der statistik und theoretischen physik. *Bull. Amer. Math. Soc*, 2(1932).

[117] D.E. Goldberg. *Genetic algorithms in search, optimization, and machine learning*. Addison-wesley, 1989.

[118] J.H. Holland. *Adaptation in natural and artificial systems: an introductory analysis with applications to biology, control, and artificial intelligence*. MIT press, 1992.

[119] Reuven Y. Rubinstein and Dirk P. Kroese. *Simulation and the Monte Carlo Method.* John Wiley & Sons, Hoboken, New Jersey, second edition, 2008.

[120] Srinivas Sriramula and Marios K Chryssanthopoulos. Quantification of uncertainty modelling in stochastic analysis of FRP composites. *Composites Part A: Applied Science and Manufacturing*, 40(11):1673–1684, 2009.

[121] C Jiang, GR Liu, and X Han. A novel method for uncertainty inverse problems and application to material characterization of composites. *Experimental Mechanics*, 48(4):539–548, 2008.

[122] S Sakata, F Ashida, T Kojima, and M Zako. Influence of uncertainty in microscopic material property on homogenized elastic property of unidirectional fiber reinforced composites. *Theoretical and Applied Mechanics Japan*, 56:67–76.

[123] P Gayathri, K Umesh, and Ranjan Ganguli. Effect of matrix cracking and material uncertainty on composite plates. *Reliability Engineering & System Safety*, 95(7):716–728, 2010.

[124] S. Sakata, F. Ashida, T. Kojima, and M. Zako. Three-dimensional stochastic analysis using a perturbation-based homogenization method for elastic properties of composite material considering microscopic uncertainty. *International Journal of Solids and Structures*, 45(3–4):894 – 907, 2008.

[125] G Georgiou, A Manan, and JE Cooper. Modeling composite wing aeroelastic behavior with uncertain damage severity and material properties. *Mechanical Systems and Signal Processing*, 32:32–43, 2012.

[126] Carl Scarth, Jonathan E. Cooper, Paul M. Weaver, and Gustavo H.C. Silva. Uncertainty quantification of aeroelastic stability of composite plate wings using lamination parameters. *Composite Structures*, 116(0):84 – 93, 2014.

[127] DJ Lekou and TP Philippidis. Mechanical property variability in FRP laminates and its effect on failure prediction. *Composites Part B: Engineering*, 39(7):1247–1256, 2008.

[128] Manuel Chiachío, Juan Chiachío, and Guillermo Rus. Reliability in composites - A selective review and survey of current development. *Composites Part B*, 43(3):902–913, 2012.

[129] John A Nairn. In R Talreja and Manson J.A.E., editors, *Polymer Matrix Composites*, chapter Matrix Microcracking in Composites, pages 403–432. Elsevier Science, Amsterdam, 2000.

[130] J.W. Lee, DH Allen, and CE Harris. Internal state variable approach for predicting stiffness reductions in fibrous laminated composites with matrix cracks. *Journal of Composite Materials*, 23(12):1273–1291, 1989.

[131] P.W.R. Beaumont, RA Dimant, and HR Shercliff. Failure processes in composite materials: getting physical. *Journal of Materials Science*, 41(20):6526–6546, 2006.

[132] KW Garrett and JE Bailey. Multiple transverse fracture in 90° cross-ply laminates of a glass fibre-reinforced polyester. *Journal of Materials Science*, 12(1):157–168, 1977.

[133] Z Hashin. Analysis of cracked laminates: a variational approach. *Mechanics of Materials*, 4(2):121–136, 1985.

[134] Peter Gudmundson and Zang Weilin. An analytic model for thermoelastic properties of composite laminates containing transverse matrix cracks. *International Journal of Solids and Structures*, 30(23):3211–3231, 1993.

[135] P Lundmark and J Varna. Constitutive relationships for laminates with ply cracks in in-plane loading. *International Journal of Damage Mechanics*, 14(3):235–259, 2005.

[136] J.N. Reddy. *Energy Principles and Variational Methods in Applied Mechanics*. Wiley, 2002.

[137] C.L. Dym and Irving H. Shames. *Solid Mechanics: A Variational Approach, Augmented Edition*. SpringerLink: Bücher. Springer, 2013.

[138] Janis Varna, Nagendra V Akshantala, and Ramesh Talreja. Crack opening displacement and the associated response of laminates with varying constraints. *International Journal of Damage Mechanics*, 8(2):174–193, 1999.

[139] R Joffe, A Krasnikovs, and J Varna. Cod-based simulation of transverse cracking and stiffness reduction in $[S/90_n]_s$ laminates. *Composites Science and Technology*, 61(5):637–656, 2001.

[140] R Joffe and J Varna. Analytical modeling of stiffness reduction in symmetric and balanced laminates due to cracks in 90 layers. *Composites Science and Technology*, 59(11):1641–1652, 1999.

[141] Peter W Manders, Tsu-Wei Chou, Frank R Jones, and John W Rock. Statistical analysis of multiple fracture in 0/90/0 glass fibre/epoxy resin laminates. *Journal of Materials Science*, 18(10):2876–2889, 1983.

[142] RJ Nuismer and SC Tan. Constitutive relations of a cracked composite lamina. *Journal of Composite Materials*, 22(4):306–321, 1988.

[143] SC Tan and RJ Nuismer. A theory for progressive matrix cracking in composite laminates. *Journal of Composite Materials*, 23(10):1029–1047, 1989.

[144] J.A. Nairn and S. Hu. In R. Talreja, editor, *Damage Mechanics of Composites Materials*, chapter Micromechanics of damage: A case study of matrix microcracking, pages 187–214. Elsevier, 1994.

[145] J.N. Reddy. *Mechanics of Laminated Composite Plates and Shells: Theory and Analysis, Second Edition*. CRC Mechanical Engineering Series.

[146] John A Nairn. The strain energy release rate of composite microcracking: a variational approach. *Journal of Composite Materials*, 23(11):1106–1129, 1989.

[147] John A Nairn. Some new variational mechanics results on composite microcracking. In *Proc. 10th International Conference on Composite Materials (ICCM-10) Whistler BC, Canada*, 1995.

[148] A. Saltelli, M. Ratto, S. Tarantola, and F. Campolongo. Sensitivity analysis practices: Strategies for model-based inference. *Reliability Engineering & System Safety*, 91(10):1109–1125, 2006.

[149] J.M. Marin, P. Pudlo, C.P. Robert, and R.J. Ryder. Approximate bayesian computational methods. *Statistics and Computing*, pages 1–14, 2011.

[150] S. Tavare, D.J. Balding, RC Griffiths, and P. Donnelly. Inferring coalescence times from dna sequence data. *Genetics*, 145(2):505, 1997.

[151] J.K. Pritchard, M.T. Seielstad, A. Perez-Lezaun, and M.W. Feldman. Population growth of human y chromosomes: a study of y chromosome microsatellites. *Molecular Biology and Evolution*, 16(12):1791–1798, 1999.

[152] P. Marjoram, J. Molitor, V. Plagnol, and S. Tavaré. Markov chain monte carlo without likelihoods. *Proceedings of the National Academy of Sciences of the United States of America*, 100(26):15324–15328, 2003.

[153] C.P. Robert and G. Casella. *Monte Carlo statistical methods, 2nd Ed.* Springer-Verlag, New York, 2004.

[154] P. Fearnhead and D. Prangle. Constructing summary statistics for approximate bayesian computation: semi-automatic approximate bayesian computation. *Journal of the Royal Statistical Society, Series B*, 74(Part 3):419–474, 2012.

[155] P. Bortot, SG Coles, and SA Sisson. Inference for stereological extremes. *Journal of the American Statistical Association*, 102(477):84–92, 2007.

[156] S.A. Sisson and Y. Fan. *Handbook of Markov Chain Monte Carlo*, chapter Likelihood-free markov chain monte carlo, pages 319–341. Chapman and Hall/CRC Press, 2011.

[157] P. Del Moral, A. Doucet, and A. Jasra. Sequential monte carlo samplers. *Journal of the Royal Statistical Society: Series B (Statistical Methodology)*, 68(3):411–436, 2006.

[158] SK Au, J. Ching, and JL Beck. Application of subset simulation methods to reliability benchmark problems. *Structural Safety*, 29(3):183–193, 2007.

[159] SA Sisson, Y. Fan, and M.M. Tanaka. Sequential monte carlo without likelihoods. *Proceedings of the National Academy of Sciences*, 104(6):1760–1765, 2007.

[160] T. Toni, D. Welch, N. Strelkowa, A. Ipsen, and M.P.H. Stumpf. Approximate bayesian computation scheme for parameter inference and model selection in dynamical systems. *Journal of the Royal Society Interface*, 6(31):187–202, 2009.

[161] SA Sisson, Y. Fan, and M.M. Tanaka. A note on backward kernel choice for sequential monte carlo without likelihoods. Technical report, University of New South Wales, 2009.

[162] M.A. Beaumont, J.M. Cornuet, J.M. Marin, and C.P. Robert. Adaptive approximate bayesian computation. *Biometrika*, 96(4):983–990, 2009.

[163] M. Baragatti, A. Grimaud, and D. Pommeret. Likelihood-free parallel tempering. *Statistics and Computing*, pages 1–15, 2011.

[164] C.C. Drovandi and A.N. Pettitt. Estimation of parameters for macroparasite population evolution using approximate Bayesian computation. *Biometrics*, 67:225–233, 2011.

[165] Pierre Moral, Arnaud Doucet, and Ajay Jasra. An adaptive sequential monte carlo method for approximate bayesian computation. *Statistics and Computing*, 22:1009–1020, 2012.

[166] Ching Jianye, SK JL Au, and JL Beck. Reliability estimation of dynamical systems subject to stochastic excitation using subset simulation with splitting. *Computer Methods in Applied Mechanics and Engineering*, 194(12-16):1557–1579, 2005.

[167] K.M. Zuev, J.L. Beck, S.K. Au, and L.S. Katafygiotis. Bayesian post-processor and other enhancements of subset simulation for estimating failure probabilities in high dimensions. *Computers & Structures*, 92-93:283–296, 2011.

[168] J.M. Marin and C.P. Robert. *Bayesian core: a practical approach to computational* B*ayesian statistics*. Springer, 2007.

[169] Monson H Hayes. *Statistical digital signal processing and modeling*. John Wiley & Sons, 2009.

[170] Ka-Veng Yuen and James L Beck. Updating properties of nonlinear dynamical systems with uncertain input. *Journal of engineering mechanics*, 129(1):9–20, 2003.

[171] Ka-Veng Yuen. *Bayesian methods for structural dynamics and civil engineering*. Wiley, 2010.

[172] E.T. Jaynes. Information theory and statistical mechanics. *Physical Review*, 106(4):620–630, 1957.

[173] A. Saxena, K Goebel, C Larrosa, V Janapati, S Roy, and FK Chang. Accelerated aging experiments for prognostics of damage growth in composites materials. In *The 8th* I*nternational* W*orkshop on* S*tructural* H*ealth* M*onitoring, F.-K. C*hang, Editor.*, volume 15, 2011.

[174] J. Chiachío, M. Chiachío, A. Saxena, G. Rus, and K. Goebel. An energy-based prognostics framework to predict fatigue damage evolution in composites. In *Proceedings of the Annual Conference of the Prognostics and Health Management Society, 2013*, volume 1, pages 363–371. Prognostics and Health Management Society, 2013.

[175] M. Chiachío, J. Chiachío, A. Saxena, G. Rus, and K. Goebel. Fatigue damage prognosis in FRP composites by combining multi-scale degradation fault modes in an uncertainty Bayesian framework. In *Proceedings of the 9th Structural Health Monitoring, 2013*, volume 1, pages 1368–1375, 2013.

[176] Cecilia C. Larrosa. *Monitoring matrix cracking in composite laminates using built-in piezoelectric sensors*. PhD thesis, Stanford University, USA, 2013.

[177] Tishun Peng, Abhinav Saxena, Kai Goebel, Yibing Xiang, Shankar Sankararaman, and Yongming Liu. A novel Bayesian imaging method for probabilistic delamination detection of composite materials. *Smart Materials and Structures*, 22(12):125019, 2013.

[178] Manuel Chiachio Ruano. *Methods for prognostics and reliability in composite materials using structural health monitoring*. PhD thesis, Universidad de Granada, Spain, 2014.